Synergistic Effects of Lubricant Additive Chemistry on Ash Properties Impacting Diesel Particulate Filter Flow Resistance and Catalyst Performance

by

Sean Munnis

B.S., Mechanical Engineering
United States Coast Guard Academy, 2007

Submitted to the Department of Mechanical Engineering in Partial Fulfillment of the Requirements for the Degrees of

MASTER OF SCIENCE IN MECHANICAL ENGINEERING

And

MASTER OF SCIENCE IN NAVAL ARCHITECTURE AND MARINE ENGINEERING

AT THE

MASSACHUSETTS INSTITUTE OF TECHNOLOGY

June 2011

Signature of Author: _____
Department of Mechanical Engineering
June 1, 2011

Certified by: _____
Victor W. Wong
Principal Research Scientist and Lecturer in Mechanical Engineering
Thesis Supervisor

Accepted by: _____
David Hardt
Chairman, Department Committee on Graduate Students

(This page intentionally left blank)

Synergistic Effects of Lubricant Additive Chemistry on Ash Properties Impacting Diesel Particulate Filter Flow Resistance and Catalyst Performance

by

Sean Munnis

Submitted to the Department of Mechanical Engineering on June 1, 2011 in Partial Fulfillment of the Requirements for the Degrees of

MASTER OF SCIENCE IN MECHANICAL ENGINEERING

&

MASTER OF SCIENCE IN NAVAL ARCHITECTURE & MARINE ENGINEERING

ABSTRACT

Diesel particulate filters (DPF) have seen widespread use in recent years in both on- and off-road applications as an effective means for meeting the increasingly stringent particulate emission regulations. Overtime, engine-out particulate matter composed of soot and incombustible ash accumulate within the DPF. Although soot can be removed by oxidation, ash remains within the filter and substantially accumulates over time leading to increased flow restriction thus a pressure drop across the filter. An increased pressure drop negatively affects the engine performance & fuel economy leading to the need for filter removal and cleaning.

The adverse effects of ash accumulation on DPF performance have been extensively studied in the past and are well know yet the underlying mechanisms for their presence are still not well understood. The ash which accumulates within a DPF is a product of a number of factors including engine wear and corrosion as well as trace metals in diesel fuel, but the majority of the engine out ash is derived from specific metallic additives placed within the diesel lubricant. This work examines the properties of ash derived from specific single lubricant additives, as well as simple combinations, and their adverse effect on DPF performance. Specific ash properties are examined such as porosity, permeability, deposit thicknesses and packing densities along the filter channel walls as a cake layer as well as the resultant end plugs in the rear of the filter channels. Through a combined approach of experiments and theoretical models, the link between the material properties and characteristics of ash derived from single additives as well as combinations can be made to their respective impact on DPF performance.

The results of this research are among a few of its kind and aim to help optimize the design of advanced diesel aftertreatment systems as well as lubricant formulations to satisfy the additive requirements for engine protection while mitigating the negative effects on DPF performance.

Thesis Supervisor: Victor W. Wong
Title: Principal Research Scientist and Lecturer in Mechanical Engineering

(This page intentionally left blank)

ACKNOWLEDGEMENTS

There are a number of people that have made my time at MIT both memorable and productive. Overall my time at this institution has helped me grow not only in the academic sense but also as a leader and efficient problem solver.

First I would like to thank my thesis advisor, Dr. Victor Wong, for giving me the opportunity to not only attend MIT but also be a part of a very interesting and relevant research topic which I will no doubt use in my future career. Dr. Wong not only helped me extensively with the financial aspect of my attendance but also was extremely flexible with my proposed class schedule being extremely understanding with my desire to obtain two master's degrees. Dr. Wong understood, acknowledged and took into consideration my desire to reach both professional and personal goals while attending MIT and I cannot thank him enough for that.

I would like to extend my sincerest thanks to Dr. Alex Sappok for his infinite amount of guidance and support throughout my research. There were countless situations in which I was stumped and troubled by research concepts, experimentation methods, troubleshooting and analysis of results. Dr. Sappok never once denied me support and always pointed me in the right direction to further my progress in an extremely cheerful and pleasant manner. Dr. Sappok is one of the best leaders, and workers, I have ever encountered and I have learned many lessons from him which I will use in my career as a Coast Guard Officer. I would be both honored and grateful to work alongside or under the supervision of Dr. Sappok at any point in my career.

I would also like to thank the United States Coast Guard for giving me the opportunity to attend graduate school during my active duty service. This was an extremely rewarding experience and I look forward to using everything I have learned to be the best Naval Engineering Officer as possible. Specifically I would like to thank LCDR Mike Plumley who encouraged me to attend MIT and gave me the guidance to make it possible.

The contributions of multiple Sloan Automotive Laboratory personnel are also in need of thanks. Thane DeWitt and Raymond Phan ensured that my experimental test set-up was working properly and always made my days (and nights) pleasurable in the lab. I would also like to thank all of the students in the laboratory who have made my time enjoyable. I have made a number of lasting friendships and I intend to stay in contact and maintain our relationships.

Lastly, but certainly not least, I would like to thank my family and friends outside of MIT. Thanks for not only visiting me in Boston and making my weekends memorable but also giving me much needed conversation outside of the institute.

(This page intentionally left blank)

Table of Contents

(This page intentionally left blank)

LIST OF FIGURES

(This page intentionally left blank)

LIST OF TABLES

NOMENCLATURE

ACEA	European Automotive Manufacturers Association
ACT	Asymmetric Cell Technology
API	American Petroleum Institute
ATS	Aftertreatment System
Ca	Calcium
CI	Compression Ignition
CMSE	MIT Center for Material Science and Engineering
CO	Carbon Monoxide
CO_2	Carbon Dioxide
DPF	Diesel Particulate Filter
ECM	Engine Control Module
EDX	Energy Dispersive X-ray Spectrometry
EGR	Ehxaust Gas Recirculation
EP	Extreme-pressure
EPA	Environmental Protection Agency
EU	European Union
HC	Hydrocarbons
JASO	Japanese Automotive Standards Organization
LNT	Lean Nox Trap
Mg	Magnesium
NAA	Neutron Activation Analysis
NI	National Instruments
NO	Nitrogen Oxide
NO_x	Oxides of Nitrogen
P	Phosphorous
Pe	Peclet Number
PM	Particulate Matter
PPB	Parts per Billion
PPM	Parts per Million
Re	Reynolds Number
RIR	Relative Intensity Ratio
RPS	Relative Pressure Drop Sensitivity
S	Sulfur
SA	Sulfated Ash
SCR	Selective Catalytic Reduction
SEM	Scanning Electron Microscope
SI	Spark Ignition
SiC	Silicon Carbide
SO_2	Sulfur Dioxide
SO_4	Sulfate

SOF	Soluble Organic Fraction
SOL	Insoluable Fraction
TDC	Top Dead Center
ULSD	Ultra Low Sulfur Diesel Fuel
XRD	X-Ray Diffreaction
ZDDP	Zinc Dialkyl-Dithio-Phosphate
Zn	Zinc
A	Area
A_f	DPF Frontal Area
D	Diffusion Coefficient
$d_{Aggregate}$	Aggregate Particle Diameter
D_H	Hydraulic Diameter
d_P	Pore Diameter
$\overline{D}_p^2$	Surface Average Sphere Diameter
$d_{Primary}$	Primary Particle Diameter
K	Permeability
L	DPF Length
P	Pressure
S	Channel Perimeter
U	Exhaust Gas Channel Velocity
U_w	Filtration Velocity
V	Exhaust Gas Velocity
v_w	Exhaust Gas Wall Velocity
W	Porous Media Thickness
$Z_{in\,/\,Out}$	Channel Inlet / Outlet Friction Coefficient
ΔP_{ash}	Ash Layer Pressure Drop
$\Delta P_{Channel}$	Channel Pressure Drop
ΔP_{In}	Pressure Drop Due to Inlet Contraction
ΔP_{Out}	Pressure Drop Due to Outlet Expansion
ΔP_{Total}	Total DPF Pressure Drop
ΔP_{Soot}	Soot Layer Pressure Drop
ΔP_{Wall}	Substrate Wall Pressure Drop
ε	Porosity
μ	Dynamic Viscosity
N	Kinematic Viscosity
ρ	Gas Density
ρPacking	Packing Density
ρTheoretical	Theoretical Density
τ	Shear Stress
ξ	Contraction / Expansion Loss Coefficient

1 INTRODUCTION

Since its introduction in the late nineteenth century, the diesel engine has been an extremely popular powering method. Diesel engines remain the method of choice for commercial land based vehicles and marine vessels, as well as personal and commercial passenger vehicles in volatile fuel markets such as Europe and Asia. By nature diesel engines have a variety of advantages over other engine types, such as higher fuel economy, reliability, durability, as well as low fuel and maintenance costs. Despite these advantages diesel engines have some drawbacks, one of which is a high amount of particulate matter (PM) emissions. The largest form of diesel engine PM is soot which has been found to be hazardous to human health and is currently regulated by strict government emission standards.

In order to trap engine out PM and conform to emission regulations, exhaust after-treatment systems must be implemented on diesel vehicles. Diesel particulate filters (DPF) mounted in the diesel's exhaust system trap over 99% of PM and have been proven to be an extremely effective way to meet government emission regulations. Because of this, nearly all diesel engines produced after 2007 in both the United States and Europe contain a DPF. There are some disadvantages that come with the use of a DPF such as engine backpressure resulting in a fuel efficiency reduction. This has encouraged the in-depth study of DPF technology and operation to optimize the essential need of these after-treatment systems.

1.1 Diesel Engine Fundamentals

The diesel engine was first patented by Rudolph Diesel in 1892 and successfully operated in 1897 in Germany. Since its initial design there have been minor improvements over time but the fundamental operating principles have remained untouched. The fundamental difference between spark ignition (SI) engines and Diesel's compression ignition (CI) cycle is the ignition's operating principle. To obtain in-cylinder combustion, the diesel cycle uses the injection of high pressure fuel into the combustion chamber that has been heated by the compression of intake air alone and not by some external method such as a spark plug used in SI engines. This method increases fuel efficiency of a CI engine substantially when compared to its SI counterpart.

In its most rudimentary form the diesel engine can be described as a reciprocating piston, internal combustion engine which relies on high pressure air compression paired with accurately timed fuel injection to produce in-cylinder combustion. During the intake stroke, air near atmospheric pressure is introduced into the combustion chamber. Compression ignition engines have typical compression ratios

in the 12-24 range which is substantially higher than those seen in SI engines which generally fall within 8-12. Because of this high compression ratio, CI engines reach in-cylinder pressures of about 4-5 MPa (40-50 bar) and temperatures around 800-1000 K (527-827 °C) during the compression stroke [1]. Just prior to the piston's top dead center (TDC) position liquid fuel is injected into the cylinder. This liquid fuel is either injected directly into the cylinder or into an adjacent pre-combustion chamber. The fuel is atomized into small droplets and entrained into the cylinder air creating a fuel-air mixture of combustible proportions. The high pressure and temperature of the compressed air are above the mixture's auto ignition point which causes spontaneous combustion. The rapid expansion of the burning mixture generates the power stroke and initiates the exhaust process for the cycle to start again.

Spark ignition engines cannot have compression ratios similar to those of CI engines because they are limited by engine knock. Because of the absence of fuel in the combustion chamber during the initial stages of the compression stroke, there is no way for a CI engine to auto ignite before the desired time causing the engine to knock. Another fundamental difference between SI and CI engines is their respective load restriction methods. Spark ignition engines generally control the load of the engine by restricting the intake air through the usage of a throttle plate. In CI engines the amount of fuel injected into the combustion chamber per cycle, not intake air amount, is the load limiting factor [1]. Although CI and SI engines have the same ultimate goal of generating power through the combustion of an air-fuel mixture, the operating manner is very different. Because of this CI engines have a multitude of advantages and disadvantages when compared to its counterpart.

1.1.1 Diesel Engine Advantages

Due to the combustion cycle previously mentioned, the diesel engine has a number of inherent advantages such as increased fuel economy, greenhouse gas and hydrocarbon (HC) reduction, durability, reliability and low fuel & maintenance costs. The advantage that is most appealing to the general public is that a diesel engine has better fuel economy than a comparable SI counterpart. Because CI engines are not limited by knock, they can run at higher compression ratios which improve fuel conversion efficiency relative to a SI engine. The overall lean fuel/air ratios and small pumping losses due to un-throttled engine operation also lead to increases the fuel conversion efficiency [1]. These characteristics translates to a 20-40% increase in fuel economy when compared to a SI engine of similar power output [2].

Because of the overall lean operation of the diesel engine there is very little, if any, unburned fuel left in crevice volumes of the combustion chamber during the compression stroke. This leads to extremely low

HC emissions for CI engines [3]. Carbon Monoxide (CO) emissions are directly related to the engine's fuel/air ratio. Since diesels always operate well on the lean side of a stoichiometric fuel/air ratio, there is sufficient oxygen to fully burn all of the fuel's carbon to CO_2 resulting in extremely low CO emission levels.

Diesel engines provide a very high amount of torque at low speeds compared to a SI equivalent. Because of this the heat released from a diesel engine occurs at slower engine speeds, at a faster rate and earlier in the combustion process. This slower engine speed also leads to low frictional losses during power generation. These factors paired with the fact that diesel engines have a compression ratio of nearly twice that of a SI engine lead to a much more robust engine design and construction resulting in a usable life up to four times that of a gasoline engine [4]. In general CI engines do not contain complicated ignition systems containing spark plugs and distributors which tend to be a source of breakdown and necessary repair. Taking into account these advantages, diesels are highly attractive for a wide variety of applications.

1.1.2 Diesel Engine Applications

Due to the advantages described in the previous sections diesel engines are attractive to a variety of applications including on-road commercial and passenger vehicles, agriculture, construction and mining equipment, railway and marine propulsion along with numerous military integrations. A study performed in 2007estimated that diesel fuel accounted for nearly 18% of all refined petroleum products with 75% of all diesel fuel produced being used for on-highway applications [5]. A study conducted in the year 2000 determined a variety of percentages that the diesel market controls within certain applications. The study showed that based off fraction of fuel energy consumed by vehicle type in the United States, diesel engines power nearly 85% of commercial trucks, 100% of marine and railway freight transport, 75% of inner-city rail transit, 62% of school buses and 100% of inner city buses. One should note that the percentage of bus applications may be outdated with the surge of natural gas / hybrid powered buses. The study also determined that 83% of construction equipment, 66% of agriculture equipment and 22% of mining equipment are diesel powered [6]. Although diesel powered vehicles only make up a very small percentage of the personal passenger market in the United States, this is not the case for both Europe and Asia in which the majority of personally owned passenger vehicles are diesel powered. As previously mentioned this is primarily due to that fuel price volatility in those specific economies.

1.1.3 Diesel Engine Emissions

The previous sections have outlined a number of advantages which make diesel engines attractive for a variety of applications but there are inherent disadvantages as well. Disadvantages stemming from the diesel's robust design include a high capital cost of acquisition, low power to weight ratio and increased amount of noise during operation. These disadvantages mostly affect the personally owned passenger vehicle market where weight, size and capital cost are of higher importance relative to the heavy duty market.

The most important technological challenge to date with diesel engines is the high nitrogen oxides (NO_x) emissions and NO_x/PM trade-off. In general it is extremely difficult to reduce both NO_x and PM emissions simultaneously where typically lowering one will increase the other and vice versa. That nature of diesel combustion is a limited mixing, high temperature, high pressure turbulent diffusion flame [1]. Nitrogen Oxide (NO) formation is strongly dependant on both temperature and oxygen concentration. Because diesel engines have both high compression ratios and run overall lean, the tendency to form NO is substantially increased. Particulate matter is formed during the combustion process and is primarily derived from unburned fuel and lubrication oil additives. In order to increase PM oxidation the cylinder temperature would need to be increased, which generally leads to an increase in NO_x emissions.

There are a number of emission reduction methods which are commonly employed to diesel engines. By retarding the fuel injection timing, a lower cylinder temperature can be achieved which would reduce the NO_x emissions but increase PM emissions and acquire a fuel efficiency penalty of up to 10% [1]. Reducing the in-cylinder temperature also lowers the exhaust gas temperature which creates much difficulty in the oxidation of collected soot within a DPF. To oxidize collected soot, a temperature above 600°C is needed if the filter does not contain a catalyst. Exhaust gas recycling (EGR) is a method that is typically used to reduce NO_X emissions by diluting the fresh intake air with a fraction of exhaust gas reducing the available amount of oxygen to form NO_X. Although this method is effective, the introduction of exhaust gas into the cylinder prior to combustion lowers the fuel conversion efficiency of the cycle reducing the overall efficiency of the engine.

Overall the balance of diesel engine emissions and efficiency penalties is a difficult decision for manufactures to make. Because the aforementioned emissions are hazardous to either the environment or human health, or both, governing bodies generally regulate their allowable amount.

1.2 Diesel Emission Regulations

Diesel fuel is a mixture of hydrocarbons which theoretically have combustion products limited to CO_2 and water vapor (H_2O). In actual applications there are many more products. The post combustion diesel pollutants generated are attributed to a variety of non-ideal processes during combustion such as unburned fuel, combustion of lubrication and fuel additives, and high temperature & pressure mixture reactions. Not all diesel emission pollutants, or suspected pollutants, are regulated by governing bodies either due to their yet-to-be-proven adverse health effects or their abundant production in nature. The pollutants that are regulated include; PM, NO_X, HC and CO.

Many components of the diesel engine's exhaust have been studied to determine their respective adverse health effects. It has been determined that exposure to diesel exhaust has acute (short-term exposure) effects including irritation and neurophysiological symptoms, as well as chronic long-term effects which can be either noncancerous or carcinogenic [7]. Much research has been directed towards the adverse effects of diesel PM. Because the PM emitted from a diesel engine is of an extremely small size (~ 0.1 μm [1]), if inhaled the particles penetrate deep within the lung tissue leading to an increased possibility of a number of health related issues such as chronic coughing, respiratory irritation & infection, aggravation of asthma symptoms and in extreme cases lung cancer [8]. These symptoms are more prevalent in small children whose undeveloped respiratory systems cannot yet fight off infections as well as members of the elderly community with emphysema, asthma and heart/lung disease.

In any given area the total air pollution is a summation of the emissions released from a number of sources ranging from internal combustion engines, power generation facilities, coal/wood stoves and municipal waste incinerators. In order to efficiently regulate specific pollutants one must know their weighted contribution from each source. For some pollutants such as methane (CH_4) and nitrous oxide (N_2O), the natural release far exceeds that contributed by SI and CI engines and therefore are not regulated engine emission products. This is not the case for CO, PM, HC and NO_X emissions in which mobile on- and off-road applications contribute greatly to the total ambient amount and are therefore regulated engine emissions. A study conducted by the Environmental Protection Agency (EPA) in 1998 determined that in industrialized countries, mobile sources contribute to as much as 50% of the NO_X inventory, 70% of the CO inventory and very sizable portions of the HC and PM inventories. Within the mobile source category, SI engines are responsible for most of the HC and CO emissions and CI and SI engines split the NO_X category at approximately 50% each. On the other hand diesel engines are the largest contributor to PM emissions within the mobile source category. Approximately 75% of $PM_{2.5}$,

particulate matter smaller than 2.5μm, can be attributed to CI engines [7,9]. With this being said, particulate matter pollution is much more prevalent in Europe due to the substantially larger amount of diesel engines in operation compared to the United States [10].

The EPA targeted diesel NO_x and PM emissions for major reduction within the last decade. Between 2002 and 2010 both Europe and the United States targeted reductions for both pollutants by a factor of 10. In 2006 the EPA also limited the sulfur contents of highway diesel fuel to no more than 15ppm [11]. The use of this ultra-low sulfur diesel fuel (ULSD) both reduces particle emissions as well as enabling the use of advanced after treatment systems which are deactivated by high fuel sulfur levels. We also see the surge of non-road diesel engines moving to ULSD in 2010, as well as railroad locomotive and marine diesels in 2012 [12].

The U.S. and the E.U. have implemented very stringent emission regulations in order to limit the amount of PM and NO_x emitted into the atmosphere. Between the years 2002-2007 a 90% PM emissions reduction was required for U.S. heavy duty diesels, a standard change from 0.10 g/hp-hr (grams per brake horsepower per hour) to 0.01 g/hp-hr. For U.S. heavy duty diesel NO_x emission, a 52% reduction was required from 2002-2007 from 2.5 g/hp-hr to 1.2 g/hp-hr subsequently followed by a 83% reduction between 2007-2010 from 1.2 g/hp-hr to 0.2 g/hp-hr. The European Union (EU) follows similar trends although they are slightly less stringent compared to the United States. Figure 1.1 graphically displays the historical U.S. heavy duty emission regulations.

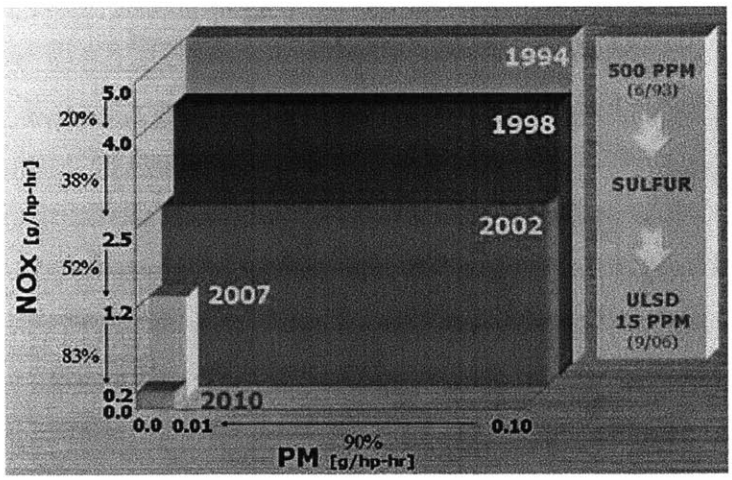

Figure 1.1: U.S. heavy duty NO_x and PM emission reduction

Along with the human health effects previously described, diesel emission PM has negative environmental effects. Depending on the temperature of formation, diesel PM is between 70%-90%

elemental carbon [1]. This elemental carbon has been determine to be the second leading cause of global warming, CO_2 being the first. It was determined that soot has a contribution factor of about 55% of that pertaining to CO_2 [13]. Elemental carbon has an extremely absorbent surface with an area of approximately 200 m^2/g. As these particles enter the atmosphere, they absorb a substantial amount if ultraviolent light and solar radiation reflected from the earth's surface. In turn these soot particles increase the top-of-the atmosphere radiative forcing, surface heating and surface dimming all of which are of great environmental concern [13]. By implementing diesel engine emission reduction measures, negative human health and environmental effects are immediately reduced.

1.3 Diesel Emission Reduction Methods

As previously described there are in-cylinder methods of reducing undesirable diesel emissions but this typically results in a permanent engine configuration during manufacture as well as a fuel efficiency penalty. Another method of reducing diesel emissions is through the implementation of an exhaust aftertreatment (AT) system. This process is a function of extra components with a specific purpose being added to the diesel engine exhaust system reducing the atmospheric emission of undesirable gases and PM. As mentioned previously HC and CO emission are relatively low for diesel engines and will not be discussed, therefore the primary focus of after-treatment systems is the mitigation of NO_X and PM emissions.

As previously mentioned the overall lean combustion within a diesel engine results in a relatively high amount of NO_X emission. Selective catalytic reduction (SCR) is one aftertreatment method to reduce NO_X emissions. A SCR is composed of a catalyzed multi-bed module that reduces NO_X to a combination of diatomic nitrogen (N_2) and water with the aid of a gaseous reducing agent (typically ammonia). Although this is an effective method, the system is dependent on the reductant and if the tank of reductant runs dry the system is useless. Another commonly used system is a lean NO_X trap. A NO_X trap employs the use of a microporous mineral, known as a zeolite, as a molecular absorbent of NO and NO_2 prior to atmospheric emission. There is a limit to which a zeolite can absorb NO_x in which it must be purged by some method such as diesel fuel or hydrogen injection. Lean NO_X traps are still a relatively new technology but have been implemented in various vehicle concepts [14].

The most effective method to reduce PM emissions has been the addition of a DPF to the diesel's exhaust system. Diesel particulate filters physically trap PM as the exhaust gases flow through the filter's porous substrate. Many filter materials and configurations have been tested and studied some with trapping efficiencies of 99% or higher. As the PM mass within the filter increases, the flow resistance

and backpressure due to the filter also increases. This results in a fuel efficiency reduction which is highly undesirable by both diesel manufactures and owners. By increasing the temperature of the DPF, the trapped soot can be oxidized resulting in the emission of SO_2 which is not a regulated product. This soot oxidation process is referred to as filter regeneration and will be discuss in subsequent sections. Even though the majority of trapped soot can be oxidized, incombustible sulfated ash is left behind which accumulates over time increasing the pressure drop across the DPF. Particulate filters have become common practice since 2007 to help meet the stringent PM regulation of 0.01 g/hp-hr.

In order to meet the stringent emission standards set forth of 0.01 g/hp-hr for PM and 0.2 g/hp-hr for NO_x the use of after-treatment systems are essential. Although these systems are effective, the optimization of these systems is necessary to mitigate the noticeable drawbacks while utilizing the systems to their potential. The optimization and further fundamental understanding of DPF technology is the motivation for this research.

(This page intentionally left blank)

2 DIESEL PARTICULATE FILTERS

In order to meet the stringent PM emission regulations the implementation of diesel aftertreatment systems such as DPFs has become very attractive. The first DPFs were used on non-road vehicles in 1980 but in 2000 PSA Peugeot Ciroën made them standard fit on passenger cars in preparation for Euro V emission standards [15]. These DPFs collect PM as the diesel exhaust gases flow through the porous media of the filter preventing emission of these harmful products to the atmosphere. Diesel particulate filters have been found to be an effective retro fit solution as well as standard manufacturing practice on all 2007 and newer diesel vehicles in the United States.

2.1 Fundamental DPF Operation

Since their conception, a number of materials and geometries have been researched regarding DPF construction and shape. The ceramic, cellular, wall-flow monolith filter has been the most popular and has seen the most usage due to its relatively low cost and high trapping efficiencies. These filters are constructed from a porous ceramic with a number of channels running longitudinally along the DPF. Each channel contains a small ceramic plug at either its inlet or outlet side designating it an inlet or outlet channel. These inlet and outlet channels are adjacently placed next to one another radialy along the filter creating the wall flow structure. As engine-out, PM saturated exhaust reaches the filter face, it enters the inlet channels. Since each inlet channel is plugged on its outlet end, the exhaust gas is forced through the porous channel walls before it exits the filter. As the exhaust gas passes through the channel walls, the ceramic filter matrix collects extremely high percentages of the PM within the exhaust. Figure 2.1 displays an actual image of a creaming wall flow DPF as well as an artist's rendition of the wall flow filtration process.

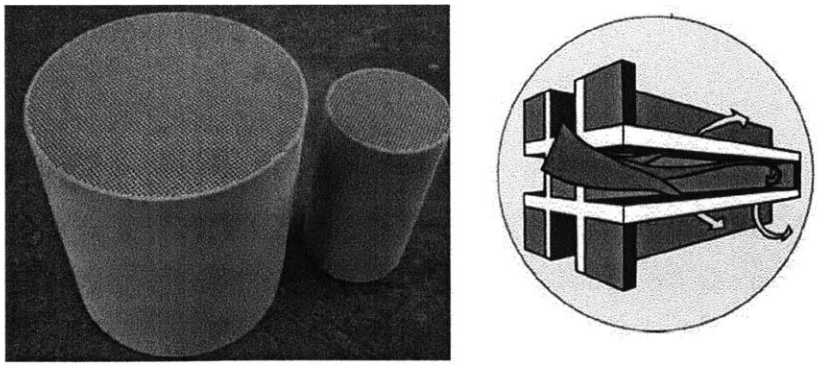

Figure 2.1: Actual ceramic DPF image and artist's rendition of wall Flow filtration. Image from HPM

There are a number of inherent advantages of to the wall flow filtration process which benefit the DPF overtime. After a period of filtration, the trapped PM acts as further filter medium increasing the DPF's filtration efficiency [16]. A negative consequence of PM accumulation within the filter is an increased flow restriction through the porous media with translates to a higher exhaust backpressure, thus decreased engine fuel economy [17]. The particulate matter within the filter is composed of both soot and inorganic sulfated ash at an approximate ratio of 99:1 [18]. The combustible portion of the PM can be oxidized at elevated temperatures of 150°C -650°C depending on both the volatility of the combustible PM fraction and whether or not the filter is catalyzed. This soot oxidation method is common referred to as a regeneration period and is either continuous or periodic.

Upon the completion of a regeneration period, the combustible soot is oxidized to CO_2 and the incombustible PM fraction (ash) remains within the filter. Overtime the amount of ash within the filter accumulates and cannot be oxidized resulting in periodic cleaning or total replacement of the DPF prior to extensive engine backpressure build-up or failure. Figure 2.2 displays longitudinal and cross section channel views of the ash build up overtime for a ceramic wall flow DPF.

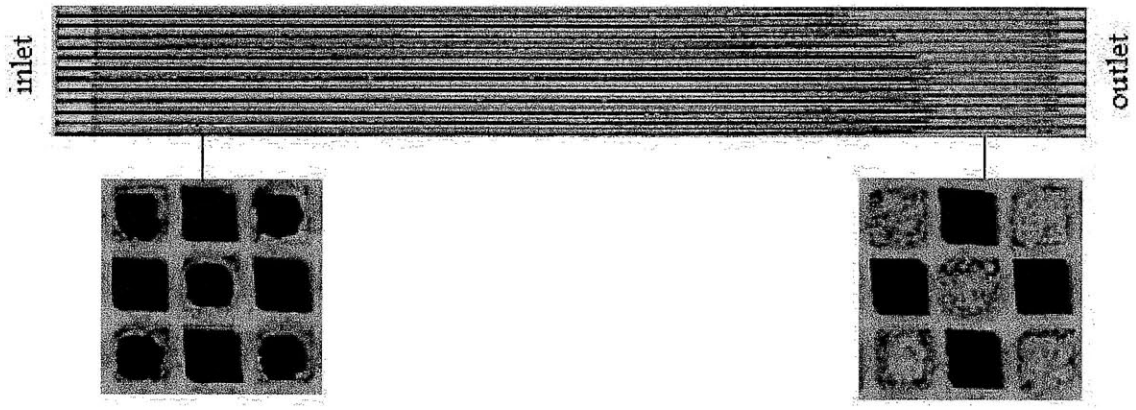

Figure 2.2: Extended ash build-up and distribution [19]

The extended ash build-up and distribution within a DPF has been studied and the fundamental deposition method is well understood. The intricacies of the deposition method will be discussed in subsequent sections but one should note that in addition to loading within the pores of the DPF substrate material, ash deposits as a thin layer on the channel walls along the length of the filter as well as an ash plug located on the outlet end of the filter channels. Through ash accumulation the ash layer along the channel walls grows in thickness which reduces the hydraulic diameter and open frontal area of the channels. As the ash plug on the outlet end of the filter channels grows in length over time, the

filter's effective length is reduced. Both of these ash distribution characteristics affect the fluid dynamics of the exhaust gases directly affecting the pressure drop across the filter [18]. The DPF's filtration efficiency, ash characteristics & distribution as well as the trapping efficiency are competing factors which needs to be understood in depth to further the comprehension of the lifecycle of these after-treatment systems. The aforementioned is the primary focus of this project.

2.2 Ash Sources: Lubrication Additives

As previously stated the ash deposits within the PM emitted from the diesel engine pose a significant problem regarding the DPF lifecycle. Although ash only makes up a small fraction of the emitted PM, it is unable to be removed from the DPF during normal engine operational procedures such as filter regeneration resulting in the need to remove & clean or replace the DPF which is both costly and time consuming. The ash that is accumulated in the DPF overtime originates from a variety of sources including trace metals found in diesel fuels, engine wear and corrosion, and primarily additives placed in the engine's lubrication oil. Although the relative contribution of these sources is dependent on a variety of factors such as lubrication formulation, engine technology and fuel type, the lubrication additive package is the largest contributor to PM ash content when a fuel born catalyst is not used [20-22]. Although combustion of diesel lubricant isn't desired, it is inevitable during typical engine operation due to small amount of oil that enters the combustion chamber by both passing by the piston rings as well as lining the cylinder wall. After the combustion of this small amount of lubrication oil takes place, the organic portions are oxidized while the incombustible residues (ash) remain.

A typical diesel lubricant will consist of 75-83% organic base oil, 5-8% viscosity modifier, and 12-18% inorganic additive package which is the primary source of PM ash [23]. Over the last several years much effort has been directed towards the mitigation and understanding of the negative effects that lubricant derived ash has on diesel aftertreatment systems. The American Petroleum Institute (API), European Automotive Manufacturers Association (ACEA) and the Japanese Automotive Standards Organization (JASO) have all recently introduced "low ash" heavy duty diesel oil which limits the amount of metallic ash, phosphorus and sulfur- based additives placed within the lubricant thus reducing the inorganic ash generated during lube oil combustion. Table 2.1 describes the additive limitations described by these "low ash" specifications. One should note that the standard to measure the sulfated ash content of fresh lubrication oil is ASTM D874 in which the oil is treated with sulfuric acid and burned until only the resultant ash remains. The ASTM test method notes that results for oils containing magnesium as well as molybdenum additives should be interpreted with caution [24].

		Content Limitations		
Specification	Year of Introduction	Sulfated Ash	Sulfur	Phosphorus
API CJ-4	2006	1.00%	0.40%	0.12%
ACEA E6	2004	1.00%	0.30%	0.08%
JASO DH-2	2005	1.00%	0.50%	0.12%

Table 2.1: International "Low Ash" Engine Oil Specifications [25-28]

Although lubrication additives are the primary culprit regarding sulfated ash generation they cannot simply be removed from the lubricant. Each additive serves an essential purpose in the successful and sustainable operation of the lubrication oil and would lead to engine failure if simply removed without a suitable replacement. The subsequent sections will describe the common lubrication components and additives in more detail regarding their purpose, generation and effects on lubrication sulfated ash.

2.2.1 Base Oil

The primary purpose of the base oil is to lubricate and act as an additive carrier. The base oil has inherent lubrication qualities including viscosity, viscosity index, pour point, and oxidation resistance [29]. The function of the lubrication additives is to enhance the already existing properties of the base oil, or to add a new property. Base oil is composed of a single or blend of base stocks which are categorized by concentrations of saturates and sulfur as well as their viscosity index [30]. The base oil composition not only determines the necessary additives required to meet the lubricant's performance expectations, but also impacts the sulfur content of the final formulation which is limited by most governing bodies. Experimental tests have been conducted to determine the extent of ash formation by base oil and its impact on DPF pressure drop. It was determined that base oil alone produces no noticeable ash anti-oxidants within a DPF resulting in a negligible increase in pressure drop [31].

2.2.2 Detergents

The primary function of a detergent additive is to act as an corrosion inhibitor. Detergents are metal salts of organic acid that generally contain some amount of excess base which is commonly in carbonate form [29]. Because of their basic nature, detergents have to ability to neutralize the acidic byproducts of both fuel combustion and the oxidation/thermal degradation of thermally liable lubricant additives. Once these acidic byproducts are neutralized, forming salts, the organic portion of the detergent commonly referred to as "soap" suspends these oxidation products within the lubricant film. The suspension of these neutral particles helps to control engine rust, corrosion and resinous buildup. The particle suspension ability of the detergent additive alone is very minor and typically inadequate for the

final lube oil formulation. Because of this, dispersant additives are generally found within lubricants as well as detergents and will be discussed in a subsequent section.

Detergents are synthesized when specific acids are combined with inorganic metallic bases. There are numerous forms of acids used in detergent generation such as arylsulfonic acid, alkylbenzenesulphonic acid and alkynaphthalenesulphonic acid to name three of many [32-35]. The reaction of these acids with inorganic bases such as metal oxides and metal carbonates results in salt formation [36]. The pH of the resultaning detergent is directly related to the amount of inorganic metal used to neutralize to acid functionality. In order to produce a basic detergent, it is necessary to add a higher than stoichiometric amount of metal during the formulation process.

Although there are a number of metals that can be used to make soaps, only a small amount produce oil-soluble detergents. Common metals that used for this purpose are calcium, magnesium, strontium and barium listed in order of preference [29]. Calcium and magnesium are most extensively used metals as detergent additives with a preference towards calcium due to its lower cost. Basic calcium sulfonates and calcium phenates make up approximately 65% and 31% of the total detergent market respectively [29].

The amount of sulfated ash generated by the detergent additive is directly related to the metal to acid ratio used in the formulation process. Higher than stoichiometric amounts of metal used in the formulation process results in a basic detergent which is desirable from an acid neutralization standpoint. Unfortunately this high metal content results in elevated sulfated ash production which is undesirable when considering DPF implementation. Detergents are the largest contributor to sulfated ash for a full formulated diesel lubricant.

2.2.3 Dispersants

The primary purpose of a dispersant is to suspend ordinarily insoluble contaminants within the bulk of the lubricant keeping engine surfaces clean. These contaminants are mainly composed of fuel and lubricant oxidation and degradation products, such as soot, resin, varnish, lacquer, and carbon [37]. The lack of a proper dispersant contained in a lubricate will lead to abrasive wear within the engine in a short period of operation.

Dispersants consist of a large non-polar group as well as a smaller polar group, typically nitrogen- or oxygen-based. These two groups suspend contaminants in different methods which can be graphically seen in figure 2.3.

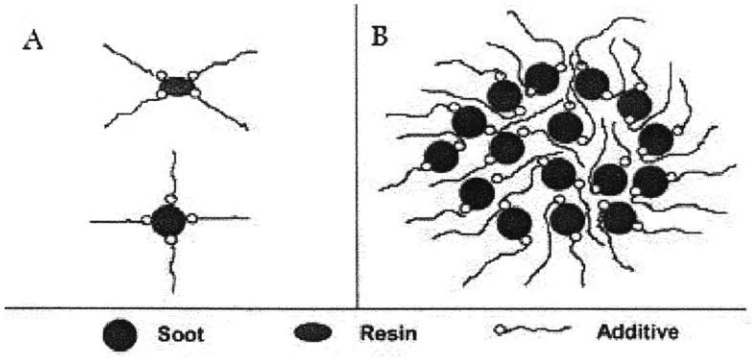

Figure 2.3: Dispersant operation by both the polar group [A] and non-polar group [B]. Figure from [38]

Figure 2.3 [A] graphically displays the operation of the polar dispersant group physically attaching themselves to polar oxidation products. Figure 2.3 [B] provides visual interpretation of how the non-polar group suspends oxidation products within the bulk of the lubricant.

Although detergents do contain some dispersive ability, it is generally not enough to produce a highly effective lubricant thus the need for additional dispersants. Detergents and dispersants are different in 3 significant ways [37]:

1. Dispersants are generally neutral in nature thus containing little to no acid-neutralization capability. Detergents are basic in nature with acid-neutralization being their primary purpose.
2. Dispersants have a much higher molecular weight than the soap portion of detergents, approximately 4-15 times. This high molecular weight is the primary factor contributing to the higher suspending and cleaning capabilities of a dispersant compared to the soap of a detergent.
3. Detergents contain metals such as magnesium and calcium where-as dispersants are metal free. Because of this, dispersants do not contribute to ash formation which affects exhaust after-treatment systems such as DPFs.

Dispersants and detergents together make up the majority of manufactured lubricant additives, about 45-50% [29].These additives work together to perform essential properties of the lubricant as a whole. The detergent neutralizes the acidic fuel and lubricant oxidation products limiting the extent of corrosive wear on then engine. Once these contaminants are neutralized, the dispersant suspends them within the bulk of the lubricant reducing the extent of abrasive wear on the engine. Once all of the detergent function is utilized, the lubricant as a whole becomes neutral in nature, it is up to the dispersant alone to suspend acidic contaminants prior to engine degradation.

2.2.4 Zinc Dithiophosphates

Zinc dialkyldithiophosphates (ZDDP) have been used in engine oils, transmission and hydraulic fluids, gear oils, greases and other lubrication applications for over 65 years. The high popularity of ZDDP is due to its ability to act as a very low cost multipurpose agent functioning as; an excellent anti-wear agent, a mild extreme-pressure (EP) agent, and an effective oxidation and corrosion inhibitor. The synthesis of ZDDP occurs by neutralizing an elemental sulfur and phosphorus based acid with zinc oxide. During this reaction, enough zinc oxide is used to neutralize the acid to a pH range that results in a product that is suitably stable to thermal degradation [39]. Similar to the process previously described for detergents, the amount of zinc oxide used to neutralize the sulfur and phosphorus based acid determines the pH of the final ZDDP product . If a basic ZDDP is synthesized, the additive will contain both neutral and basic zinc salts. Although this is desirable from an acid neutralization point of view, it has been reported that basic zinc salts are sensitive to increased temperatures and tend to thermally decompose [40].

As previously mentioned, ZDDP will thermally decompose during normal engine operating temperatures giving off volatile compounds such olefin, alkyl disulfide and alkyl mercaptan [39]. These volatile compounds contribute to the necessity of both detergents and dispersants which were previously mentioned. The thermal degradation of ZDDP is not necessarily undesirable. During typically engine operation, surface asperities present on the metal parts penetrate the lubrication film increasing metal-to-metal contact. The ZDDP reacts with these surface asperities to reduce this contact. Similarly, if the oil film collapses due to a high enough engine load, the ZDDP reacts with the entire metal surface reducing wear and preventing surface welding [39]. In turn it is the products of the ZDDP thermal oxidation that are the active anti-wear agents.

The primary components of ZDDP are sulfur, phosphorus and zinc. As seen in table 2.1, recent lube oil specifications limit the amount of allowable phosphorus. Because of this, the ZDDP treatment level in a typical engine oil is limited to about 0.5-1.5%. ZDDP does contribute to the sulfated ash content of a lubricant due to the amount of incombustible metals present. Because a typical lubricant has a relatively small amount of ZDDP treatment, it is not as strong an ash contributor compared to detergents but should still be investigated regarding its effects on DPFs.

2.3 Ash Effects on DPF Performance

In recent years much effort has been directed to identify how lubricant additives and their resulting ash negatively affect the performance of diesel aftertreatment systems. Many common results have been found and are generally agreed upon but the intricacies as to why they are observed are still unclear.

Because of this further investigation is necessary to fundamentally understand why specific phenomena reoccur in experimental and field DPF testing.

As mentioned previously, the ash accumulated within the DPF is derived mostly from the additives package placed in the lubricant. Because of this, it has been seen that the ash content within a DPF increases with both the lubricant's sulfated ash level and the rate of oil consumption. Taking into account the composition of the lubricant, the ash is mostly composed of Zn, Mg and Ca sulfates, phosphates and oxides [22,41-45]. Although the sulfated ash level effects the amount of ash produced, it cannot be used to accurately predict the amount of ash produced. This is primarily due to the differences in lubricant additive and formulation volatility which in turn effects the consumption rate [43,45,46]. The lubricant additive package greatly effects the ash composition, morphology and distribution within a DPF. This in turn effects the extent of the filter's pressure differential as the ash load increases [47].

Research has shown that ash accumulation effects DPF performance but a fundamental understanding as to why, although well understood, is still not complete. Because ash is primarily derived from lubricant additives, one must study individual and synergistic effects of these additives to determine their respective effects on DPF performance.

2.3.1 DPF Pressure Drop

As any filter is introduced into an exhaust system, an exhaust backpressure is observed due to the newly introduced flow restriction. This is the case for a DPF. As the DPF accumulates ash over time, the filtration area is reduced increasing the flow restriction. As the flow restriction is increased, the differential pressure between the inlet and the outlet of the filter increases. This differential pressure is commonly referred to as pressure drop and is one of the main focal areas of DPF research. A great deal of experimental tests have been performed to determine the effects of ash load on DPF pressure drop, a portion of these tests are graphically displayed in figure 2.4.

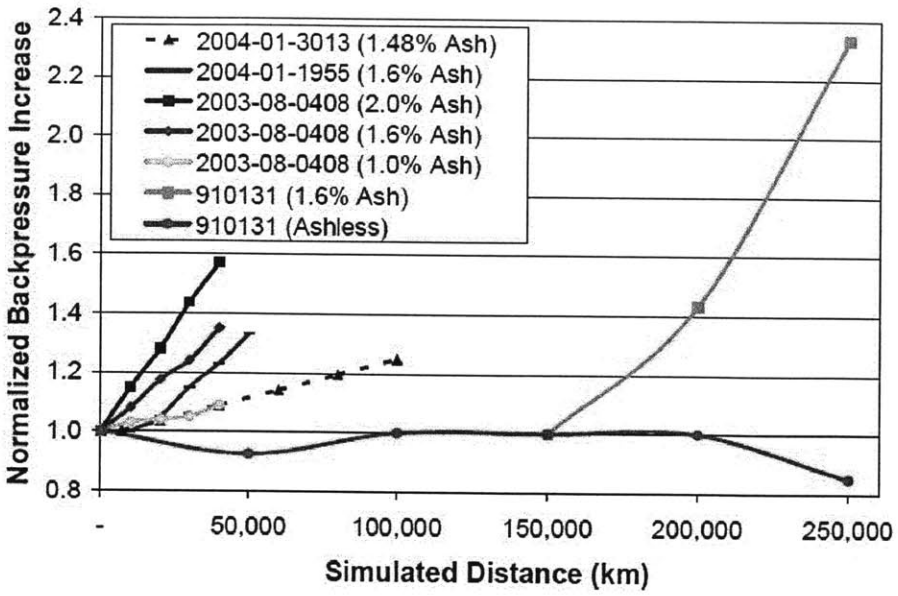

Figure 2.4: Exhaust backpressure as a function of simulated driving distance (Ash Load) [20]

Figure 2.4 displays a number of tests which confirm that as ash load increase, so does the exhaust back pressure. It is interesting to note that the sulfated ash level does not directly affect the DPF ash accumulation over a certain simulated driving distance. This confirms the aforementioned observation that lubricant chemistry and additive volatility are important factors that lead to the mass of ash accumulation. To compound this observation further, authors noted that the mass of accumulated ash did not correspond to the exhaust backpressure confirming the fact that ash composition and morphology are important characteristics for research. This phenomenon was observed when Bardasz et al. tested 10 lubricant formulations of 1.8% sulfated ash all with different lubricant additive chemistries [42]. It is important to note that more complications arise during the synergistic effects of both soot and ash loaded DPFs. This topic will be discussed in further sections.

2.3.2 Lubricant Chemistry Effects

Many studies, including some of those previously mentioned, have been directed towards determining how lubricant chemistry affects both ash properties and DPF pressure drop. Although the lubricant additives are vital to the oil's functionality, the presence and concentration of each additive will greatly affect the material properties and morphology of the oil's resulting ash. As these ash properties change, so does the extent and mechanisms by which the ash affects DPF pressure drop.

A study was conducted in 2003 by Takeuchi et al. to determine how lubricant chemistry impacts deposit formations. Eight lubrication oil formulations were tested with varying amounts of Ca-based detergent,

borated dispersant and ZDDP. Table 2.2 displays the lube oil test matrix used with corresponding sulfated ash levels.

Candidate Oil	1	2	3	4	5	6	7	8
Borated Dispersant	L	L	L	L	H	H	H	H
ZDDP Anti-Wear	L	L	H	H	L	L	H	H
Ca-Detergent	L	H	L	H	L	H	L	H
Sulfated Ash %	0.428	0.765	0.567	0.86	0.454	0.799	0.641	0.921

Table 2.2: Lube Oil Test Matrix for 2003 Chevron Study [48]

The "L" and "H" classifications refer to amount (low or high) of each variable that was formulated in the lubrication oil. The various sulfated ash levels of the lubricants confirm the previously mentioned statement that the amount or presence of lubrications additives affects sulfated ash content. The tests concluded that there was no noticeable effect on DPF pressure drop due to the boron based dispersant, nor was any boron found within the accumulated ash. It was also concluded that although the Ca-based detergent contributed most towards the amount of ash produced, the ZDDP additive had the greatest impact on DPF pressure drop [48]. These results can be seen graphically in figure 2.5.

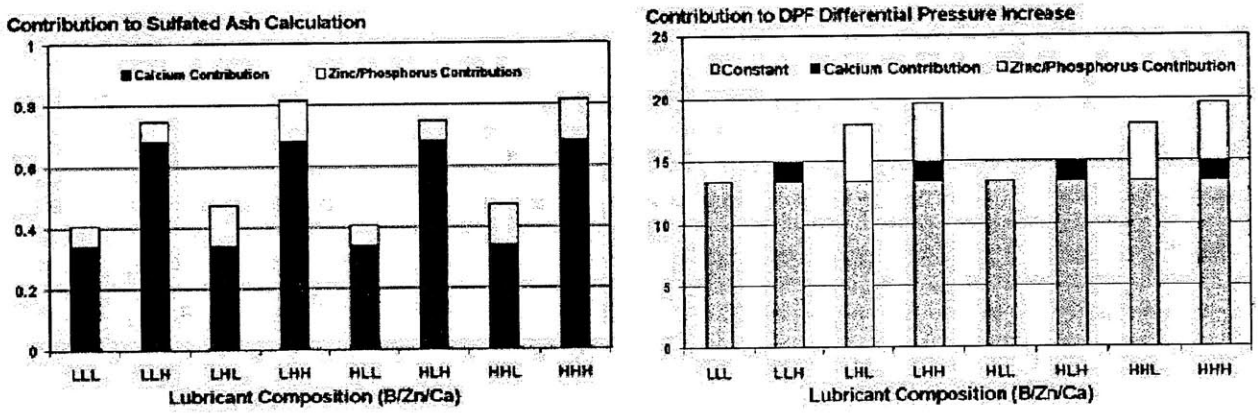

Figure 2.5: Lubrication additive contribution to ash and DPF pressure drop [48]

A similar study was conducted in 2005 by Bardasz et al. which tested 10 lubrication formulations each at 1.8% sulfated ash content. The altered variables for the 10 different formulations were Ca-vs.Mg-based detergent, type of ZDDP used, high or low phosphorus level and the presence or absence of boron. One of the conclusions of this study was the confirmation that the amount of oil consumption is directly related to the amount of accumulated ash in a DPF. Another finding was that the mass of accumulated ash did not necessarily relate to DPF pressure drop in any discernable way [49]. These results can be seen graphically in figure 2.6.

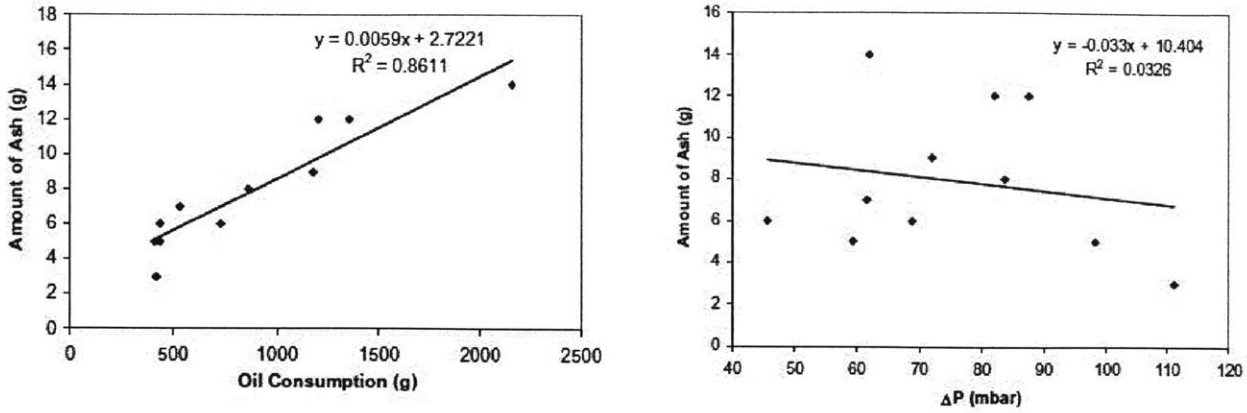

Figure 2.6: Ash mass relation to oil consumption and DPF pressure drop [42]

The authors also concluded that lubrication phosphorus level does not directly relate to DPF pressure drop. It was hypothesized that a complex interaction may exist between the phosphorus and filter's platinum catalyst creating a synergistic effect on the ash composition affecting DPF pressure drop.

A more recent study was conducted by Sappok et al. in 2010. A portion of this study was devoted to the effect that ash derived from individual additives has on DPF pressure drop. During this study, 3 lube oils at 1% sulfated ash were tested; a fully formulated CJ-4 oil, a formulation containing just a Ca-based detergent, and a formulation containing just ZDDP. It was concluded that for a given mass of ash accumulation, the Ca-detergent derived ash produced the highest pressure drop, followed by the CJ-4 and lastly the ZDDP additive [47]. These results can be seen graphically in figure 2.7.

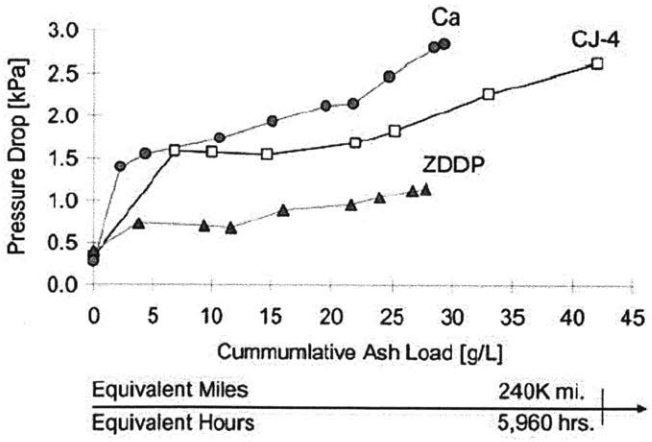

Figure 2.7: DPF pressure drop as a function of ash load for ash derived by individual additives [47]

This study determined that ash derived solely from the ZDDP additive produces a pressure drop on the order of half that of the Ca-based ash. Ash morphology and composition were also studied to determine the pressure drop effects of a number of variables such as ash packing density, porosity, permeability

and elemental composition. These variable effects will be discussed further in subsequent sections. This confirms that individual additive effects impact DPF performance greatly and should be investigated further.

2.3.3 Ash Distribution Effects

The previous section described how lubrication chemistry affects ash composition and morphology which in turn affects DPF pressure drop. Another factor to consider is the bulk ash distribution throughout the filter as well as individual channels. The ash deposition process will be discussed in detail in a subsequent section, but as available channel volume is decreased due to ash accumulation, pressure drop is affected. Research has shown that regeneration strategy as well as lubricant chemistry affects both the ash layer thickness along the channel walls as well as the ash end plug which begins to form at higher ash loads [47, 49]. These distribution effects directly relate to the exhaust flow characteristics and play a major role in the observed DPF pressure drop.

2.4 Project Objectives

Although many studies have been performed to help understand how lubricant ash affects DPF performance, the fundamental understanding to which underlying mechanisms contribute to this performance degradation is limited. This investigation attempts to expand on the research conducted by Sappok et al. in 2010. The primary objective of this project is to further the knowledge on how accumulated ash composition and morphology affect DPF pressure drop and catalyst degradation. By performing tests using variants on lubricant chemistries, ash derived from individual additives and combinations thereof can be related to pressure drop. To further this research, correlations of DPF performance can be related to ash morphology and composition variables such as; ash distribution, packing density, theoretical density, elemental composition, porosity, permeability, and particle size.

By understanding the individual and synergistic affects that lubrication additives have on DPF performance, the optimization of advanced diesel aftertreatment systems can be reached. This fundamental understanding also hopes to influence both the optimization of diesel lubricant formulation as well as future lubricant specifications/limitations.

(This page intentionally left blank)

3 FUNDAMENTAL UNDERSTANDING

As previously mentioned, the introduction of a DPF as an aftertreatment system produces an inevitable backpressure on the engine's exhaust. The extent of this backpressure is dependent on a variety of factors such as filter geometry & properties, exhaust gas characteristics, and accumulated soot and ash properties. Numerous studies have been performed to understand the fundamental impact these factors have on pressure drop. More recent studies have been specifically directed to understanding the time lapse sequence and effects that ash and soot accumulation have on DPFs. With this being said, the understanding of how lubricant chemistry affects ash properties and DPF performance is still in its preliminary stages. The further understanding of this issue is the motive for this research. To fully understand how ash properties and accumulation affect DPF pressure drop it is beneficial to first understand each parameter influencing pressure drop.

3.1 DPF Pressure Drop

Introducing a clean DPF into the exhaust stream of a diesel engine produces a substantial flow restriction, thus increasing engine backpressure. The influence of a clean DPF has been well studied and general principles can be related to an ash and/or soot loaded filter. The accumulation of ash and soot decrease the available filtration area by reducing the individual channel's hydraulic diameter and available channel length. Since accumulated soot and ash are porous, exhaust gas does still have ability to flow through the filter after substantial PM accumulation. The properties of the accumulated soot and ash directly affect the extent of flow resistance, thus the extent of DPF pressure drop. Figure 3.1 is a graphical interpretation of geometrical alterations as ash and soot accumulate in the filter's channels.

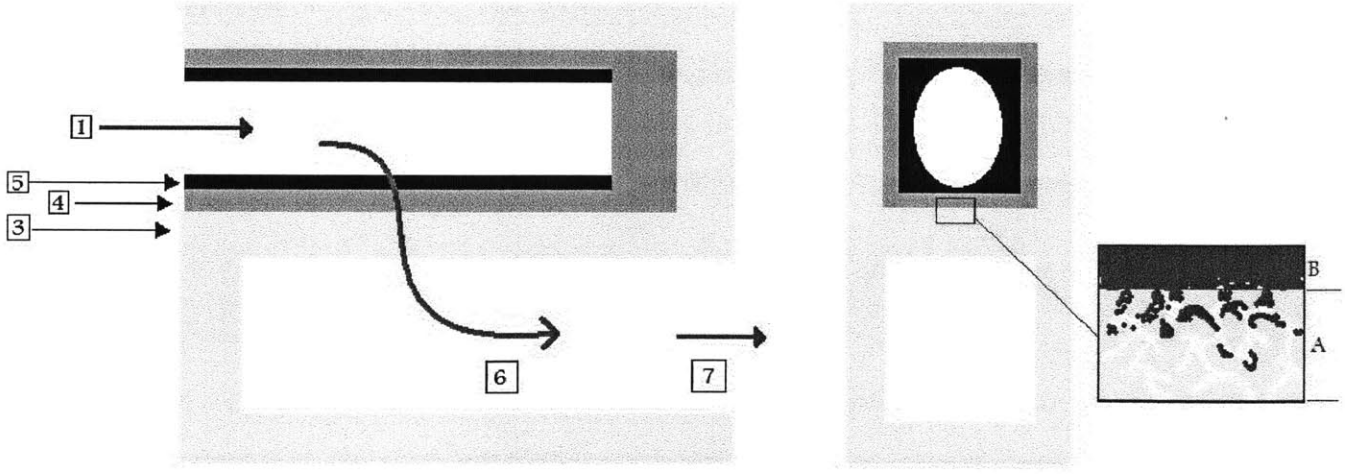

Figure 3.1: Soot and ash accumulation in DPF channel (Inset depicts accumulation in DPF pores)

When considering all of the variables that affect the total pressure drop across a DPF, the largest contributor is the flow through the channel's porous media. The porous media takes into consideration the channel wall along with the porous ash and soot layer if present. Sappok generated a table of pressure drop contribution variables and their relating factors. Table 3.1 displays this data with numerical correspondence to figure 3.1 [50].

Pressure Drop Contribution Variable		Key Parameters	Controlling Properties	Reynolds Number (Re)	Pressure Drop Contribution %
1	Inlet Losses (Contraction)	Open Frontal Area	Filter Geometry, Ash and Soot Layer Thickness	Transition	<3%
2	Frictional Losses Along Inlet Channel Walls	Channel Hydraulic Diameter	Filter Geometry, Ash and Soot Layer Thickness	< 2,100	5% - 30%
		Available Channel Length	Filter Geometry, Ash and Soot End-Plug Formation		
3	Frictional Losses from Flow Through Channel Wall	Channel Wall Permeability	Filer Properties, Extent of Ash and Soot Depth Filtration (A)	<<1	50% - 90%
		Channel Wall Thickness	Filter Geometry		
		Available Filtration Area	Filter Geometry		
4	Frictional Losses from Flow Through Ash Layer	Ash Permeability	Ash Porosity, Pore Size		
		Ash Thickness	Ash Packing Density		
		Available Filtration Area	Ash Layer Thickness, End-Plug Formation		
5	Frictional Losses from Flow Through Soot Layer	Soot Permeability	Soot Porosity, Pore Size		
		Soot Layer Thickness	Soot Packing Density		
		Available Filtration Area	Soot Layer Thickness		
6	Frictional Losses Along Outlet Channel Walls	Channel Hydraulic Diameter	Filter Geometry	<2,100	~ 5%
		Available Channel Length	Filter Geometry		
7	Outlet Losses (Expansion)	Open Frontal Area	Filter Geometry	Transition	<3%

Table 3.1: Key DPF Pressure Drop Contribution Factors. Adapted from [50-51]

As PM laden exhaust gases enter the DPF, they need to contract to fit within the filter's channels. The Inlet loss contributes to a minor portion of the DPFs total pressure drop. As the exhaust gases are forced to flow through the porous filter media, the PM is extracted from the exhaust gas. The largest pressure drop contribution is due to the exhaust gases flowing through the bulk porous media (substrate + ash layer + soot layer). This variable changes as the ash and soot layer properties are altered. Initially the DPF has a relatively high amount of open pore volume. Because of this, the initial PM deposited in the DPF is accumulated within the pores of the substrate (depth filtration). Part "A" in the inlet of figure 3.1 graphically interprets this depth filtration. Depth filtration causes a very steep rise in pressure drop over a small amount of mass accumulation. This high initial rise in pressure drop is due to the accumulated PM causing an alteration in substrate permeability and porosity. Once the substrate pores have been

saturated with PM, ash and soot begin to form a thin layer on top of the porous media (cake filtration). Cake filtration and the growth of the cake layer increases the filtration efficiency of the filter due to the addition of porous media thickness that the exhaust gases are forced to flow through. The growth of the cake layer increases the pressure drop of the filter rather linearly and in a less drastic manner than depth filtration. The cake layer of an ash accumulated channel is depicted in the inlet of figure 3.1 labeled "B". These filtration methods can be seen on a pressure drop versus time graph similar to figure 3.2.

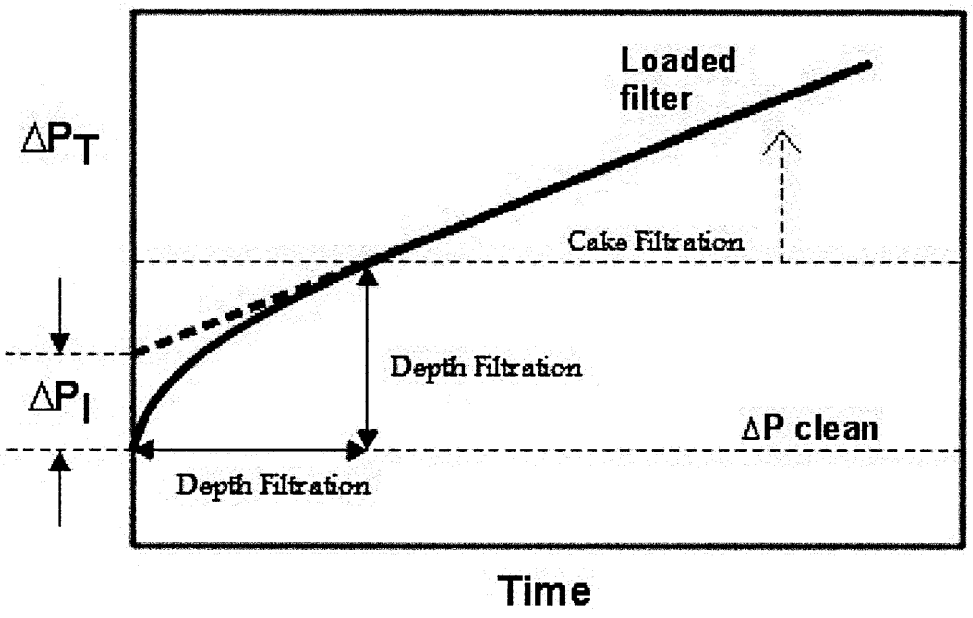

Figure 3.2: Pressure drop as a function of depth and cake filtration. Adapted from [52]

Figure 3.2 is consistent with most research that has been conducted on DPFs. The depth filtration of soot and ash display a steep non-linear increase in pressure drop over time. As the pores become occupied with PM and a cake layer builds, a fairly linear pressure drop increase over time is observed. This non linear increase due to depth filtration causes difficulty in pressure drop estimation modeling due to its dynamic nature. The total pressure drop of the DPF is a factor of numerous variables that are altered over time. The fundamental understanding of these factors is essential to a high level of insight into the lifecycle of a DPF.

3.1.1 Zero-Dimension DPF Pressure Drop Model

The key factors contributing to the total pressure drop across a DPF can be captured in a zero-dimension pressure drop model. This basic, widely used model will help highlight the underlying properties which affect the total pressure drop of a DPF and promote further research and advanced modeling

techniques. Mathematically the total pressure drop can be broken into six broad variables and is described as:

$$\Delta P_{Total} = \Delta P_{In} + \Delta P_{Out} + \Delta P_{Channel} + \Delta P_{Wall} + \Delta P_{Ash} + \Delta P_{Soot} \quad (3.1)$$

where $\Delta P_{In/Out}$ is associated with the respective contraction and expansion of the diesel exhaust gases as it enters and exits the DPF, $\Delta P_{Channel}$ is associated with the frictional losses along the channel walls, and $\Delta P_{Wall/Ash/Soot}$ contribute to the losses associated with the flow through the porous media layer composed of substrate, ash and soot.

The losses associated with the contraction and expansion of the exhaust gases can be described as:

$$\Delta P_{In/Out} = K_{In/Out} \frac{\rho V^2}{2} \quad (3.2)$$

where ρ is the exhaust gas density, V is the exhaust gas velocity and $K_{In/Out}$ describes the frictional coefficients for contraction (in) and expansion (out) as:

$$K_{In} = (-0.415\frac{A_F}{A} + 1.08) \quad (3.3) \quad \text{and} \quad K_{Out} = \left(1 - \frac{A_F}{A}\right)^2 \quad (3.4).$$

The area terms in the above equations refer to the open frontal area, A_F, and total surface area of the respective filter face. Equations (3.3) and (3.4) are associated with frictional losses due to laminar flow which is not always the case. The frictional coefficients for turbulent flow are approximately 50% lower than those for laminar flow proving that our laminar assumption would be the most conservative but may be an overestimation. If flow is know to be turbulent or transitional the appropriate frictional coefficients can be used [53].

During flow, frictional losses occur as the gases pass over the channel walls down the length of the filter. These frictional losses are described as:

$$\Delta P_{Channel} = 4f\left(\frac{L}{D_H}\right)\left(\frac{\rho V^2}{2}\right) \quad (3.5)$$

where D_H is the channel diameter (or hydraulic diameter for loaded filters), L is the channel length, ρ is the exhaust gas density, V is the exhaust gas velocity and f is the dimensionless Fanning friction factor described as:

$$f = \frac{K}{\mathrm{Re}} \tag{3.6}$$

where Re is the flow's corresponding Reynolds number and K is a constant coefficient of 14.23 for channels of square cross sectional opening and 16.00 for round cross sectional openings [53]. Although the pressure drop due to channel friction is typically a small portion of the DPF total pressure drop, as the hydraulic diameter is substantially reduce it begins to play a larger role. This has been noticed with highly loaded ash and soot filters. Another note is that the cross sectional channel opening generally transitions from square to circular as the ash load of the filter increases [50].

As previously mentioned, the largest contributor to the total pressure drop of the DPF is due to the flow through the porous media layer of substrate, ash and soot. This contribution can be explained in totality through the Forchheimer-extended Darcy equation as:

$$\Delta P_{Wall} = \left(\frac{\mu}{K_p}\right) v_w w + \beta \rho (v_w)^2 \tag{3.7}$$

Equation 3.7 takes into account the laminar to turbulent flow transition by including an additional inertial term. The Reynolds numbers associated with the flow through our porous media layer are generally much smaller than one. Because of this the inertial terms are approximated as a first order term resulting in a simplified from of Darcy's Law described as:

$$\Delta P_{Wall} = \left(\frac{\mu}{K_p}\right) v_w w \tag{3.8}$$

where μ is the dynamic viscosity of the exhaust gas, v_w is the velocity of the exhaust gas through the porous media layer, w is the thickness of the material layer consisting of substrate along with ash and soot if present, and K_p is the bulk permeability of the porous media layer. As ash and soot accumulate within the DPF, the material thickness (w) increases. For a clean DPF, K_p is solely the permeability of the substrate but as ash and soot are deposited within the bulk material, the permeability is altered.

This permeability is affected by both depth and cake filtration, thus is dynamic throughout the loading process [52].

As previously mentioned the bulk permeability of the porous material layer is a dynamic variable over time for a DPF's lifecycle. Permeability, K_p, is a function of porosity and pore diameter. For the substrate wall this calculation is characterized by the Kozeny-Carman correlation:

$$K_w = \frac{1}{5.6}\varepsilon^{5.5} {d_P}^2 \tag{3.9}$$

where K_w is the permeability of the substrate wall, d_P is the pore diameter and ε is the porosity of the substrate. Typically the pore size for the substrate is a distribution and the average pore size is used in equation 3.9. Both average pore size and substrate porosity are variables that are specified by the manufacturer. Once an ash or soot layer is built up along the channel walls, their specific permeability values can be described by:

$$\varepsilon = 1 - \frac{\rho_{Packing}}{\rho_{Theoreticd}} \tag{3.10}$$

where $\rho_{Theoreticd}$ is the powder's true density based off its material composition and $\rho_{Packing}$ is its packing density. The packing density directly impacts the ash layer characteristics, occupied volume and hydraulic diameter within the filter. The properties of the filter's substrate are generally supplied by the manufacturer but the properties of the ash and soot layer are much less straightforward. As ash and soot enter the DPF pores during depth filtration, the substrate's permeability, porosity and mean pore size change. As ash and soot layers form within the channels, these previously mentioned properties are much less characteristically consistent and difficult to determine.

While extensive effort has been devoted to understand the properties of soot layers and their formation principles, the understanding of these parameters regarding ash is still in its preliminary stages. Sappok furthered the understanding of these properties and characteristics for ash layers and also noted that these parameters alter with lubrication chemistry as well [47, 50].

3.2 Material Properties and Characteristics

The previous section described how various material properties of both the DPF substrate and accumulated PM affect the total pressure drop across the filter. A great deal of research has been devoted to determining and understanding these properties. The filter substrate's material properties are typically provided from the manufacturer, but as PM accumulation occurs they begin to change. The properties of ash and soot layers have been studied in recent year but a complete understanding has yet to be found.

3.2.1 DPF Substrate Properties

As mentioned the material properties and characteristics of the DPF substrate are generally well understood prior to PM loading. Although the two most common types of substrate used in diesel particulate filters are cordierite, a ceramic composition, and silicon carbide (SiC), neither is a perfect combination of desired features. Cordierite is characterized by good thermal shock resistance and relative low cost, but has an insufficient melting temperature to sustain some runaway regeneration cases. SiC displays a higher limiting operating temperature and favorable pore network structure but displays low thermal shock resistance and at a high relative cost. A compellation of relative parameters for both SiC and cordierite filters can be seen in Table 3.2.

	Substrate Material	
Property	**Cordierite**	**SiC**
Channel Width (mm)	1.3 -2.1	1.0 - 1.6
Wall Thickness (mm)	0.3 - 0.5	0.3 - 0.8
Permeability (x 10^{-12} m^2)	0.5	1.24
Porosity	45 - 50	42 - 58
Mean Pore Size (μm)	13 -34	8 - 17
Melting Temp (°C)	1450	2400
Thermal Expansion (1/°C)	0.7 x 10^{-6}	4.5 x 10^{-6}
Elastic Modulus, Axial (Gpa)	4.7	33.3
Strength, Axial (Mpa)	2.6	18.6
Thermal Shock Parameter	790	124
Thermal Conductivity (W/mK)	<2	20
Relative Cost	Low	High

Table 3.2: Properties of Common DPF Substrates Cordierite and SiC [52]

The first five parameters directly relate to the filter property changes that occur during PM loading. Mean pore size relates to the amount and size of PM that can fill each pore. The porosity relates to the amount of open volume space that can potentially be filled with PM. From table 3.2 it can be seen that both filter materials are on the order of 50% porous. This is due to the complex network of pores that distributes all throughout the filter's channel walls.

There are also a number of developmental DPF materials such as zirconium phosphate, mullite and silicon nitride. Although these materials have been tested and determined to have a number of desirable traits, they are all still in the research phase with limited applicability [54-56].

3.2.2 Ash Properties

To completely understand of how ash affects the performance of a DPF, it is important to quantify key ash properties then link them to DPF pressure drop and performance. Doing this produces the possibly to identify which ash characteristics and relations thereof impact DPF performance the most. Knowing how ash characteristics and DPF pressure drop relate to one another will help promote the optimization of DPF design, operation and loading procedure. Numerous lab and field studies have been performed within the last 10-15 years that has measured these ash properties; this data has been summarized in table 3.3.

Source (SAE Tech Paper)	Theoretical Density (g/cm^3)	Packing Density (g/cm^3)	Porosity (%)	Permeability (m^2)	Test Type
2000-01-1016	---	0.4 - 1.0	---	$2.8 - 7.4 \times 10^{-14}$	Lab
2001-01-0190	3.13	0.54	83	---	Field
2004-01-0948	2.5	0.4	85	$\sim 5 \times 10^{-12}$	Field
2005-01-3716	2.85	---	---	---	Field
2006-01-3257	---	0.31 - 0.52	---	---	Field
2008-01-0331	---	0.45	---	---	Field
2009-01-1086	---	0.17 - 0.34		---	
Field Test -A	---	0.34		---	Field
Field Test -B	---	0.17	90 -95	---	Field
Field Test -C	---	0.18		---	Field
Lab Test -A	---	0.26		---	Lab
2010-01-1213	3.4	0.3	91.1	---	Lab

Table 3.3: Key Ash Properties Determined from Ash and Field Tests [31, 47, 54, 57-61]

The equations explained in section 3.1.1 provide mathematical evidence that the above ash properties directly relate to the variables contributing to the total pressure drop of the DPF. Understanding these properties will generate a better understanding of why the total pressure drop is affected.

More recent studies have been conducted to determine the ash properties derived from lubricants of various chemistries. Understanding the ash properties derived from various individual lubricant additives and additive combinations will provide insight on the nature of ash derived from fully formulated oil. Table 3.4 provides the data determined from lab tests using two lube oil formulations; ashless base oil with a Ca-detergent additive only, and ashless base oil with a ZDDP additive only. This data is also compared with a fully formulated CJ-4.

Ash Type	Theoretical Density (g/cm^3)	Packing Density (g/cm^3)	Porosity (%)	Test Type
Base Oil + Ca Detergent	3	0.25	90.9	Lab
Base Oil + ZDDP	3.9	0.19	95.1	Lab
CJ-4	3.4	0.3	91.1	Lab

Table 3.4: Ash Properties of Various Lubricant Chemistries [47]

This data proves that lubricant chemistry, the presence and amount of each additive, alters the properties of the ash produced. Each lubricant chemistry tested in the above study had a sulfated ash content of 1% while producing drastically different pressure drops for a given ash load. The results from the above study provided a portion of the motivation behind this project to expand on experimental knowledge of various lubrication oil formulations.

Two other importation ash properties to be noted are particle size and ash layer thickness. It is seen through the aforementioned mathematical equations that hydraulic diameter and porous media thickness directly influence the total pressure drop on a DPF. Particle size also affect pressure drop by relating to the amount of depth filtration, and substrate permeability/porosity alteration that occurs. The particle size and layer thickness measure in a number of tests can be seen in table 3.5.

Source (SAE Tech Paper)	Particle Size (μm)	Layer Thickness (μm)
2000-01-1016	1 - 10	---
2001-01-0190	$d_{primary}$ 0.1 - 0.5	---
2004-01-0948	2.4 - 37.6	---
2004-01-3013	---	73 - 298
2005-01-3716	0.4 - 8	---
2006-01-0874	1	---
2006-01-3416	---	44 - 94
2010-01-1213	---	
Base + Ca	---	180
Base + ZDDP	---	150
CJ-4	---	~ 200

Table 3.5: Ash Particle Size and Layer Thickness from Various Studies [43, 45, 47, 54, 57-59, 62]

It should be noted that the various experimental procedures and measuring methods may partly explain the large range of values reported in Table 3.5. The extent of PM loading also directly impacts the ash layer thickness along the channel walls. With this being said it is important to note how lubricant chemistry affects ash layer thickness. The results presented in the above table for the "Base + Ca" and "Base + ZDDP" tests were both loaded to approximately the same level of ash loading with an estimated 17% difference in ash layer thickness.

Numerous experiments have also determined that ash particles follow a bimodal size distribution with large particles in the 10-100 μm diameter range being agglomerates of smaller particles in the 0.2 – 1.0 μm diameter range. The results of on size distribution test and scanning electron microscope (SEM) images can be seen in figure 3.3.

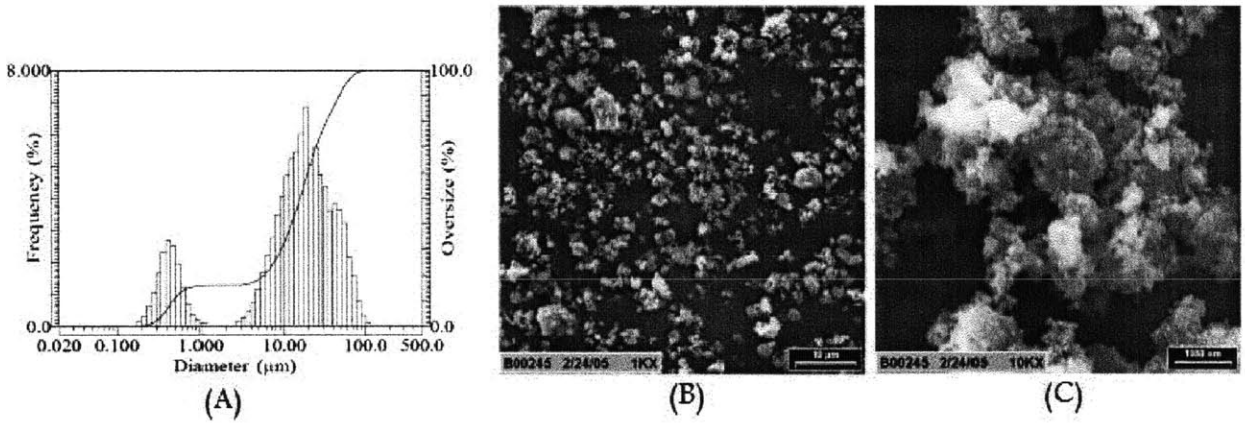

Figure 3.3: Ash Bimodal size distribution with respective SEM images [59]

Figure 3.3A describes a bimodal size distribution with averages of 0.4 and 20 μm. Figure 3.3 B&C describe this distribution as larger agglomerated particles being composed of smaller ash particles.

Experimental and computational research has also shown that the regeneration method affects the ash layer thickness and ash plug length. It has been determined that filters regenerated periodically tend to accumulate ash plugs in the rear of the DPF overtime, whereas filters being continuously regenerated accumulate a even layer thickness with little ash plug generation. This is generally attributed to the fact that when filters are periodically regenerated, the ash PM is re-entrained in the exhaust flow relocating the respective particles further down the DPF. These substantial differences in bulk ash distribution may have a large effect on the total pressure drop of the DPF [63].

The results of the described experimental tests prove that both exhaust conditions and lubricant chemistry have a direct effect on the properties of the resulting ash PM. It has also been shown that these ash properties contribute the total DPF pressure drop. In order to understand to components of the DPF pressure drop more fully, further investigations into lubricant chemistry are needed. This information will contribute to the optimization of diesel oil formation and regulation.

3.2.3 Soot Properties

Unlike the properties surrounding ash, an extensive amount of research has been conducted on the properties of soot particles, layers and controlling properties. From a particle size perspective, soot particles are much smaller than ash particles. Similar to ash, soot particles follow a bimodal size distribution with primary particles ranging from 10 -40nm while agglomerated particles have a size on the order of 100nm [64,65]. Comparing these measured soot particles sizes with those for ash found in table 3.5, we see that soot particles are smaller by an approximate order or magnitude.

Other studies have shown that soot packing densities are on the order of 0.1 g/cm^3 and layer permeability range between 1.5 x 10^{-14} m^2 to 3.3 x 10^{-14} m^2 [66,67]. When compared to the values for ash in table 3.3, ash packing densities are 2 to 5 times that of soot and ash layer permeability values range between 2 to 100 times those of soot.

A study conducted in 2002 reported that soot packing density and permeability were a function of the flow's Peclet number (Pe), which a measure of inertial versus diffusional deposition:

$$Pe = \frac{U_w d_{Primary}}{D} \tag{3.11}$$

where U_W if the filtration velocity, $d_{Primary}$ is the primary particle diameter and D is the diffusion coefficient. A high Pe signals primarily in inertial deposition which results in a more densely packed later. A low Pe represents particles primarily deposited by diffusion resulting in a more loosely packed layer [68]. Other mathematical correlations have been made and reported in the literature resulting in soot permeability calculations and a better understanding of how soot directly affects pressure drop. Because the nature of this study is in regards to lubricant chemistry effects on DPF performance, these details will not be described.

3.3 Deposition Mechanisms and Cake Filtration Theory

Cake filtration theory has been studied for over a century and is understood relatively well. As individual particles are collected along the cell channel wall they generate an ash layer. As this ash layer is generated, the method of particle deposition determines the ash layer's properties. Multiple theoretical and experimental tests have been performed to understand these phenomena.

A simulation experiment was performed in the 1980s by Houi et al. in which a statistical model was used to describe the particle deposition mechanisms and cake layer growth. The authors performed two simulations. The first simulation, Type A, was used to determine deposit structures using only a small number of particles (1000), and the second simulation, Type B, used a larger amount of particles to determine the macroscopic structure of the cake layer. The simulations were based off random, Brownian motion (diffusive) and the results can be seen in figure 3.4.

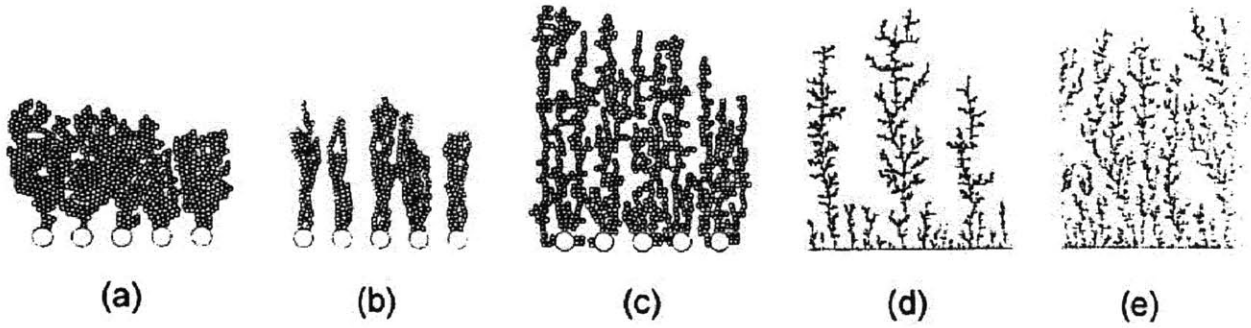

Figure 3.4: Simulation results of 1000 particles deposited on collectors (a-c) and macroscopic cake layer formation (d, e) [69].

The results displayed in Figure 3.4 (a-c) represent particle deposition for particles with much smaller diameter than the filter pores, which is similar to the case of soot and ash deposition in a DPF. The outline circles on the bottom of figure 3.4 (a-c) represent the collectors. Figure 3.4 (d, e) describe the macroscopic formation of the cake layer. It can be seen through these simulations that the ash and soot particles are deposited on the cake layer to form tree-like structures that grow over time. The authors describe a "sticking probability" which determines whether or not the particle collides and attach itself to the tree-like structure or simply bounces off. This sticking probability is based off the angle of incidence of the individual particles that are entrained in the flow which collide with the cake layer built. The authors observed that the density of the cake layer is inversely proportional to the "sticking probability". As the particles bounce off a variety of tree-like structures in the cake layer, they eventually settle in a final resting place. Because they are not attached to the first structure they hit, the overall density of the cake layer increases. It was also noted that these tree-like structures will become unstable

overtime and the fluid flow or colliding particles will cause them to collapse and form ash bridges. These ash bridges have the capability of branching over multiple filter pores creating an inability for them to be filled with PM [69].

Further research has determined that the cake layer growth is related to the flow's Peclet number (Pe). It was determined that as the Pe decreases, the tree-like particle formations begin to appear. This leads to a larger thickness and lower density of the cake layer. Along these same lines, as the angle of incidence is increased, similar tree-like deposits are formed resulting in a more open structure. For a given angle of incidence, as the flow velocity is increased, the layer density is increased [70,71]. Figure 3.5 graphically depicts the morphology of the ash layer created under various conditions.

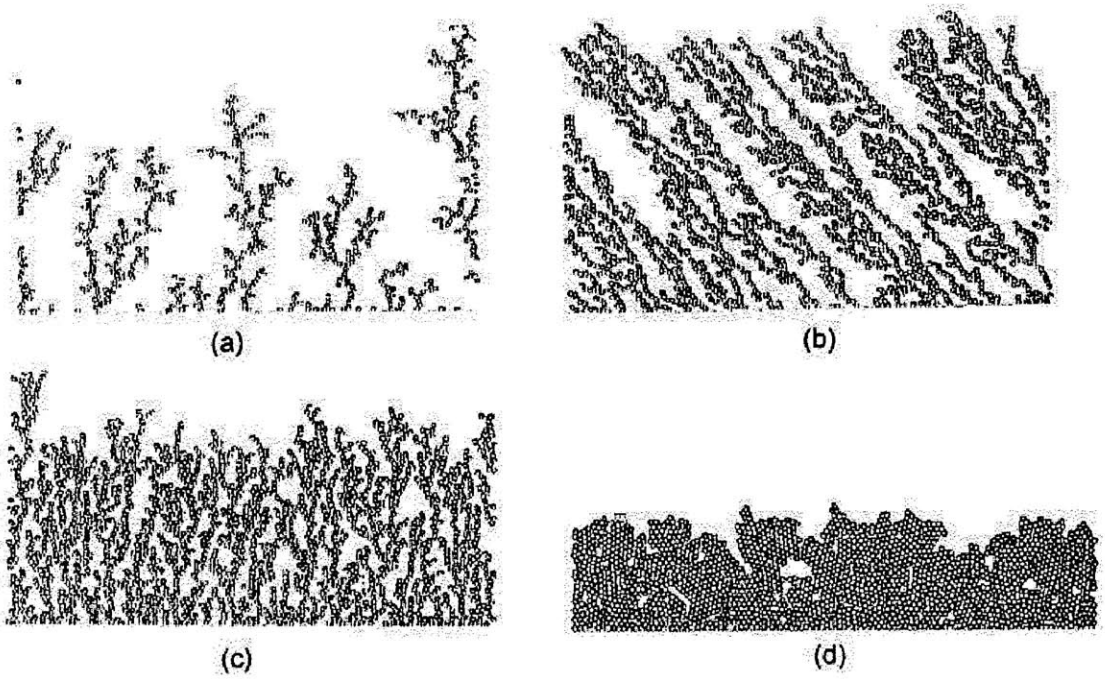

Figure 3.5: Cake layer growth for entirely diffusional deposition (a), ballistic deposition at a 60° incident angle (b), ballistic deposition normal to filter surface (c), ballistic deposition with 'rolling events' (d). [71]

Figure 3.5 provides graphical depictions of the results mentioned above. Figure 3.5 (d) displays the ash layer generated with multiple "rolling events", or deposit restructuring, occurring. This results from the tree-like structures being unstable over time which causes them to break and be re-deposited which produces a more densely packed cake layer.

Experimental results have shown that initially the ash accumulation in a DPF will penetrate into the matrix of pores within the filter media (depth filtration) which leads to a steep increase in pressure drop. This alters the porous media's porosity and permeability. After a small amount of PM is deposited in the

pores, a cake layer begins to build which results in a relatively linear pressure drop increase which has a small slope than that of depth filtration. This cake layer build up produces a smaller hydraulic diameter which in turn would increase the incident angle of arriving particles.

Based off experimental results and particulate description, the cake layer of ash accumulation within a diesel particulate filter will resemble a network of interconnected tree-like structures as opposed to a layer of densely packed particulate spheres. The alteration of ash morphology, incidence angle and flow velocity may affect the cake layer morphology which is directly related to the total DPF pressure drop.

3.4 Additional Ash Property Considerations

Extensive work has been performed to produce models for clean DPF operation as well as the effects of soot deposition but little has been directed towards ash effects. Fundamental equations were described in previous sections regarding the effects that fundamental ash properties have on total DPF pressure drop. This type of work is recent and needs to be studied in more detail to be fully understood.

A study performed in 2003 proposed an ash "stickiness factor" with regard to ash transport. This "stickiness factor" is related to the tendency of tree-like ash deposits reaching their critical shear stress and being re-entrained in the exhaust flow. The critical shear stress of the ash was estimated to be a function of the ash properties (composition based off lubricant chemistry) and thermal history which determines the "stickiness factor". Figure 3.6 provides simulation results for ash transport for ash of varying "stickiness" [72].

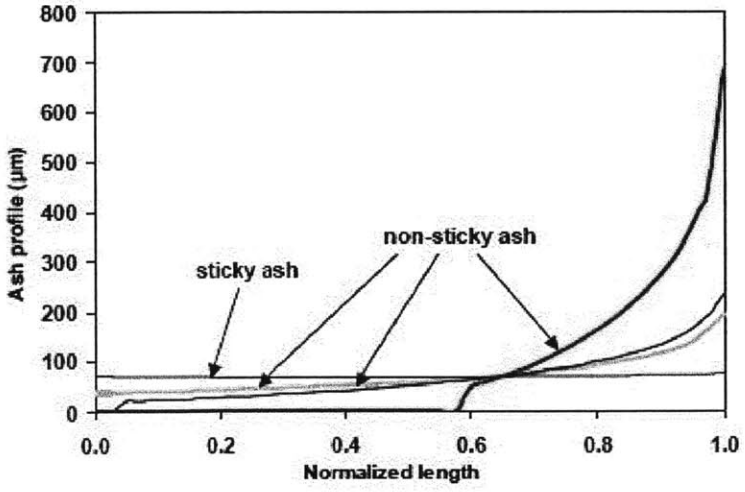

Figure 3.6: Simulated ash profiles for varying levels of ash stickiness. [72]

It can be seen from figure 3.6 that as ash stickiness increases, the cake layer thickness increased and there is little ash end plug formation. Intuitively this makes sense being that if it is less sticky ash, it will have a tendency to shear off from the cake layer and be deposited towards the back of the filter. The author noted that this is a conceptual study and much more research must be devoted to this topic. As noted above, ash composition and morphology is presumed to be a factor of the ash stickiness. This provided some motivation for the conducted research in determining how lubrication chemistry affects the ash "stickiness" and resulting deposition profile and transport process.

3.5 Ash and Soot Distribution and Modeling

The fundamental equations described earlier in this section prove that ash morphology and distribution relate directly to the total pressure drop of a DPF. Because of this it is of special interest as to the manner in which both ash and soot are deposited within the filter. Although PM distribution is often non-uniform both radially and along the channel length, the general deposition trends have been proven to be the same [47, 50, 57].

In a clean DPF, PM is initially trapped in the surface pores of the porous media. As previously mentioned this is referred to as depth filtration and has a large effect on DPF pressure drop. The extent of depth filtration is generally low and does not seem to occur at particulate loads greater than 5 g/L [47,50]. Figure 3.7 graphically depicts depth filtration with SEM images.

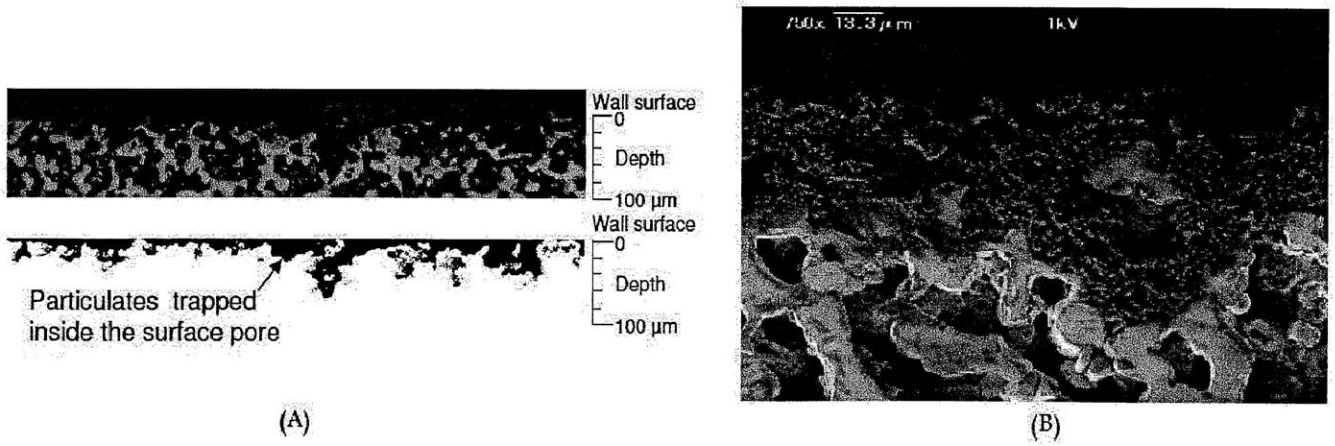

Figure 3.7: SEM images of depth filtration in a SiC DPF. Adapted from [73]

Figure 3.7 (A) graphically displays depth filtration within the filter matrix. It is seen that the extent of depth filtration is generally limited to the surface pores with some exceptions extending deeper into the

filter matrix. Figure 3.7 (B) is a higher magnification image of depth filtration within the filter matrix which displays similar characteristics to those of 3.7 (A). As previously motioned, depth filtration occurs at PM loads on the order of 5g/L and lower and produces a steep rise in DPF pressure drop. This can be seen in the three experimental test cases displayed in figure 3.8 by the steep initial pressure drop slopes. Although depth filtration doesn't change the filter channel geometry, it does alter the porosity and permeability of the porous media.

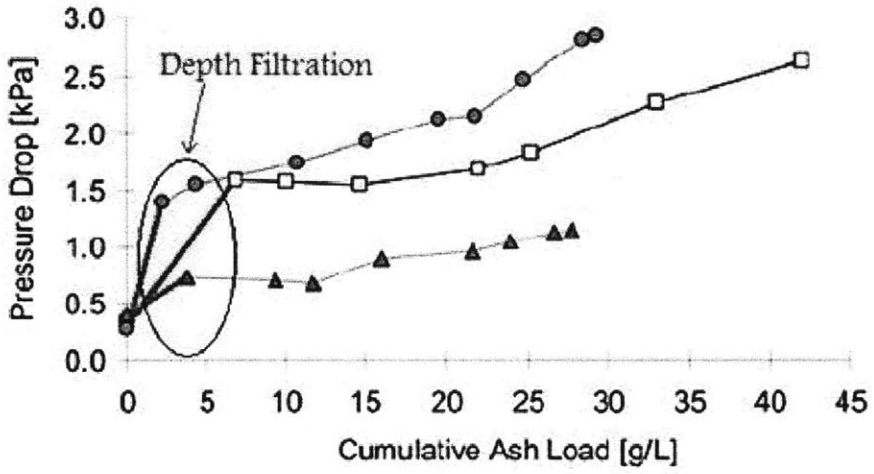

Figure 3.8: Pressure drop due to depth filtration highlighted. Experimental data taken from [47].

Depth filtration generally ends after the surface pores of the filter matrix are filled with PM or ash bridging occurs over the surface pores. After depth filtration has ceased, cake filtration occurs which builds a layer of PM along the filter channel walls. Cake layer formation begins to alter the channel geometry by reducing the channel's hydraulic diameter which influences the flow characteristics. Because the ash layer is porous in nature, as the cake layer builds, the available porous media for filtration increases which in turn increases the filter's trapping efficiency.

The cake layer thickness is a function of the ash's packing density and critical shear stress which was previously mentioned. As the cake layer reaches a "critical thickness" in which its max allowable shear stress is reached, layer ash begins to break off and deposit to the end of the filter creating a plug. Ash plug formation tends to occur at ash loads on the order of 12 g/L and does not become a significant factor until higher ash loads are reached (~20g/L) [47, 50]. Figure 3.9 displays cross-sectional views of filter channels with substantial ash layers and plugs obtained through this research.

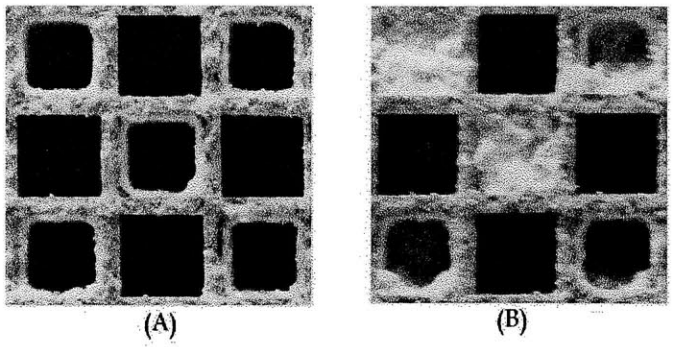

Figure 3.9: Cross sectional channel views displaying ash cake layers and end plugs.

The ash cake layer not only changes the channel geometry but also provides a larger porous media thickness for the exhaust gas to flow through increasing the resistance. As the ash end plug begins to form, the available channel length begins to decrease. This influences pressure drop by reducing the available filtration area and channel geometry. Although not as drastic as depth filtration, cake filtration and end plug formation increase pressure drop as the accumulated PM mass within the DPF increases. Figure 3.10 highlights the portion of pressure drop graphs which cake filtration are responsible for.

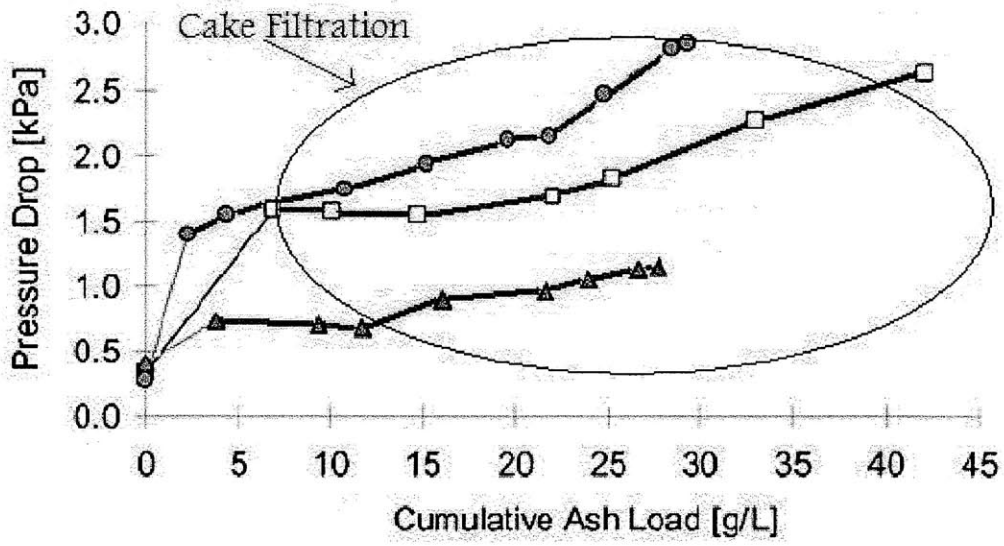

Figure 3.10: Pressure drop due to cake filtration highlighted. Experimental data taken from [47].

As the inlet filter channels collect PM, the outlet filter channels stay entirely clean. This produces an inaccuracy in our zero dimensional model described earlier in this section but is accepted due to the fact that this research is mostly experimental in nature.

For both soot and ash, an end plug volume fraction is used to quantify the amount of ash collected within the cake layer vice the end plug in the back of the filter. The eng plug fraction is defined as:

$$End_P Fraction = \frac{Vol\_End\_Plug}{Total\_Volume} \tag{3.12}$$

which is the ratio of the volume of ash or soot accumulation in the end plug to the total volume of ash or soot accumulated in the filter. It was described earlier that the volume of ash accumulated in the filter is dependent on the ash's packing density. It has been proven that end plug and channel wall ash accumulation packing densities vary which must be considered in advanced pressure drop models and the end plug fraction variable [47,50]. More advanced and accurate models are necessary to fully understand the dynamic process of PM accumulation in a DPF and its respective effects. This is not the focus of this research but cannot be neglected.

3.6 Modeling Ash Properties

The pressure drop of a DPF is directly affected by ash properties such as packing density, porosity and permeability. Some of these properties, such as packing density, are relatively simple to measure but others such as permeability are not as straightforward. A primary focus of this research is to enhance the understanding of how lubricant chemistry ties to these ash properties which influence DPF pressure drop.

As previously mentioned, permeability is a direct function of porosity and mean particle diameter. Porosity and particle diameter can be determined by a variety of experimental procedures, which will subsequently be discussed further, but permeability must be calculated. Over the past several decades a number of numerical permeability relationships have been determined, the most commonly used are described below.

The Rumpf & Gupte relationship is one of the most widely used permeability relationships in DPF technology including substrate, ash and soot layers. This relationship was determined by randomly packing spherical particles with porosities (ε) ranging from $0.35 - 0.7$, Reynolds numbers (Re_P) ranging from $10^{-2} - 10^{2}$, and particle diameters with $D_{P,max} / D_{P,min} \sim 7$. The Rumpf & Gupte relationship is defined as:

$$k = \frac{\varepsilon^{5.5}}{5.6}\overline{D}^{2}_{P2} \tag{3.13}$$

where k is the calculated permeability, ε is the measured porosity, and $\overline{D}_{P2}$ is the surface average sphere diameter. If the porous layer has a higher permeability ($\varepsilon \geq 0.8$), the Carman-Kozeny equation is generally used:

$$k = \frac{\varepsilon^{3}}{180(1-\varepsilon)^{2}}\overline{D}^{2}_{P2} \tag{3.14}.$$

In conditions in which the structures are highly porous ($\varepsilon \geq 0.95$) or no longer sphere-like shaped these relationships tend to break down. When these conditions are encountered, relationships for "flow through porous media" are no longer used and "flow around submerged structures" are generally utilized.

(This page intentionally left blank)

4 EXPERIMENTAL SET-UP AND APPROACH

The primary objective of this research is to determine the composition and morphology of ash derived from specific lubricant chemistries, and then relate these ash properties to their negative effects on DPF performance. To conduct this type of research using fleet field data, it would take upwards of 150,000 on road miles with constant engine monitoring techniques being used [42,47]. Because of this it is more effective to construct and utilize an accelerated ash loading system for DPFs with in situ monitoring techniques. For the experiments conducted through this research, a Cummins ISB 300 and a specifically designed accelerated ash loading system coupled to the engine's exhaust set-up was used. This accelerated ash loading system has been historically proven to generate and deposit engine-out ash in a realistic manner.

4.1 Approach

As previously mentioned, to obtain and analyze field aged DPFs is both costly and time consuming. Although this method provides the most realistic data pertaining to DPF and lubricant optimization, it is impractical to base research solely on these samples. Because of this it is important to used accelerated loading techniques to produce more time efficient results to help determine the underlying mechanisms regarding DPF ash loading and performance degradation. Along these same lines, it is essential to periodically compare lab and field results whenever possible to ensure that the accelerated ash loading system resembles that of a field diesel engine as closely as possible. Because of the variability of field diesel engines, it is difficult to pinpoint the underlying mechanisms which contribute to ash properties. This provides a benefit to lab research by being able to specifically control experiments knowing the exact formulation nature of the ash. Although accelerated ash systems are essential, their formulation mechanisms must be analyzed to ensure a suitable comparison to field samples.

4.1.1 Accelerated Ash Loading Methods

Several accelerated ash loading systems exist but their results may not necessarily simulate field results in an accurate manner. The primary method used to increase the amount of ash generated is by increasing the lubrication consumption rate in the power cylinder. The most prevalent technique used to do this is by doping lubricant into the engine fuel. In a literature review by Bodek et al. it was noted that fuel doping differs from natural oil consumption in at least four ways [20]:

- Fuel doping only accelerates one of two oil consumption methods, the flow around the top piston ring. This method only accounts for 60% of natural oil consumption when compared to evaporative [48].
- Fuel doping changes the soot to ash proportion in the "exhaust", therefore neglecting any reaction that takes place between the two especially during regeneration.
- Fuel doped oil is burned in the diffusion flame front and not in the air rich regions it would generally occupy.
- Oil doping may disturb the micelles within the lubricant which may form unburnable sludge of metallic compounds [73].

Fuel doping also neglects the recent studies concerning the elemental lubricant consumption variations due to volatility differences. Although these lubricant compound consumption variations are not fully understood, they may be important in understanding the morphology of field generated ash. Studies conducted by Bardasz et al. utilized the fuel doping accelerated ash method to determine the negative effects of ash on DPFs. When a high sulfated ash lubricant (2.23%) was doped into the fuel, the axial ash deposit profile was relatively uniform along the filter's length. When a low sulfated ash lubricant (0.63%) was doped into the fuel or a high sulfated ash lubricant was strictly used in the sump without doping, ash deposits increased towards the back of the filter and were not uniform along the filters length [49]. Taking all of this into consideration the fuel doping accelerated ash method, although effective, must be criticized.

Another accelerated ash method is used in which oil mist is injected into the engine's intake manifold and then burned in the combustion chamber. This is slightly more accurate than fuel doping because it addresses the third and fourth above bulleted issues [20]. Research conducted by Sutton et al. utilized the oil misting technique. The accelerated and un-accelerated results displayed similar ash deposit profiles but the pre- and post-regeneration backpressure effects were found to be drastically different [74]. Other research utilized oil misting along with undersized DPFs (DPF to volume ratio of 0.88) to further accelerate the ash loading rate. It was determined that this did not closely resemble natural oil consumption and ash loading effects due to a resultant non-linear pressure drop response only seen at high ash loads [45]. This historical data proves that although the oil misting technique better resembles natural oil consumption when compared to fuel doping, it is not entirely representative of typical diesel engine operation and other methods should be explored.

4.1.2 Historical MIT Approach

Over the past several years an accelerated ash system was constructed and utilized at the Massachusetts Institute of Technology which closely parallels the results found from field study analysis. Although no system will completely resemble natural diesel and after-treatment system operation, the system used in this research has proved to provide accurate results in a relatively short amount of time. One of the benefits of the system used is the flexibility to independently change a number of variables during testing such as simulated exhaust temperature and flow rate, oil consumption rate, lubricant chemistry consumed, DPF size and material used, and the soot and ash interactions throughout the test duration. This flexibility provides the ability to help isolate individual underlying mechanisms of ash generation and their resultant effect on DPF performance.

Utilizing the subsequently described accelerated ash system, this research attempts to quantify the ash morphology of various lubricant chemistries and their negative effect on DPF performance. Because of the system's operating mechanisms, oil which would not be suitable for engine operation can be used to generate ash and help understand the underlying mechanism of lubricant chemistry on DPF performance.

4.2 Accelerated Ash System

The DPF volume used in these studies was 2.47 liters. This volume is relatively under-sized compared to a full size DPF which accounts for a portion of the accelerated ash loading. The ash loading system was designed to ash load a conventional D5.66" (14.38 cm) x 6" (15.24 cm) DPF to 40 g/L in approximately 100 hours. This is a substantial amount of accelerated ash accumulation considering 40g/L ash corresponds roughly to 300,000 on-road miles [46].

The accelerated ash loading system independently utilizes both a Cummins ISB engine and a separate diesel combustion chamber to load the DPF with PM. The Industrial diesel burner with a custom combustion chamber is used to burn lubrication oil and deposit ash in the DPF. The Cummins ISB engine is used to deposit realistic exhaust gas, primarily soot, into the filter. These two systems are run independently from one another. A schematic of the accelerated ash loading system can be seen in figure 4.1.

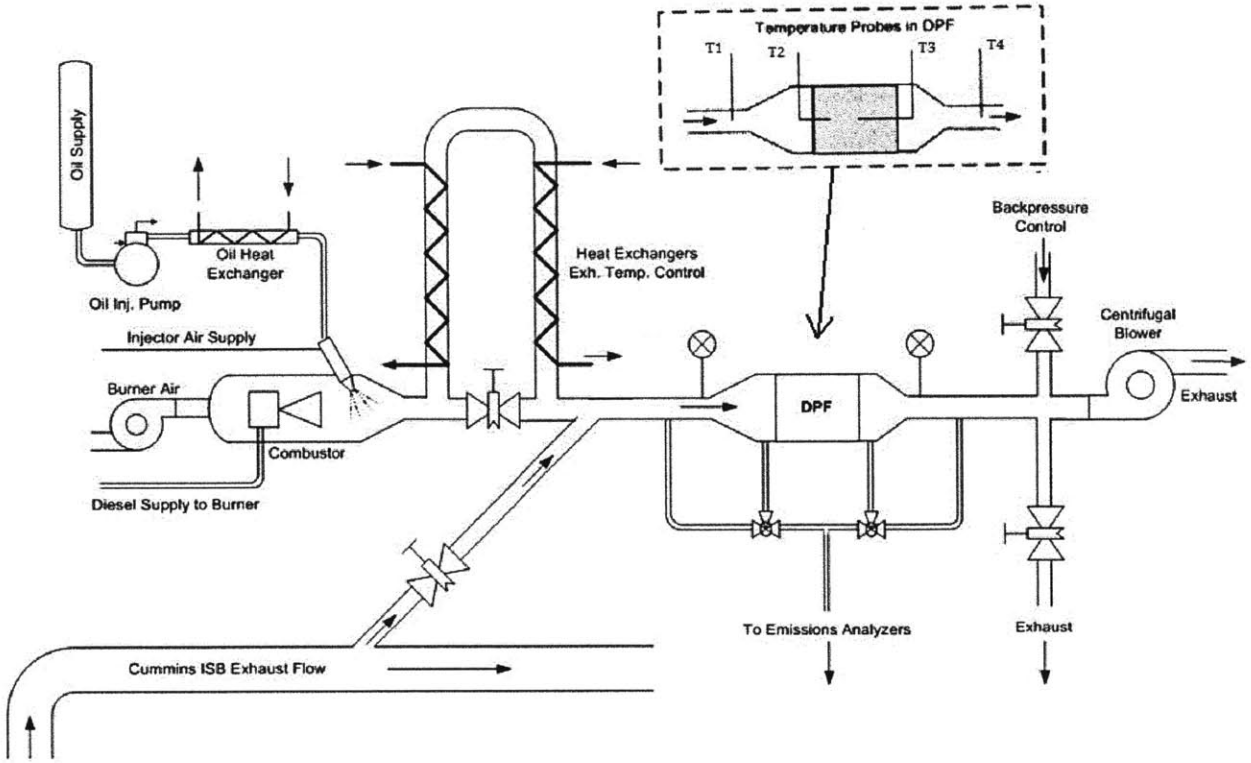

Figure 4.1: Configuration of accelerated ash loading and after-treatment system used in this research.

Figure 4.1 accurately describes the accelerated ash loading system used in this research. The oil supply line is filled with oil of any desired chemistry. Because the oil is used solely for ignition, it does not necessarily need to exhibit the full additive package needed for a fully functional lubricant. This creates some flexibility as to what oils can be studied including base oil, individual additives and combinations along with fully formulated oils. The oil is delivered by an air assisted oil injector located atop the custom diesel burner and is fed by a computer controlled constant volume pump. The variability in combustor air flow and oil injection parameters offers some control over combustion quality and its products. Table 4.1 displays the ash loading system's operating specifications.

System Parameter	Description
Fuel Consumption	1.5 - 7.6 L/h
Oil Consumption	0.94 - 9.4 ml/min
Injection Pressure	700 - 1400 kPa
Air Flow	266 - 1130 slpm
DPF Inlet Temperature	200 800 °C

Table 4.1: Accelerated ash loading system specifications [50].

The heat exchanger downstream the combustion chamber is used to control the combustor exhaust temperature independent of burner settings. The use of this heat exchanger can control DPF inlet

temperatures between 200 – 800 °C enabling online filter continuous or periodic regeneration. Because the industrial diesel combustor runs igniting diesel fuel, a small amount of soot is produced while ash loading. The use of the heat exchanger enables the possibility of oxidizing this unwanted soot when strictly ash loading is preferred.

Downstream of the system's heat exchanger and upstream of the mounted DPF there is a connection stemming from the Cummins ISB. This enables the possibility of loading the mounted DPF with a portion of the engine's exhaust flow. This is primarily used to load the DPF with soot. Because these two systems are separate (but can be run together), soot can be loaded onto a filter which already contains any amount of accumulated ash. This leads the better possibility of understanding the synergistic effects of ash and soot on DPF performance.

The DPF is located downstream of the heat exchanger with four thermo couples attached. The inlet and outlet face of the filter have thermocouples attached (fig 4.1 T2 & T3) to accurately display the actual filter temperatures. Just upstream and downstream of the respective filter faces; two more thermocouples are attached (fig 4.1 T1 & T4) which measure the exhaust gas temperatures. Downstream of the mounted DPF is a centrifugal blower which provides addition control over gas flow rates through the DPF while PM loading. This centrifugal blower provides the majority of the flow rate through the system. When not loading, this blower is used to conduct space velocity tests to evaluate DPF pressure drop.

The ample amount of piping from the combustion chamber to the DPF provides a lot of surface area for PM collection. This unwanted loss of PM within the system piping, and not the DPF, is unavoidable but does not change the accuracy of the DPF accumulation measurements.

4.3 Engine Specifications and Capabilities

The accelerated DPF ageing set-up contains a 6 cylinder, 5.9 liter, four-stroke, turbocharged, direct injection Cummins ISB diesel engine. In order to meet the stringent diesel emission regulations discussed earlier, the engine utilizes a number of advanced technologies such as a Bosch high-pressure common rail fuel injection system, Holset variable geometry turbocharger, and cooled exhaust gas recirculation (EGR). Overall the engine is rated at 300hp (224 kW) at 2500 rpm and 660 ft-lb (890 N-m) at 1600 rpm. Table 4.2 contains specifics on other engine parameters.

Model	ISB 300
Maximum Torque	890 N-m @ 1600 rpm
Maximum Power	224 kW @ 2500 rpm
Number of Cylinders	6, in-line
Combustion System	4 stroke, direct injection
Injection System	Common Rail
Aspiration	Variable geometry turbocharger and intercooler
Displaced Volume	5.9 liters
Compression Ratio	17.2:1
Cylinder Head Layout	4 valves / cylinder
Injection Nozzle	O.D. = 158 μ_m
	L = 1.00 mm
	8 sac-less nozzles per injector
Injection Pressure	800 - 1600 bar

Table 4.2: Cummins ISB 300 Engine Specifications [50]

The stock engine system was also instrument laden with National Instruments (NI) measuring and recording devices. These devices were divided into a slow speed and high speed modules (SCXI-1102B and SCXI-1100 respectively) which receive and record a variety of temperatures, pressures and flow rates. These modules with their appropriate signal filters were connected to a PCI-6024E data acquisition board. In addition to the fixed NI instrumentation, the engine set-up was outfitted with a variety of particle / gaseous sampling capabilities. Although these capabilities were utilized in past research they were not used for the research further described.

4.4 Analytical Techniques

Using the data acquisition systems and the experimental set-up we can acquire important results such as DPF temperature, pressure drop and weight resulting in filter ash load. Once these results are obtained during the experimental test runs, data which characterizes the chemical and physical nature of the accumulated ash can be acquired during the filter's post mortem analysis using various analytical techniques.

4.4.1 Scanning Electron Microscopy

Scanning electron microscopy (SEM) was used to obtain high resolution, three-dimensional images of ash deposits and build up on DPF samples at a near one nanometer scale. The microscopy analysis was carried out at the MIT Center for Material Science and Technology (CMSE). Analysis of these images can help determine extent of ash depth filtration, individual and agglomerate particle size as well as ash layer thickness.

Energy dispersive x-ray (EDX) analysis was used in conjunction with SEM to determine specific elemental composition of ash particles. This technique provides qualitative information on the ash composition and distribution of the lubrication elements in a give ash sample. Comparing multiple EDX images provides the ability to hypothesize about the elemental compounds which the ash is composed of.

4.4.2 X-Ray Diffraction Analysis

X-Ray Diffraction (XRD) is a technique used to determine the chemical compounds in a given sample. An incident x-ray beam is aimed at a powder sample compressed in pellet form and a resultant spectrum is obtained. The intensities and location of the spectral peaks relate to various type, crystalline phase and relative quantities of the various chemical compounds in the powder sample. A Rigaku Powder Diffractometer at the MIT CMSE was used.

(This page intentionally left blank)

5 EXPERIMENTAL PROCEDURES AND TEST MATRIX

This section outlines the details of the various tests conducted as part of this research. Various lubrication formulations were run in efforts to quantify their ash's effects on DPF performance. This section details the lubrication, fuel and filter specifications as well as the experimental procedure conducted.

5.1 Lubricant and Fuel Specifications

The goal of this research was to determine how the ash derived from specific lubricant chemistries effect DPF performance degradation. Much research has been conducted on fully formulated CJ-4 lubricants but the effects on individual additives and combinations thereof are still in the preliminary stages. Research conducted by Sappok et al. investigated the effects of ash derived from four lubricant chemistries, a formulated CJ-4 and ash-less base oil for upper and lower bounds, as well as base oil treated with Ca detergent and a base oil treated with ZDDP for individual additive effects. This research attempts to extend the test matrix conducted by Sappok by three specifically formulated lubricant chemistries. The specifications of the lubricant oils can be seen below in Table 5.1.

Lubricant	N [ppm]	Ca [ppm]	Mg [ppm]	P [ppm]	Zn [ppm]	S [ppm]	Mo [ppm]	Estimated S.A. Content [%]	ASTM S.A. Content [%]
Base + Mg	700	< 1	2070	< 1	< 1	460	< 1	1.0741	1.047
Base + Ca & ZDDP	700	2480	< 1	1180	1280	2750	< 1	1.8557	1.048
Base + Mg & ZDDP	700	< 1	1730	1180	1280	2840	< 1	1.8189	1.058

Table 5.1: Lubricant composition for the oils used in this research.

Table 5.1 describes the chemistries of the three lubricant formulations used in this research; a base oil with solely a magnesium detergent additive, a base oil with a calcium detergent and ZDDP additive package, and a base oil with a magnesium detergent and ZDDP additive package. These three oils extend the matrix conducted by Sappok by investigating the second most used detergent as well as the initial stages of the synergistic effects of both calcium and magnesium based detergents paired with ZDDP.

All of the lubricants were formulated to 1% sulfated ash [SA] content which provides the comparability to fully formulated CJ-4 oil. Once obtained from the manufacture, the lubricant SA content was estimated using commonly found sulfated ash conversion factors seen in table 5.2 as well as experimentally measured using ASTM D874.

Element	Metal % → SA %
Zn	1.25
S	3.1
Mg	4.5
Ca	3.4
Ba	1.7

Table 5.2: Sulfated ash conversion factors [75].

Elements not found in table 5.2 are noted to have little effect on SA content and should not be included in the SA estimation. It is important to note that these conversion factors are unreliable when a lubricant is formulated with a magnesium-based detergent or a boron-based dispersant [75]. The disparity between the estimated and actual SA contents noted in table 5.1 confirms the necessity to conduct the ASTM to determine the correct SA content of the lubricants used. In our case, the three lubricant formulations were indeed very close to 1% SA content as suggested by the manufacturer.

All of the fuel used in the experiments, both for the Cummins engine and the accelerated ash burning system, was ultra-low sulfur diesel (ULSD). By definition ULSD contains no more than 15 ppm of sulfur and is a necessity to meet the stringent emission regulations mentioned in section 1 of this document. An elemental analysis of the fuel was conducted by Sappok to ensure that the fuel had no contribution to SA production. The results of the elemental analysis can be found in Table 5.3.

ASTM D5185						
Element	Ca	Mg	P	Na	K	Zn
ULSD [ppb]	<97	<56	<1180	<2010	<2690	<155

Table 5.3: Elemental analysis of test fuel. Taking from [50]

It was also noted that in all test cases the trace metals were below the minimum detectable limits of the analyzer which ranged from 100 to 1,000 ppb [50].

5.2 Particulate Filters

Conventional cordierite DPFs, all produced by the same manufacturer, were used in the tests for this research. The filter geometry was 200 cells per square inch with wall thicknesses of 0.012 inch (200/12). The filters also contained a platinum-based catalyst. Table 5.4 displays details on the filter geometry and specifications.

Substrate	Catalyst	Dimensions	Cell Density	Wall Thickness	Filter Volume
Cordierite	Pt	D5.66" x 6" (D14.38 x 15.24 cm)	200 cpsi (31 cells/cm^2)	0.012" (0.03mm)	2.47 L

Table 5.4: Properties of diesel particulate filters used in this research.

5.3 Accelerated Ash Loading

The accelerated ash system used in these tests has been validated in previous research ensuring the validity of its results. The experimental procedure consisted of filter preparation, ash loading, intermittent soot loading and a detailed post mortem analysis. The ash and soot loading is performed on the filter to quantify the performance degradation the ash and PM has on the DPF. The post mortem analysis is conducted to quantify the ash properties which lead to this degradation. Throughout all of these steps, various parameters and measurements were taken to provide the further understanding desired from this research.

5.3.1 Filter Preparation

Before starting the experimental loading procedure, the filters described in section 5.2 needed to be properly prepared. The first step in completing this preparation is to properly mat and can the raw filter. Once the filter is surrounded by filter matting and properly inserted into its supportive containment canning, it is necessary to "degreen" the filter. This procedure consists of heating the filter and supportive canning to an elevated temperature for an extended period of time. This temperature elevation ensures that proper thermal expansion of the matting occurs which ensures that 100% of the exhaust flow is directed through the filter and not around its outer surface. The degreening procedure consisted of subsequently increasing the filter's temperature for a specified period of time. The procedure is as follows:

1. ~300°C for 30 minutes
2. ~500°C for 30 minutes
3. ~650°C for 120 minutes

Following this procedure ensures that the matting is gradually expanded to its desired position creating optimal flow for testing. Once this procedure is completed, the filter loading is commenced.

5.3.2 Ash Loading

Throughout this research a fully loaded filter is considered to contain on the order of 25g/L ash (2.47 liter DPF). To accumulate this mass of ash, the accelerated loading previously described was used in conjunction with the different lubricant formulations listed in table 5.1. This mass of ash roughly equates to 65-70 hours of loading and the consumption of approximately 4.5 gallons of lubrication oil. This procedure roughly equated to 175,000 miles or 4,500 hours of DPF operation. In one case a DPF

was chosen to be loaded only to 12g/L which would equate to about half the miles and hours previously mentioned.

All of the filters loaded in this research were periodically regenerated for 15 minutes after an hour of ash loading. The inlet filter face maintains approximate temperatures of 250°C during ash loading and 625°C during regeneration. The regeneration temperature and time is in extreme excess for platinum catalyzed filers which ensured complete soot oxidation within the filter. Graphs of the filter's face temperature (fig 4.1 "T2") and pressure drop over time for a typical loading cycle under periodic regeneration can be seen in figures 5.1 and 5.2.

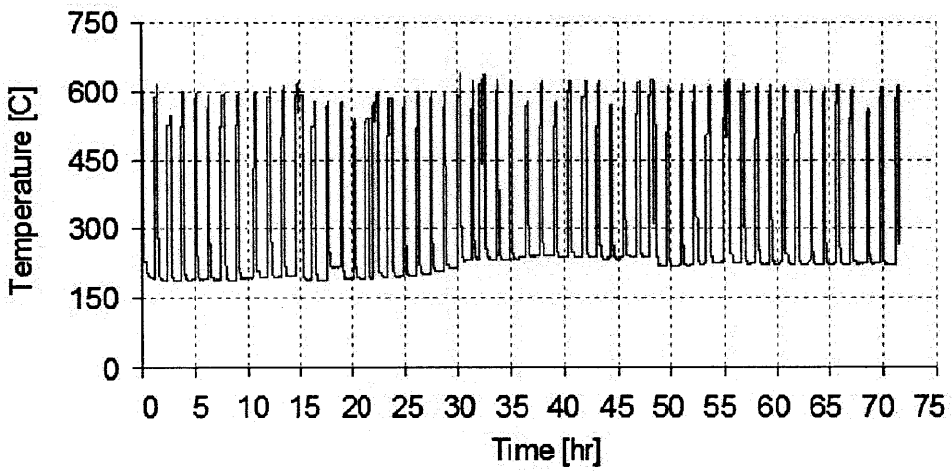

Figure 5.1: Typical DPF inlet temperature profile for periodic loading and regeneration cycles.

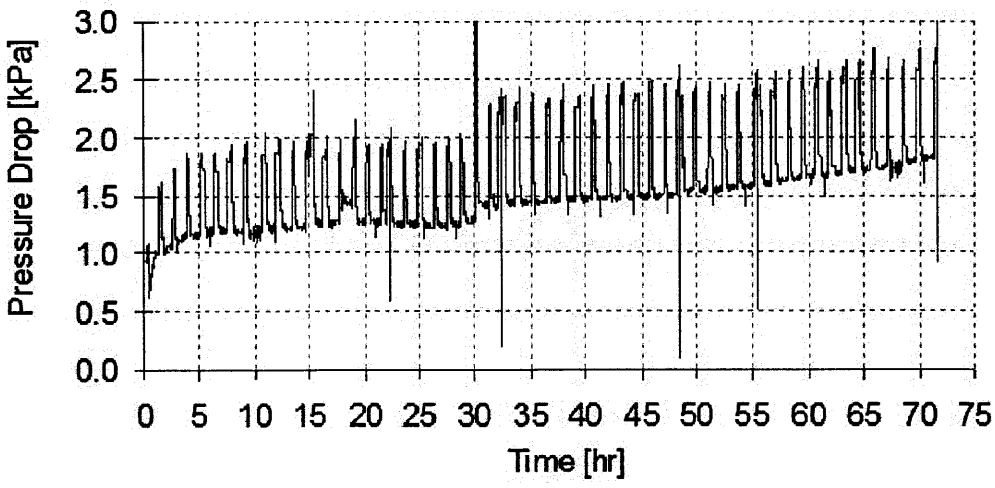

Figure 5.2: Typical DPF pressure drop profile for periodic loading and regeneration cycles.

Periodically throughout the loading procedure the filter assembly is removed from the system and weighed on an Acculab VA-12KG balance with a 0.02g resolution. Weighing the filter is performed to

establish the mass of accumulated ash within the filter determining its ash load. When weighing the filter it is essential to ensure the entire filter is at a temperature above 100°C producing the inability for water vapor collection to occure which would create inaccuracies in the ash load determination. Paired with the determination of a given ash load, a room temperature space velocity test was performed to determine the filter's corresponding pressure drop.

It can be seen in figure 5.2 that overtime the average pressure drop increases due to the elevated amount of ash accumulation within the filter throughout the experiment. It is also interesting to note that the average pressure drop increases much more rapidly during the beginning of the experiment. This is due to the process of depth filtration by the filter at the initial loading stages, which as previously mentioned has a higher effect on pressure drop.

5.4 Soot Loading

The Cummins ISB engine was used to soot load the DPFs and quantify the performance degradation. These soot tests were performed on both clean and various stages of ash loading filters. The engine provided both a means to compare the negative effects on DPFs from engine out soot and ash from the accelerated loading system, as well as a means to test ash loaded filters with real engine exhaust and PM.

Soot loading occurred at three stages of filter ash loading including clean (0 g/L), half loaded (~12 g/L) and fully loaded (~24 g/L). The soot loading procedure consisted of four stages of soot loading which can be seen in table 5.5.

Soot Stage	Loading Duration	Engine Load	Approximate Soot Load	Approximate Soot Loading Rate
1	30 minutes (30 total)	224 N/m	2 g/L	3.5 g/L per hr
2	60 minutes (90 total)	225 N/m	3 g/L	1.0 g/L per hr
3	90 minutes (180 total)	226 N/m	4.5 g/L	1.0 g/L per hr
4	105 minutes (285 total)	227 N/m	6 g/L	0.86 g/L per hr

Table 5.5: Soot loading procedure conducted on clean and ash loaded filters.

In between each soot loading stage the filter was weighed at an elevated temperature above 100°C to determine the extent of PM accumulation. Once the soot load was determined, a room temperature space velocity test was conducted to determine a DPF pressure drop associated with the extent of soot (and ash if present) in the filter.

This soot loading procedure provides a thorough analysis of DPF degradation of at various levels of PM loading. It also provides data on the synergistic effects of ash and soot subsequently loaded on a DPF. This research aims to determine the combined effects of soot loading on top of ash layers derived from different lubricant chemistries.

5.5 Filter Post Mortem Analysis

After all of the performance degradation characteristics have been identified through the ash and soot loading, a thorough post mortem analysis was conducted on each of the test filters. This post mortem analysis allowed for the measurement and characterization of ash morphology, properties and distribution along the DPF channels. A similar post mortem analysis was conducted on field samples to produce a proper correlation to the accelerated loading samples. The results of this post mortem analysis provide valuable information which correlates lubricant chemistry, exhaust conditions and thermal history to the measureable ash properties which directly relate to DPF pressure drop as described in section 3.

5.5.1 Laboratory Aged Filters

All of the filters loaded with ash by means of the accelerated ash loading system for this research were subjected to the post-mortem analysis. Table 5.6 describes the various filters and lubricants with an associated on-road equivalent aging estimate.

Lubricant	Filter Type	Ash Load (g/L)	Regeneration Type	Equivalent On-Road Aging
Base Oil + Mg	CDPF - Pt	23.8	Periodic	170k mi.
Base Oil + Ca & ZDDP	CDPF - Pt	25.02	Periodic	175k mi.
Base Oil + Mg & ZDDP	CDPF - Pt	11.8	Periodic	65k mi.
Base Oil + Mg & ZDDP	CDPF - Pt	22.67	Periodic	165k mi.

Table 5.6: Laboratory-aged filters subjected to post-mortem analysis.

5.5.2 Ash Measurements

The same post-mortem procedure was performed on each of the laboratory loaded filters. Once the fully loaded filter is removed from the canning assembly, it is axially cut in half. One of the halves is preserved for future testing and analysis while the other is further segmented into smaller pieces for examination. Figure 5.3 depicts how the analyzed half is further segmented.

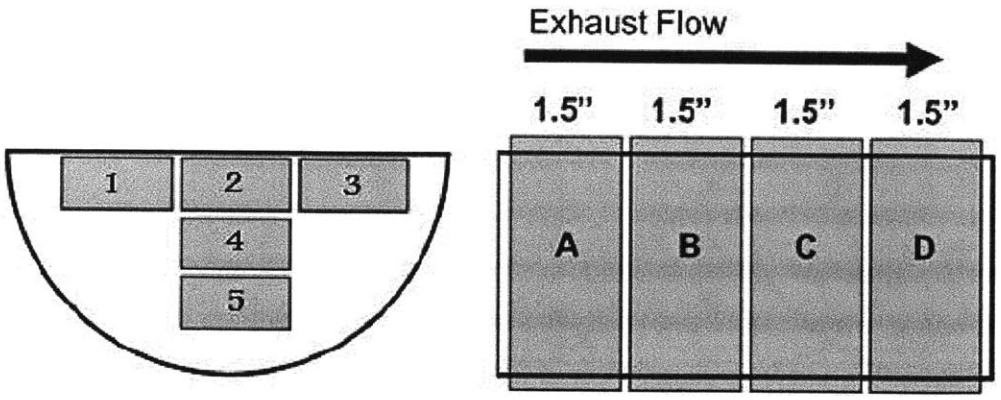

Figure 5.3: DPF post-mortem segmentation.

Each filter half was segmented axially into four 1.5 inch long sections. The axial sections were further divided into five radial samples. Each of these five samples contains approximately 140 to 200 cells and was 1.5 inches in length. Therefore each tested filter in divided into a total of 20 samples providing the ability to determine the radial and axial distribution of the determined ash characteristics.

For each of these samples, ash layer thickness, hydraulic diameter, accumulated ash volume and packing density were determined. To determine the ash layer thickness two images were taken per sample, one for each face of the sample. Figure 5.4 provides an example of an image from a sample face.

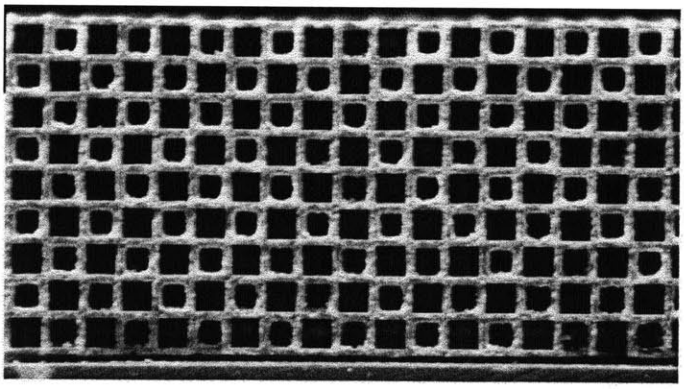

Figure 5.4: Example of an image taken of the face of a filter sample.

Because there were images taken of the inlet and outlet faces of the filter samples, a total of fourty images were taken per filter. To accurately determine the average ash layer thickness and hydraulic diameter for each sample face, the images were zoomed in and analyzed with commercially available processing software. An example of the zoomed in image marked with the measurements taken can be seen in figure 5.5.

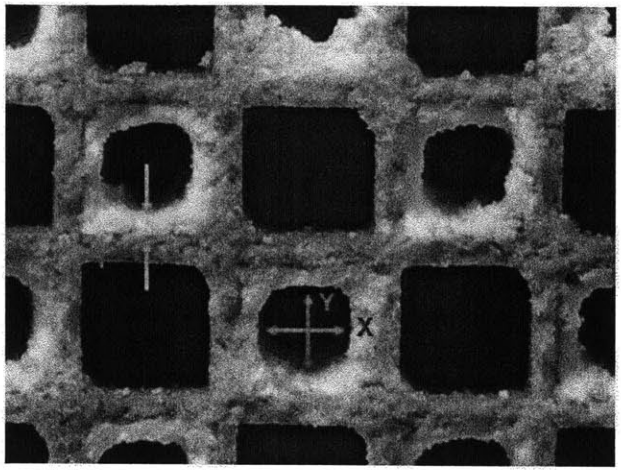

Figure 5.5: Example of zoomed in image and marked measurements taken.

Two measurements were taken on each loaded channel. To accurately determine the ash layer thickness and hydraulic diameter of the entire sample face, 50-75% of the sample's loaded channels were measured and averaged. Aside from the loaded channels, 3 clean channels were measured and averaged to determine their corresponding dimensions. For the samples taken from the outlet end of the entire filter, denoted by "D" in figure 5.3, the loaded channels were completely filled with an ash plug. To determine the amount of ash contained within one of these plugged channels, the clean channel dimensions were used assuming all of the available channel volume contained ash. Knowing the average ash layer thickness of each sample face, the layer distribution of the sample can be determined assuming a linear trend. By combining the distributions of all 20 samples, the reconstruction of the axial and radial ash layer distributions for the entire filter can be completed.

The ash volume contained within each sample was also determined. By measuring the average ash layer thicknesses on both sample faces, the volume of ash within a channel can be determined knowing the sample's length and assuming a linear axial layer distribution. Using this calculated ash volume within a single channel along with the number of loaded channels per sample; the volume of ash within the entire sample can be calculated. Similarly to layer thickness, the ash volume of the "D" samples was determined by using the available volume of a clean channel in conjunction with the number of loaded channels per sample. After calculating the ash volume contained in each of the 20 samples, the ash volume distribution of the entire filter can be reconstructed in the radial and axial directions.

Aside from determining the ash distribution profile, ash packing density was also calculated. The determination of ash plug and layer packing density utilized the ash volume calculations and the following process:

1. Inlet and outlet face of each sample imaged and analyzed as described above
2. Ash loaded filter sections weighed
3. Ash tapped out (~ 5 minutes)
4. Samples imaged and reweighed
5. Ash blown out using compressed air
6. Clean filter sections weighed
7. Packing density computed from known ash volume and ash weights

For filter samples that did not contain an ash plug, step 4 in the above process was omitted. The imaging and reweighing of the sample after the ash plug is removed provides the ability to determine the packing density gradient between the ash plug and the ash layer. Similarly to the ash layer thickness and volume calculations, the determination of packing density for all 20 samples was utilized to reconstruct the packing density distribution of the entire filter.

Some of the ash collected from step 3 of the above packing density procedure was then used for a XRD analysis. The resultant spectrum of the XRD analysis was analyzed to determine the compounds composing the tested ash. The relative intensity ratio (RIR) of each of the compounds within the ash provides a percentage of abundance for each compound relative to one another. As well as the RIR, each of the compounds within the ash has a true density which was determined from past research on that individual compound. These variables were then used to calculate the theoretical density of the ash by:

$$\rho_{Theoretical} = \sum_n \rho_{TRUE}^n \times RA \tag{6.1}$$

where the ash theoretical density, $\rho_{Theoretical}$, is the sum of all of the compounds true densities, ρ_{TRUE}^n, multiplied by their respective abundance percentage, "RA". Using this in conjunction with the determined ash packing density, ash porosity can be determined by:

$$\varepsilon = 1 - \frac{\rho_{Packing}}{\rho_{Theoretical}} \tag{6.2}$$

where ε is the ash porosity, $\rho_{Packing}$ is the ash packing density and $\rho_{Theoretical}$ is the ash's theoretical density calculated from equation 6.2. It should be noted that the ash particles comprising the agglomerates and accumulated structures are likely to be porous or hollow. These porous particles relate to determined ash porosities in upward of 90 – 95% [50]. Because of this, it has been noted that

the porosity determined from equation 6.3 must be corrected to account for porous and/or hollow particle structures before being applied to permeability calculations.

Lastly, core samples of the DPF were subjected to a SEM-EDX analysis. Two samples per filter were removed, one ash layer taken from section "B" in figure 5.3, and one of the ash plug taken from section "D". These filter samples were then impregnated with epoxy, polished and coated with 9nm of carbon. These samples were then analyzed using SEM imagery to determine the extent of depth filtration, confirmation the ash layer thickness, and to observe the particle and agglomerate structure. Using the EDX function of the microscope, mapping images for individual elements were taken for the ash layers. These mapping images provide information on the elemental composition and distribution within the ash at the microscopic level.

The post-mortem analysis conducted after the ash loading and performance evaluation provides a variety of data pertaining to ash composition, morphology and distribution. These determined variables were expected to differ among various lubricant chemistries and then related back to the DPF performance determined during the experimentation phase.

(This page intentionally left blank)

6 ASH CHEMISTRY IMPACT ON DPF PRESSURE DROP

This section will present and describe the experimental results found through this research. Table 5.6 describes the four test cases that were conducted and analyzed. The lubricant formulations used were chosen to expand on the research conducted by A. Sappok in 2009.

The results for the laboratory loaded filters during the performance and evaluation phase described a number of valuable characteristics including ash effects on pressure drop as well as pressure drop sensitivity to soot loading on top of ash layers. The post mortem analysis on each filter helps determine and quantify ash characteristics such as layer thickness and packing density, plug length and packing density, elemental distribution, extent of depth filtration as well as composition.

6.1 Variability Studies

Before the experimental results are presented, it is important to determine and quantify any variability that may influence the accuracy of the results. Two variability tests were conducted to determine the variations in measured filter mass, thus determined ash and/or PM accumulation, as well as witnessed pressure drop from the conducted space velocity tests.

6.1.1 Filter Mass Variability

Through the experimental procedure described in the previous chapter, the filter is weighed numerous times to determine the extent of ash and/or PM accumulation in the filter. To ensure the accuracy of these results, it is important to quantify how both the experimental instrumentation and procedure affect these measurements.

The procedure of the mass variability test was as follows:

1. Weigh the ash accumulated filter at room temperature
2. Weigh calibration mass of 7 kg on the scaled used for the filter
3. Regenerate the filter to a filter inlet face temperature of approximately 700°C
4. Remove the filter and probe the filter with a thermocouple along its centerline and outer edge to measure filter's temperature gradient. The thermocouple probe extended 2 inches into the filter.
5. Weigh the filter while it is hot
6. Repeat step 4
7. Repeat steps 3-6 at a number of filter temperatures

This procedure quantifies both the scale's repeatability as well as the effects of filter temperature on DPF mass. The above procedure was conducted 3 times providing a total of 24 filter mass measurements at various temperatures. As previously mentioned, the filter is weighed at elevated temperatures above 100°C numerous times to quantify its accumulated ash and/or PM load. In the case of ash loading, the filter is weighed immediately after it experiences a regeneration cycle in which its temperature could be upwards of 700°C. The specific temperature that the filter is weighed at is determined by the user based off their specific tolerance to heat. Because of this, it is feasible that the filter could be weighed throughout the experiment at a temperature range of 100 - 700°C which may cause some possible variation in its measured mass. The calibration weights used to ensure scale repeatability were chosen to be 7kg because this is the approximate weight of the combined filter and canning assembly which was loaded. The filter used in this variability study was a cordierite, Pt-catalyzed DPF with an ash load of 22.7 g/L. To determine the filter's centerline and outer temperatures, a 2 inch K-type thermocouple was probed 2inches into respective centerline and outer channels of the filter. A 3 inch thermocouple probe was initially used to determine the core temperature of the six inch long filter, but became very ductile at elevated temperatures and proved to be difficult to manipulate to obtain the desired measurements. It should also be noted, that the filter was probed with the K-type thermocouple on the outlet filter face to ensure that no part of the filter's ash layer was disturbed.

An Acculab VA-12KG balance with a 0.02g resolution was used for the measurements throughout the experiment. This resolution is high enough for the filter assemblies used which are typically on the order of 7kg. Step 2 of the above procedure proved that the scale was extremely repeatable. After using the same calibration weights in triplicate on 3 separate days, the measured values only differed 0.02g. This confirms that the instrumentation used to determine the filter's ash and/or PM accumulation is accurate and repeatable.

Through the 24 mass measurements as a function of filter temperature, the same general trend was seen. As the filter's temperature is increased, the observed mass decreases. The slopes of the three test cases can be seen in figure 6.1. These slopes were generated by plotting only the first and last data point, lowest and highest temperature, for each of the three tests cases.

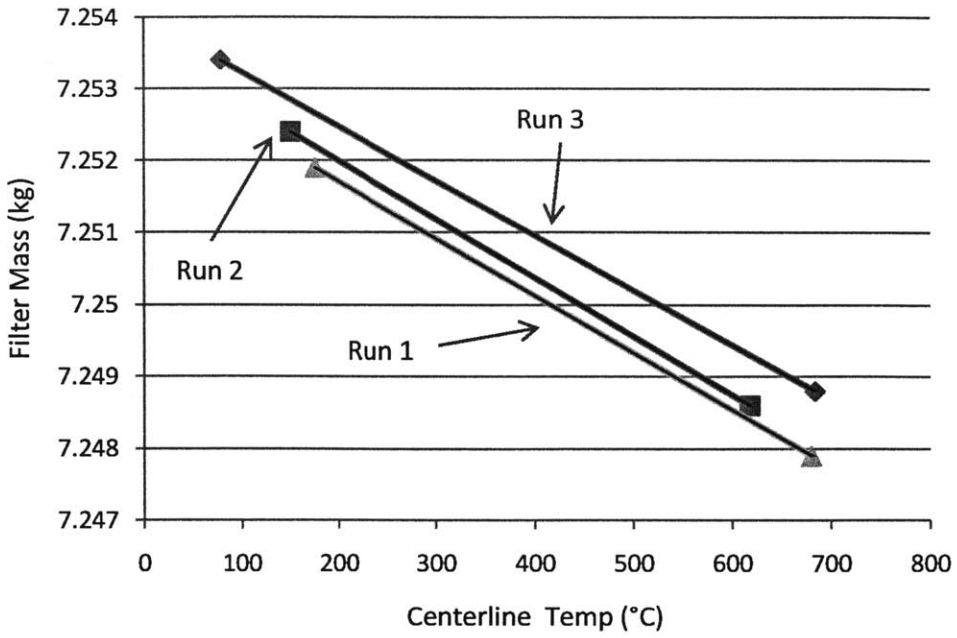

Figure 6.1: Filter mass versus temperature slopes for the three test runs.

It can be seen that the three tests conducted have very similar slopes relating to a mass variability of approximately 5 grams for our measured temperature range of 100-700°C.

Figure 6.2 presents the measured filter centerline and edge temperatures for one of the three experimental runs.

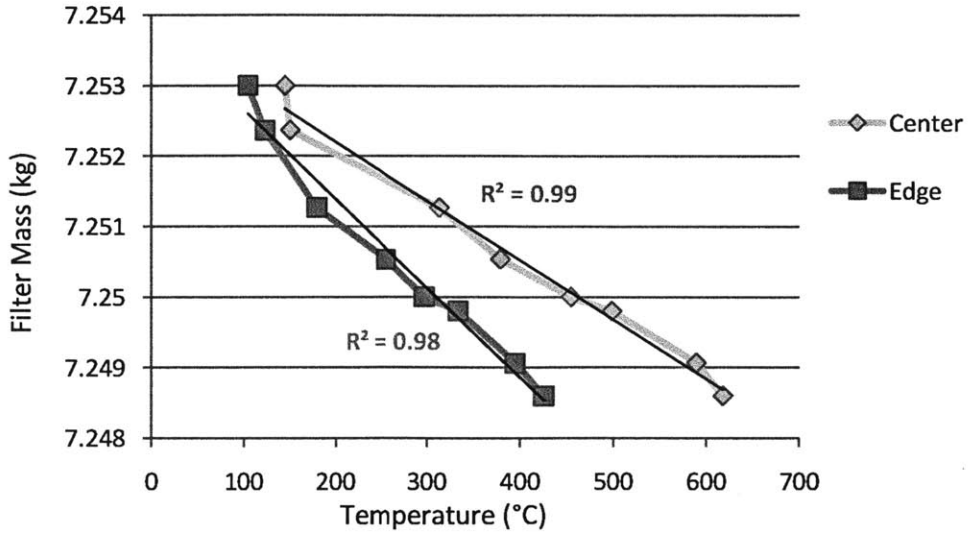

Figure 6.2: Filter mass as a function of filter edge and centerline temperatures for run 2 of mass variability test.

Figure 6.2 describes that for a given filter temperature for a heated filter, the filter's edge is substantially cooler than the filter's core. Over the course of this variability test, the edge versus centerline temperatures ranged from 25°C - 200°C with the larger differentials witnessed at the higher mean filter temperatures. Intuitively this makes sense because as the filter temperature increases through a regeneration cycle, the hot exhaust gases flow through the entire filter increasing the filter's mean temperature. Once the hot exhaust gases cease to flow through the filter, the outer surface of the cylindrical filter witnesses the largest temperature differential being in close contact with the ambient air temperature. Because the filter is ceramic, it has a low heat transfer coefficient which in turn would keep the centerline at an elevated temperature. Once the filter is cooled by ambient air, the filter has the ability to becoming more uniform in temperature resulting in a lower edge-to-centerline temperature differential.

As seen in figure 6.1, the results of this mass variability test present a possible 5 gram mass disparity at the temperature range in which the filter's mass could be measured during this research. As described in the literature, the reason for this trend is due to the hot, less dense air being contained in the filter producing a small buoyant force within the filter. This buoyant force will reduce the apparent mass of the filter witness by the scale [76]. Because of this possible mass variability, all ash and/or PM loads described in the following results of this research have a possible variation of ± 2.02 g/L. A detailed list of all of the data within the variability study as well as all of the individual graphs for each run can be found in the appendix table A-1 and appendix figure A-1.

6.1.2 Measured Pressure Drop Variability

Throughout the experimental process, a standard 6-point space velocity test was conducted approximately 20-25 times to quantify the pressure drop for a given filter condition. These tests are conducted at room temperature with ambient air to easily estimate the properties of the working fluid within the filter. If the filter's condition is not altered between space velocity tests they should produce the same results.

The purpose of this test was to determine the variability, thus leading to the quantification of possible experimental error, for the pressure drop measurements stemming from the space velocity tests. The variability experimental procedure was as follows:

1. Weigh the filter at room temperature
2. Perform a space velocity test at room temperature
3. Heat filter to an inlet face temperature of 650°C

4. Let filter cool with ambient air until inlet face temperature is 100°C
5. Perform space velocity at inlet face temperature of 100°C

The above procedure was conducted once a day for three days. This experimental procedure quantified both the space velocity variability for a given ash load, as well as the effects of filter temperature on space velocity measurements. As previously mentioned, the space velocity measurements were taken when the filter inlet face was at room temperature. After the filter mass variability experiment was conducted, it was determined that a filter with a room temperature inlet face could very possibly have an inner core temperature of 80-100°C. Because of this, it was determined that the effects of "hot air" space velocity tests must be considered. Figure 6.3 displays the results from the 3-day space velocity variability tests.

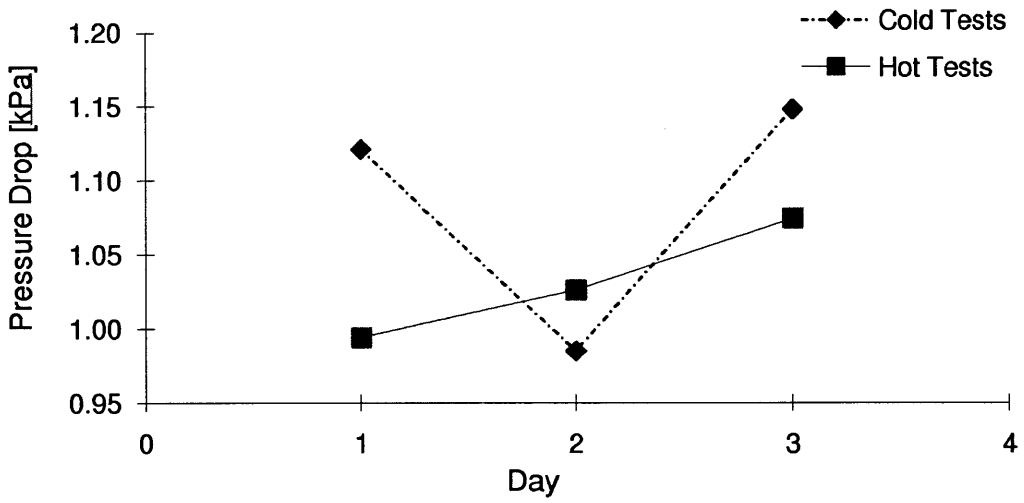

Figure 6.3: Pressure drop day-to-day variability for a given ash load from both room temperature and hot space velocity tests.

The filter used for this space velocity variability test was loaded to 22.7 g/L of ash. It can be seen from figure 6.3 that for a given ash load the pressure drop has a variability of approximately 0.16 kPa. It was interesting to note that although the "hot" space velocity test results differ from those at room temperature; they fell within the overall day-to-day variability of the room temperature results and therefore slightly elevated filter temperatures are not a large factor of possible error. The various space velocity graphs for each of these tests can be seen in the appendix figure A-2 for the interested reader.

6.2 Lubricant Chemistry Specified Ash Effects of on Pressure Drop

This research paired with previous studies attempts to identify the effects that individual lubricant additives as well as additive combinations have on DPF performance. As previously mentioned, this research expands on that conducted by Sappok in 2009. The experimental methodology, procedure and post mortem analysis were identical allowing for direct comparison of the two sets of results. Table 6.1 presents the test cases which were compared.

Lubricant	Filter Type	Ash Load (g/L)	Regeneration Type	Past Research
Base Oil + Ca	CDPF - Pt	29	Periodic	Sappok
Base Oil + ZDDP	CDPF - Pt	28	Periodic	Sappok
Base Oil + Mg	CDPF - Pt	23.8	Periodic	
Base Oil + Ca & ZDDP	CDPF - Pt	25.02	Periodic	
Base Oil + Mg & ZDDP	CDPF - Pt	11.8	Periodic	
Base Oil + Mg & ZDDP	CDPF - Pt	22.67	Periodic	
CJ-4	CDPF - Pt	42	Periodic	Sappok
CJ-4	CDPF - Pt	12	Periodic	Sappok

Table 6.1: Compared test cases conducted as part of this research and by Sappok in 2009.

As far as past research on the effects of individual additives are concerned, base oil + Ca was conducted because Ca-based detergents are the most prevalent in lubricant oils. Base oil + ZDDP was also conducted because ZDDP is the most common multi-functional anti-wear additive. To expand on this individual lubricant test matrix, this research conducted a test on a lubricant formulation of base oil + Mg because although more costly, Mg-based detergents are the second most common detergents manufactured for lubrication oils.

This research also performed tests on specific lubricant formulations containing multiple additives to help understand their synergistic effects. The two combinations chosen were the two detergents individually paired with the ZDDP additive. These combinations were then compared to past research on the fully formulated CJ-4 oil. A fourth test was conducted on a Mg + ZDDP combination only taken to half ash load, approximately 12g/L.

6.2.1 Individual Additive Effects on DPF Pressure Drop

The effect of individual additive-derived ash on DPF pressure drop can be seen in figure 6.4. The three tests compared were the effects of a Ca-detergent, Mg-detergent and ZDDP independently at ash loads from 0 g/L to approximately 25 g/L. As previously mentioned, all of the tested lubricant oils were blended to approximately 1% sulfated ash but the elemental content differed.

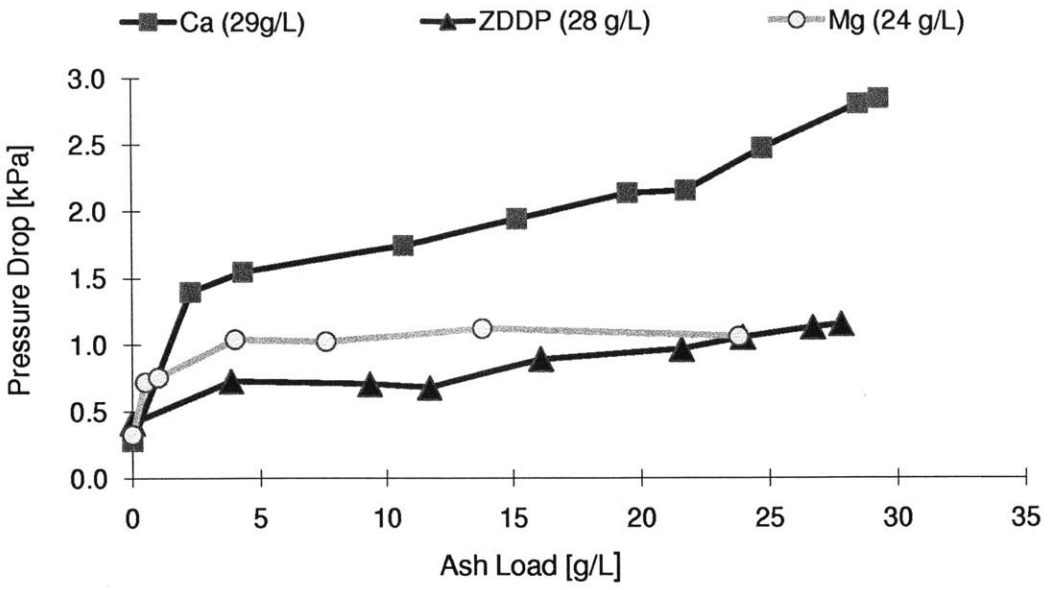

Figure 6.4: Pressure drop trends as a function of ash load for lubrication oils formulated to 1% sulfated ash with individual lubricant additives of Ca & Mg-based detergents and ZDDP respectively. Test results from base oil + Ca and base oil + ZDDP taken from [50].

It can be seen from figure 6.4 that the lubricant composed of the Ca-based detergent creates the highest pressure drop increase as a function of ash load. On the other hand, the base oil + ZDDP and the base oil + Mg lubricant formulations have substantially smaller pressure drop increases compared to that of the base oil + Ca test.

Both the calcium and magnesium cases display very rapid initial pressure drop increases which is representative of depth filtration. The effects of depth filtration are much less pronounced for the ZDDP test case. It is evident from the ash load at the end of this rapid increase that all three oils produce relatively similar amounts of ash contained within the filter's pore matrix. Though it will be discussed in more detail later, it was observed through the post mortem analysis that only the surface pores of the channel substrate performed ash collection and there was relatively no deep penetration of ash. In fact, although the surface pores of the substrate collected some ash, this ash "depth filtration" largely results from ash simply covered the pores with very little penetration into the substrate at all. The pressure drop differences between these three cases after the cake layer begins to form are likely related to ash particle packing density and permeability. The morphology and packing characteristics of the magnesium and ZDDP cases should differ greatly from those of the calcium case which would account for the lower pressure drop increase after similar amounts of ash are trapped in the filter pores during depth filtration.

It is also interesting to note the differences between how the ash cake layer build up affects the DPF pressure drop. Figure 6.5 graphs the cake layer build up trends for each individual additive test case and applies a linear trend line for slope analysis.

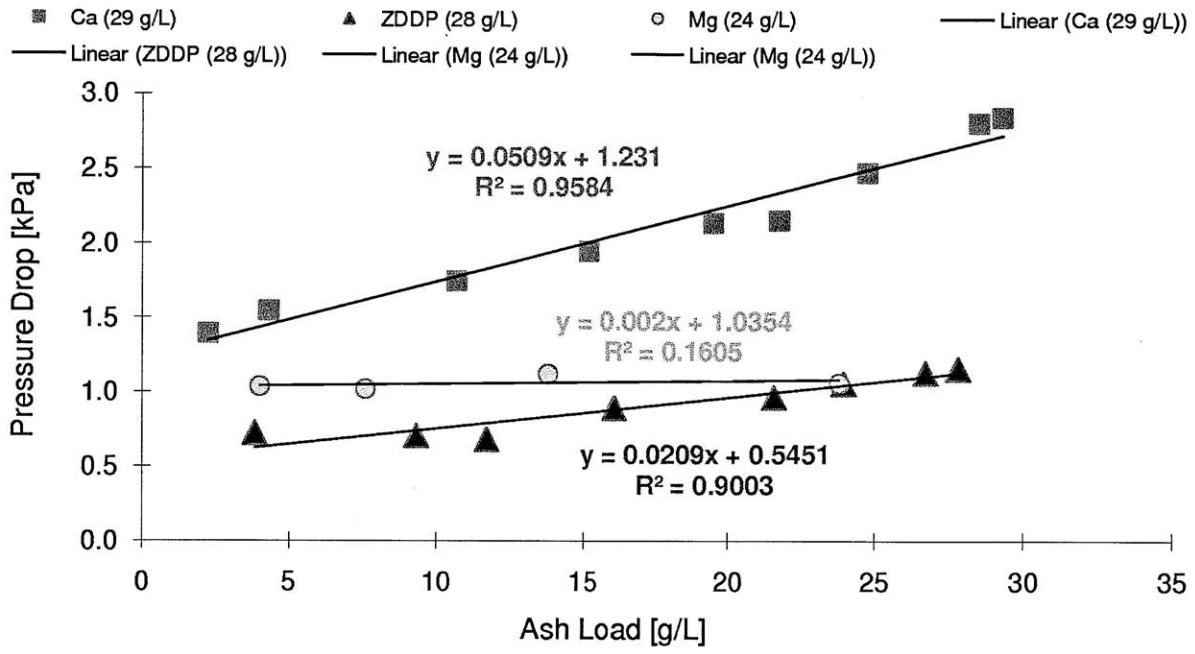

Figure 6.5 :Pressure drop trends as a function of ash load for cake layer build up from lubrication oils formulated to 1% sulfated ash with individual lubricant additives of Ca & Mg-based detergents and ZDDP respectively. Cake layer pressure drop slopes presented. Test results from base oil + Ca and base oil + ZDDP taken from [50].

It can be seen from the cake layer pressure drop slopes that the calcium case produces a higher pressure drop increase for a given amount of added ash compared to the magnesium and ZDDP cases. The magnesium case has an extremely low slope representing that the cake layer build up has little impact on the pressure drop increase of the filter. The initial hypothesis for these trends relate to the packing characteristics and permeability of the cake layer. It is intuitive to assume that the calcium cake layer packs in a manner that produces a higher resistance to air flow whereas the magnesium and ZDDP cases pack in a manner that only slightly restricts air flow. This could be based off particle shape in which spherical particles pack closer together whereas abnormal shapes create a more porous ash layer.

6.2.2 Additive Combination Effects on DPF Pressure Drop

The effect of ash generated from combinations of specific additives on DPF pressure drop can be seen in figure 6.6. The three test cases include a Ca-detergent plus ZDDP, Mg-detergent plus ZDDP and a fully-formulated CJ-4 oil each at ash loads from 0 g/L to approximately 25 g/L. As previously mentioned, all of

the tested lubricant oils were blended to approximately 1% sulfated ash but the elemental content differed.

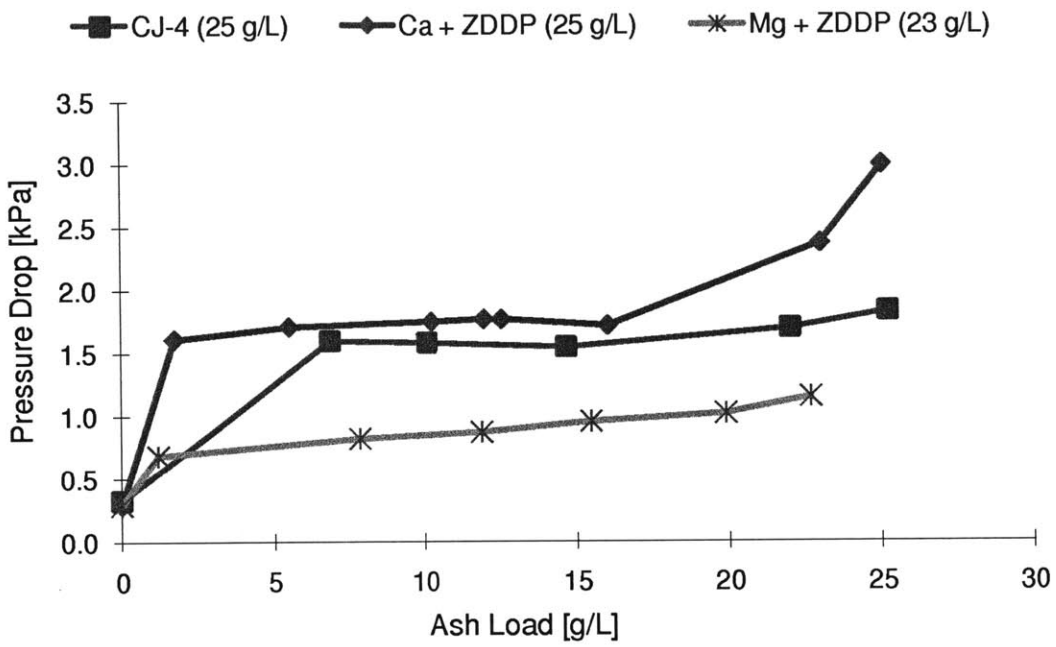

Figure 6.6:Pressure drop trends as a function of ash load for lubrication oils formulated to 1% sulfated ash with combinations of lubricant additives; Ca & Mg-based detergents +ZDDP and CJ-4 respectively. Test results for CJ-4 taken from [50].

It can be seen from figure 6.6 that the lubricant oils containing a Ca-based detergent, CJ-4 and Ca plus ZDDP, display the highest pressure drops as a function of ash load. The Mg plus ZDDP case produces a substantially lower pressure drop compared to the other combinations tested. Taking the individual additive and combination tests into consideration, it seems that the Ca-based detergent provides the largest increase in DPF pressure drop.

All three test cases display rapid initial increases in pressure drop which can be contributed to "depth filtration". The extent of this rapid pressure drop increase seems to stop at approximately 2g/L ash accumulation for the Ca +ZDDP and Mg +ZDDP cases. The lack of data points between 0 g/L and 5 g/L ash for the CJ-4 case creates an inability to determine the transition of depth to cake filtration and the resulting pressure drop characteristics. Similar to the individual additive cases, the mass of ash accumulated during depth filtration is comparable in all test cases, therefore making the in-pore packing and the particle characteristics of the pore covering ash the likely cause of the pressure drop differences between the test cases. As far as pressure drop magnitude is concerned, the additive combinations

display traits similar to those expected after the individual additive tests were complete. The Mg plus ZDDP case displays pressure drops similar to a combination of the Mg and ZDDP individual tests where the Ca plus ZDDP case resembles a combination of the Ca and ZDDP tests individually.

It is also interesting to note the differences between how the ash cake layer build up affects the DPF pressure drop. Figure 6.7 graphs the cake layer build up trends for the additive combination tests and applies a linear trend line for slope analysis.

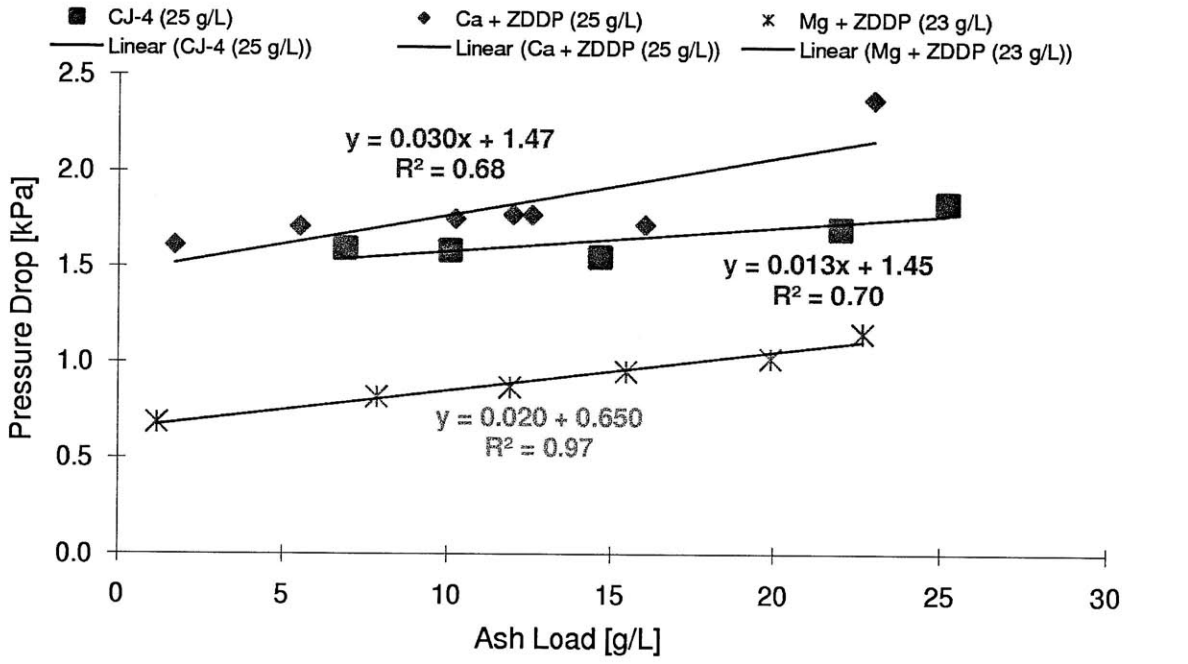

s

Figure 6.7: Pressure drop trends as a function of ash load for cake layer build up from lubrication oils formulated to 1% sulfated ash with additive combinations of Ca +ZDDP, Mg +ZDDP and CJ-4 respectively. Cake layer pressure drop slopes presented. Data for CJ-4 test taken from [50]

Figure 6.7 displays how the ash addition onto the ash cake layer affects the overall pressure drop of the DPF. It can be seen that the Ca plus ZDDP case has the largest slope of all the additive combination tests resulting in the largest pressure drop increase for a specified increase in ash accumulation. It is interesting to note that one of the synergistic additive effects is that the cake layer pressure drop slopes tend to balance out between one another compared to those of the individual additives. For the additive combinations, the majority of the differences in the pressure drop magnitudes as a function of ash load reside in the "depth filtration" range of 0 g/L to 3 g/L. This may relate to the synergistic effects that additive combinations have on cake layer packing density and permeability.

For comparison purposes, the individual additive pressure drop curves were plotted alongside those of the additive combinations in figure 6.8. It can be seen that the aforementioned trend holds true that the lubricant formulations containing a Ca-based detergent display the highest pressure drop for a given ash load mostly due to its extreme pressure drop increase within the depth filtration regime.

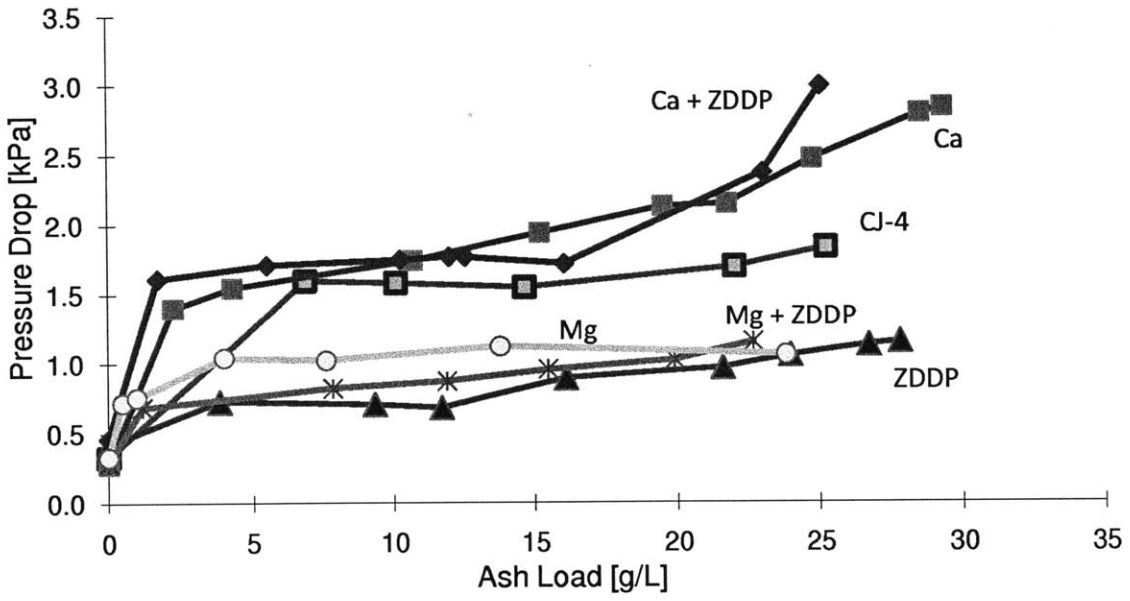

Figure 6.8: Pressure drop trends as a function of ash load for all lubricant formulations blended to 1% sulfated ash. Test results for CJ-4, Base + Ca and Base + ZDDP taken from [50].

Detailed graphs for each individual test case run throughout this research as well as space velocity curves for each pressure drop data point can be found in the appendix figures A-3 through A-5.

6.3 Combined Soot and Ash Effects on DPF Pressure Drop

As previously mentioned, the majority of the engine out PM is composed of soot. As the soot is trapped in the DPF, the pressure drop across the filter is affected. Overtime as the soot is regenerated the incombustible ash remains and builds a cake layer along the channel walls. While this ash is retained in the filter, soot is constantly being deposited on top of the ash layer. Because of this it is important to determine the impact of ash plus soot in the DPF on the filter's pressure drop.

When soot is loaded on a clean DPF, the pressure drop follows a similar trend to that described during ash loading. Throughout the initial loading stage, a steep rise in pressure drop is observed due to soot depth filtration. As a cake layer of soot begins to form and grow, the pressure drop gradually increases

with the addition of PM at a rate substantially less than that observed during depth filtration. Figure 6.9 presents the DPF pressure drop as a function of PM load on a clean filter with no substantial ash accumulation. It is important to distinguish that in field applications ash and soot are always deposited in the DPF together. As previous mentioned, typical engine out PM contains approximately 1% incombustible ash by mass while the remaining 99% is typically soot. After this PM is accumulated in the DPF the soot portion of the PM can be regenerated while the incombustible ash remains. Although through this research the effects of ash and soot are measured separately, they are deposited together and it is important to distinguish this fundamental difference.

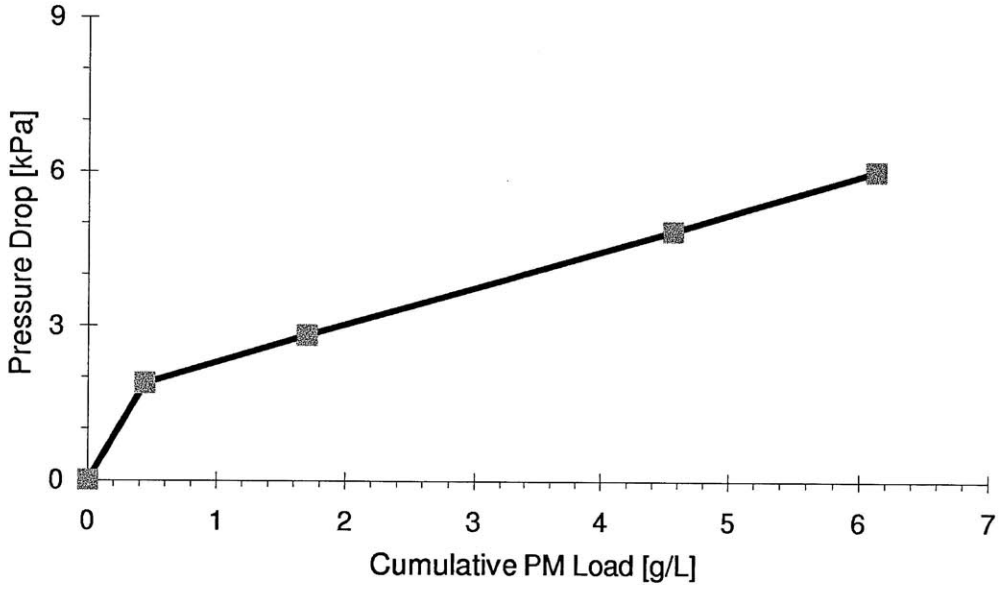

Figure 6.9: Pressure drop trend as a function of PM load for a DPF with no ash accumulation.

Ash derived from various lubricant chemistries contain different material properties and packing characteristics. These various ash characteristics likely influence the combined effects on DPF performance that soot has on ash cake layers.

6.3.1 Soot and Individual Additive Ash Effects on Pressure Drop

Figure 6.10 presents a summary of data on the combined effects of soot and ash derived from the single additive test cases. The pressure drop profile for a DPF with no ash accumulation is also displayed for comparison. In all of the test cases, DPFs containing ash show higher levels of pressure drop with no soot accumulation relative to the clean case. This initial pressure drop difference at 0g/L PM accumulation is due to the ash deposits alone. Furthermore, the presence of an ash layer provides a physical barrier which presents depth filtration of accumulated soot.

For the filter with no ash present, soot depth filtration is clearly visible by the rapid pressure drop increase between 0 g/L and 0.5 g/L of accumulated PM. On the other hand, the ash pre-loaded filters do not display this rapid pressure drop increase and the physical ash barrier prohibiting soot depth filtration is beneficial from a pressure drop perspective at low soot loads. Instead of the soot accumulating in the filter pores further increasing the pressure drop rapidly, it seems to build a second cake layer on top of the ash cake layer already formed.

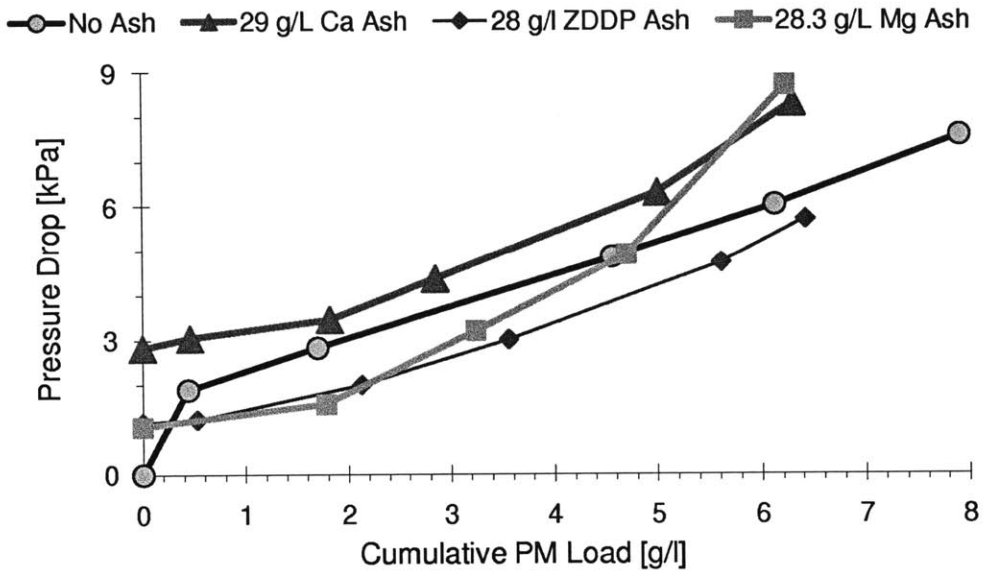

Figure 6. 10: Pressure drop as a function of soot load on Pt-catalyzed DPFs fully loaded with ash derived from single additives. Data for Base + Ca and Base + ZDDP cases taken from [50].

All of the test cases displayed similar trends. Of the three single additives tested, the calcium ash had the largest pressure drop at the final stage of ash loading. Because of this, the initial pressure drop point at 0g/L of PM accumulation is the highest for the calcium case and substantially lower for the ZDDP and magnesium cases. Because the initial pressure drop was so low for ZDDP and magnesium, the presence of their respective ashes is beneficial at lower PM loads. The extent of pressure drop increase due to depth filtration of the base oil + ZDDP and base oil + Mg ashes is lower than the pressure drop increase due to soot depth filtration. Because of this, from a pressure drop perspective it could be more beneficial to prevent the soot depth filtration with an ash layer and forgo the initial pressure drop difference at 0g/L PM accumulation. This is not the case for the calcium ash loaded filter. Because the pressure drop contributed to depth and cake filtration of ash alone generates such a high pressure drop, the calcium ash cake layer provides no added benefit compared to the clean filter. Individual pressure

drop graphs at various stages of ash loading with corresponding space velocity curves for the base + Mg test case can be found in the appendix figure A-6.

6.3.2 Soot and Combination Additive Ash Effects on Pressure Drop

Figure 6.11 presents a summary of data on the combined effects of soot and ash derived from the test cases using combinations of additives. The pressure drop profile for a DPF with no ash accumulation is also displayed for comparison. Similarly to the cases of single additive derived ash, DPFs containing ash show higher levels of pressure drop with no soot accumulation relative to the clean case. This initial pressure drop difference at 0g/L PM accumulation is attributed to the presence and pressure drop increase witnessed from ash deposits alone.

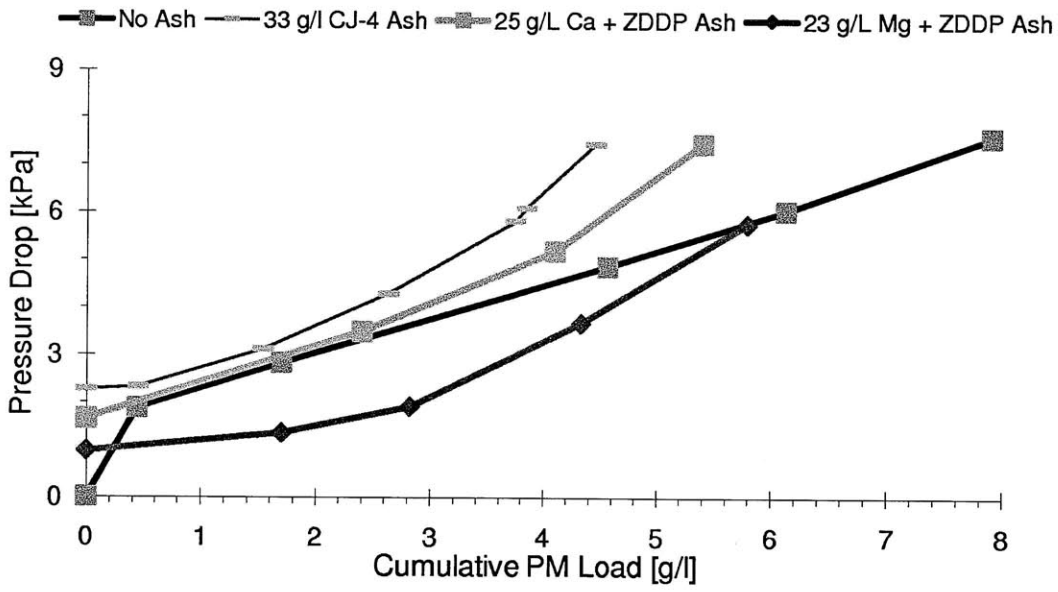

Figure 6. 11: Pressure drop as a function of soot load on Pt-catalyzed DPFs fully loaded with ash derived from additive combinations. Data for CJ-4 case taken from [50].

Similarly to that described in the previous section, all pressure drop profiles follow similar trends. Because the filter fully loaded with Mg + ZDDP ash produces a relatively low pressure drop compared to the other cases, the ash cake layer provides an initial benefit compared to the clean filter by prohibiting the depth filtration of soot. This is not the case with the filters fully loaded with CJ-4 and Ca + ZDDP ash due to their relatively high pressure drop at 0g/L PM accumulation.

Figure 6.12 presents the pressure drop data as a function of soot load for all of the fully ash loaded filters for comparative purposes. In the cases not containing any Ca-based detergent, 6.12 (a), the pressure drop due to full ash accumulation of approximately 25 g/L was relatively low compared to the

other cases. Because of this, the presence of the ash layer provides a benefit from a pressure drop due to soot accumulation because the depth filtration is prohibited. The test cases containing Ca-based detergents, 6.12 (b), prevented soot depth filtration as well, but since the initial pressure drop due solely to the ash was relatively high, it did not provide any added benefit compared to the clean filter case.

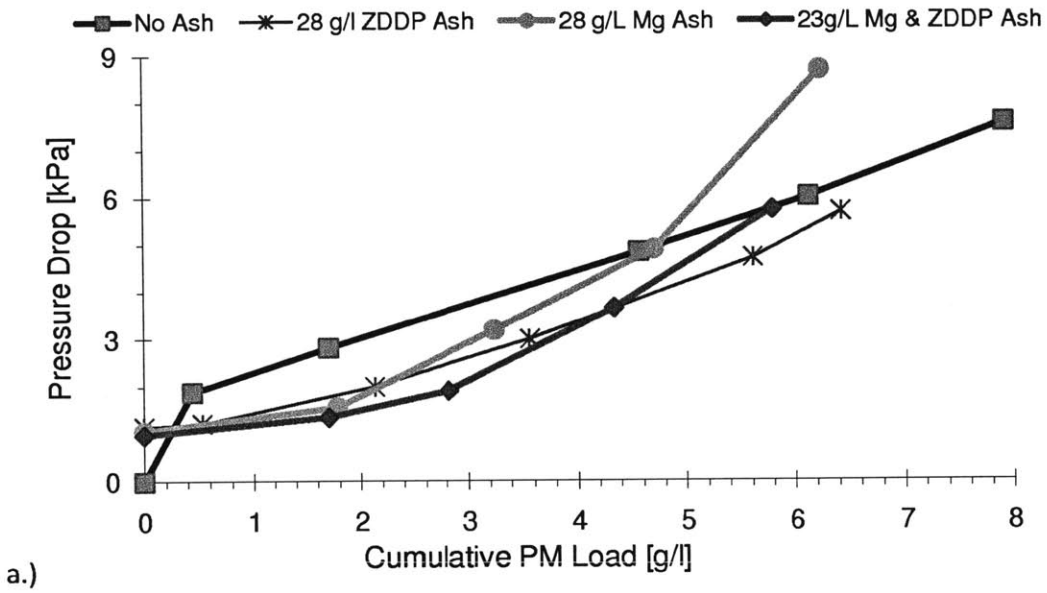

a.)

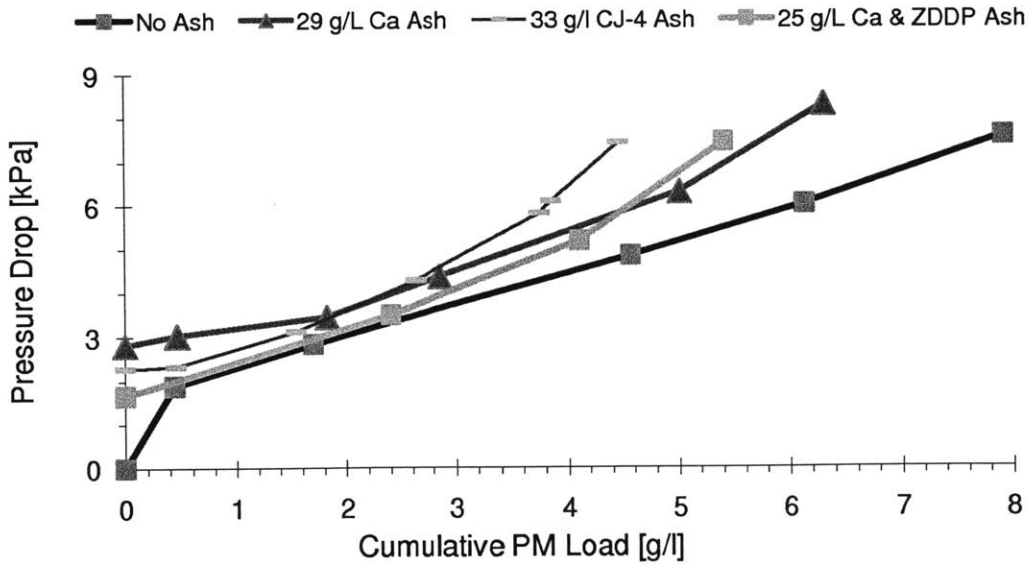

b.)

Figure 6.12: Pressure drop as a function of soot load on Pt-catalyzed DPFs fully loaded with ash for all conducted tests. Data for CJ-4, Ca, and ZDDP cases taken from [50].

A full catalog of graphs for the test case conducted in this research including pressure drop as a function of PM load for various ash loads and space velocity graphs can be found in the appendix figures A-6 through A-8.

6.3.3 DPF Pressure Drop Sensitivity

Figures 6.13 and 6.14 show the pressure drop trends as a function of accumulated PM load for DPFs with and without ash. For both cases, two distinct pressure drop regimes are observed and labeled (I) and (II).

For the fully ash loaded filters, there is a distinct slope alteration which separates the two pressure drop regimes. This slope alteration is seen to occur at approximately 3 g/L of cumulative PM load for all levels of ash loading ranging from 12.5 to 42 g/L [50]. For the clean DPF loaded with PM, the pressure drop regimes are distinguished by two distinct slopes which correspond to the transition from depth to cake filtration at approximately 0.4 g/L of accumulated PM. This is not the case for the fully ash loaded filters due the ash layer's ability to prohibit soot depth filtration.

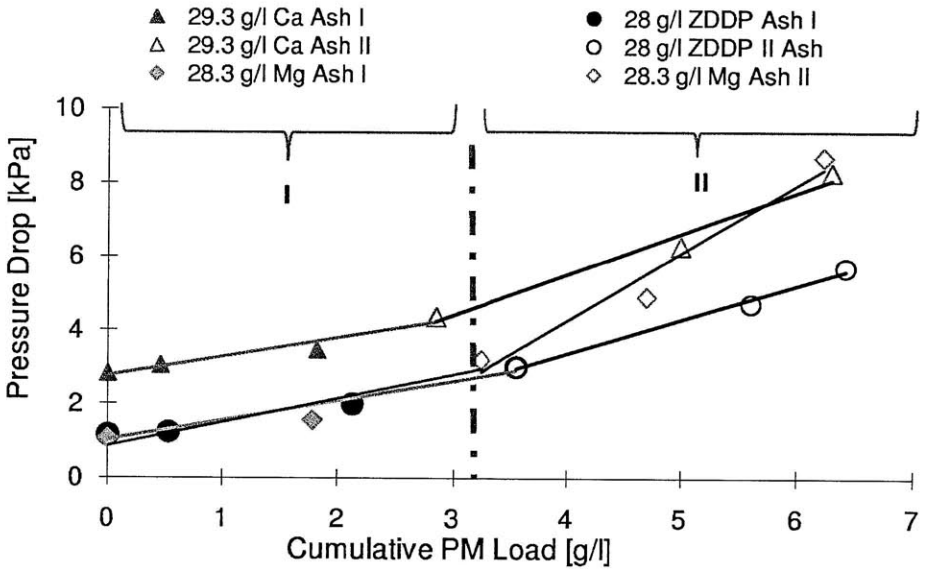

Figure 6.13: Definition of pressure drop regimes (I) and (II) observed with soot accumulation on ash loaded DPFs at 20,000 hr^{-1} space velocity.

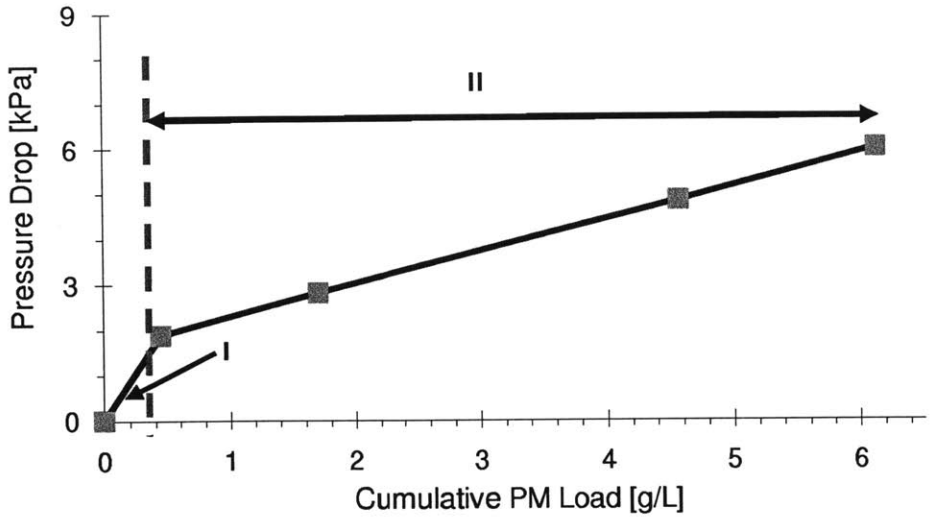

Figure 6.14: Typical depth (I) and cake (II) filtration regimes for soot accumulation in a DPF with no ash at 20,000 hr^{-1} space velocity.

By overlapping the pressure drop profiles for the DPFs with and without ash, comparative pressure drop regimes can be defined. Because the slope transitions for the fully loaded and clean DPFs occur at different points, three regimes are generated and as follows:

- Response to soot loading up to 0.4 g/L
- Response to soot loading from 0.4 → 3.0 g/L
- Response to soot loads in excess of 3.0 g/L

The slopes of the pressure drop curves for ash loaded DPFs, similar to those seen in figure 6.13, define the pressure drop sensitivity to additional soot accumulation within the filter. In this manner pressure drop sensitivity (RPS) is defined as:

$$RPS = \left(\frac{\partial \Delta P}{\partial PM}\right)_{Ash,i} \div \left(\frac{\partial \Delta P}{\partial PM}\right)_{Clean,i} \tag{6.1}$$

which is simply the slope of the pressure drop curve of the ash loaded filter normalized by the slope of the pressure drop curve for the clean filter at the corresponding pressure drop regime, denoted by "i". A RPS value of unity indicates no difference in performance compared to a filter without ash accumulation. An RPS value greater than one indicates an increase in pressure drop sensitivity and values less than one indicates a decrease in pressure drop sensitivity. By directly comparing the RPS of the various tests cases, it can be determined how the accumulation of soot impacts pressure drop for ash cake layers of various compositions. This was completed for all ash loaded filters.

Figure 6.15 compares the RPS for soot accumulated on ash cake layers derived from lubricant oils with a single additive.

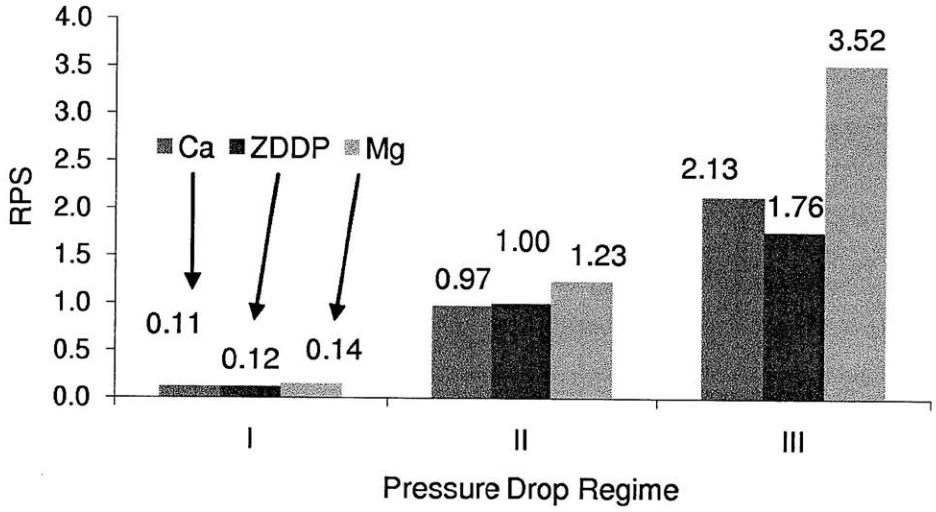

Figure 6.15: RPS comparison for ash layers derived from lubricants containing a single additive. Data for Ca and ZDDP cases taken from [50].

It can be seen from figure 6.15 that for all test cases pertaining to single additive lubricants, the RPS values are extremely low for regime I. This is due to the presence of an ash layer prohibiting the rapid pressure drop increase due to soot depth filtration. It should be noted that these low RPS values describe a lower increase in pressure drop as PM is accumulated, not a lower pressure drop magnitude, compared to a clean DPF. For regime II, the calcium and ZDDP derived ashes produce an RPS similar to that of a clean DPF whereas the magnesium based ash's RPS is higher than one. For soot loads higher than 3.0 g/L, regime III, magnesium has the highest RPS followed by calcium and lastly ZDDP. These results generate the observation that although magnesium-derived ash alone doesn't contribute greatly to pressure drop increase of a DPF, the combined effect of soot and magnesium-derived ash on pressure drop is greater than that of the Ca and ZDDP ash. It is hypothesized that the packing characteristics and morphology of magnesium derived ash interact with soot in a different, more detrimental from a pressure drop perspective, manner compared to the Ca and ZDDP derived ashes. This is likely due to the presence of a substantially larger ash end plug formation for the magnesium based ash compared to the other test cases which drastically decreases each channel's respective filtration area. It has been seen in past research by Sappok that this increased ash plug length has a very large affect on pressure drop response to soot loaded on top of ash layers and since this variable is very different between the test

cases it is likely the cause. Ash transport and distribution differences between the test cases will be described in detail in a subsequent section.

Figure 6.16 compares the RPS for soot accumulated on ash cake layers derived from lubricant oils with various additive combinations.

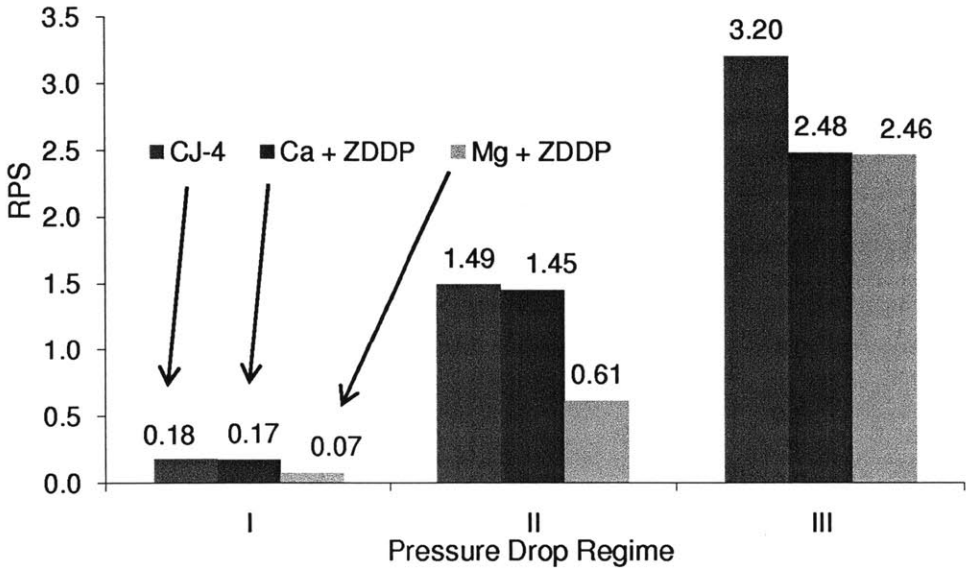

Figure 6.16: RPS comparison for ash layers derived from lubricants containing multiple additives. Data for CJ-4 case taken from [50].

Similar to the regime "I" observations seen in figure 6.15, all test cases pertaining to lubricants with multiple additives have a very low RPS value due to the presence of an ash layer prohibiting the rapid pressure drop increase due to soot depth filtration. The observations seen in figure 6.16 within regimes "II" & "III" are much less predictable. In regime "II" the CJ-4 and Ca +ZDDP lubricants have RPS values greater than one while the Mg +ZDDP test case is less than one. For regime "III", the fully formulated CJ-4 lubricant has the highest RPS value, followed by the Ca + ZDDP and lastly the Mg + ZDDP. The morphology of the ashes produced from additive combinations seem to differ from those of individual additives and are not as predictable.

Figure 6.17 compares all of the experimental RPS values determined in this research. The observations of figure 6.17 will help identify any synergistic effects that the additives may have regarding RPS.

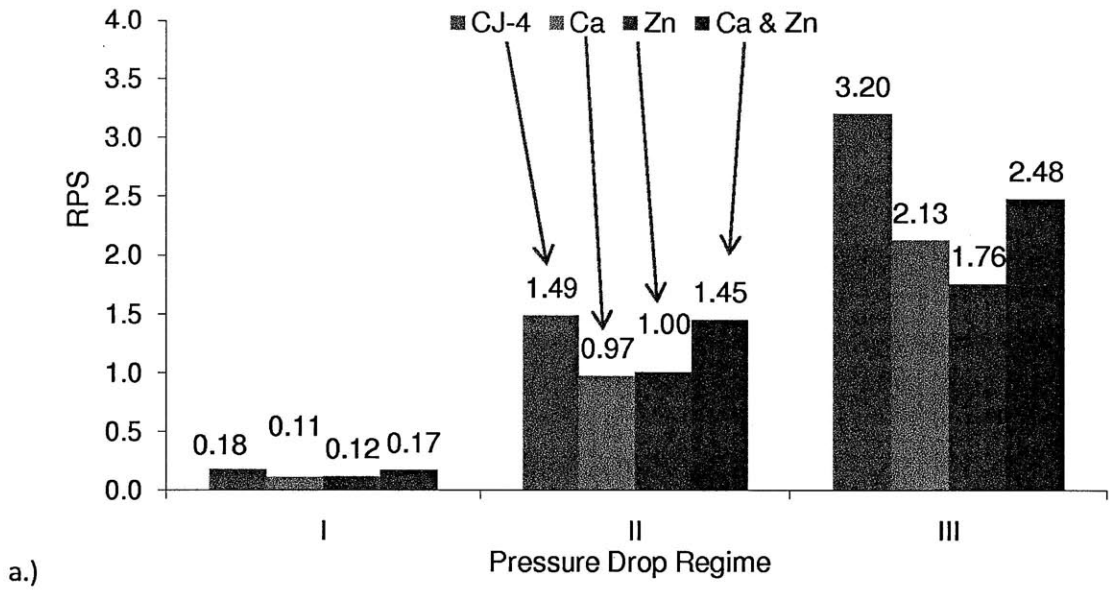

a.)

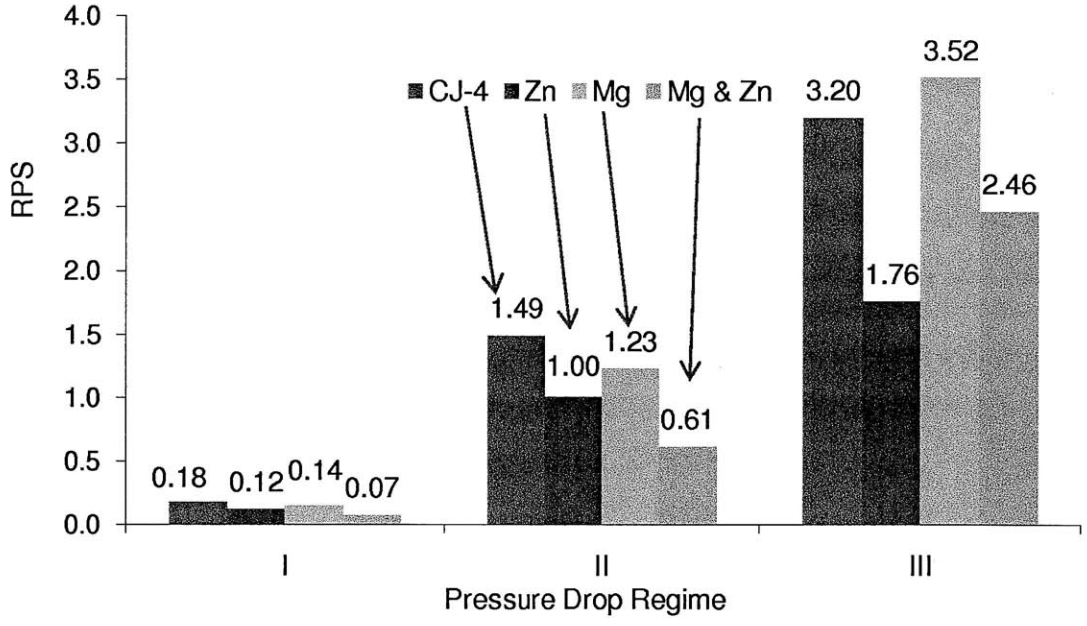

b.)

Figure 6.17: RPS comparison for all tested lubricants. Data for CJ-4, Ca, and ZDDP cases taken from [50].

Analysis of figure 6.17 leads to some interesting observations, particularly in regimes "II" & "III", about the effects of additive combinations on RPS. By comparing the base oil + ZDDP, base oil + Mg and Mg + ZDDP test cases, 6.17 (b), it can be seen that the addition of ZDDP with magnesium has a beneficial RPS effect when compared to the RPS values of magnesium alone. On the contrary, figure 6.17 (a) displays that the addition of ZDDP to calcium generates a negative synergistic effect pertaining to RPS compared to the calcium additive alone. These observations are likely due to the morphological differences that

occur when the ash is derived from various lubricant chemistries. As different additives are placed together in a lubricant, the resultant ash is comprised of various compounds of the individual element which the additives contain. These resultant ash compounds have their own specific characteristics, such as density and particle size, which directly affect the properties of the entire ash layer such as porosity, permeability and ash "stickiness". As ZDDP is added to the magnesium detergent, the resultant ash likely becomes less prone to transport. This results in a smaller ash end plug length which creates a RPS benefit compared to the ash derived from solely the magnesium detergent. On the other hand, as ZDDP is added to the calcium detergent, the resultant ash is more likely to transport compared to the ash derived from solely the calcium detergent. Because of this, the ash plug for the Ca plus ZDDP test case is larger and thus a negative RPS effect compared to the Ca-ash test case is observed.These observations further stress the importance of ash formation and how lubricant chemistry affects the resultant ash properties on an additive by additive basis. Graphs for individual RPS determinations for each test can be found in the appendix figure A-9.

(This page intentionally left blank)

7 POST-MORTEM ANALYSIS RESULTS

For each of the tests performed as part of this research, as well as those conducted by Sappok in 2009, a thorough post-mortem analysis was conducted on the resultant ash-loaded filters once the performance evaluation was complete. The results of the post-mortem analysis aim to quantify key ash properties that directly influence pressure drop such as packing density, distribution throughout the filter as well as permeability and composition. Images were also taken using an SEM to determine the extent of depth filtration and elemental distribution. The complete post-mortem procedure was described in chapter 5.0 and was help constant for all the filters compared throughout this section.

7.1 Ash Layer Thickness and Distribution

As described in chapter 5, each ash loaded filter was sectioned in order to determine the ash layer thickness and distribution throughout the filter both in the axial and radial directions. These characteristics were expected to change with altered lubricant chemistry and as described in chapter three directly impact the total pressure drop observed on a loaded DPF. Table 6.1 described the tests cases which were analyzed with the aforementioned post-mortem analysis. The first piece of data that is obtained through this analysis is ash layer thick and distribution throughout the filter. Through commercially available computer imaging software, numerous data points were measured and averaged to get an accurate account of their magnitude as well a variability estimate based off the resultant standard deviations.

7.1.1 Single Additive Lubricant Formulations

The filters loaded with ash derived from single lubricant additives were subjected to the post-mortem analysis following the ash loading and performance evaluation phases of the experiments. The ash generated from these three test cases displayed clear visual difference in composition and morphology both in the cake layer and in the end plug. Furthermore, the transport of the ash slightly differs from test to test with differences in layer thickness and end plug length. A direct comparison of two filter samples from the same positions within each of the three DPFs is shown in figure 7.1. Figure 7.1 (a-c) display images at 57mm from the DPF inlet face to depict visual difference in the ash cake layer deposited along the channel walls. Figure 7.1 (d-f) display images 133mm from the DPF inlet face to depict visual difference in ash plug length, uniformity and morphology.

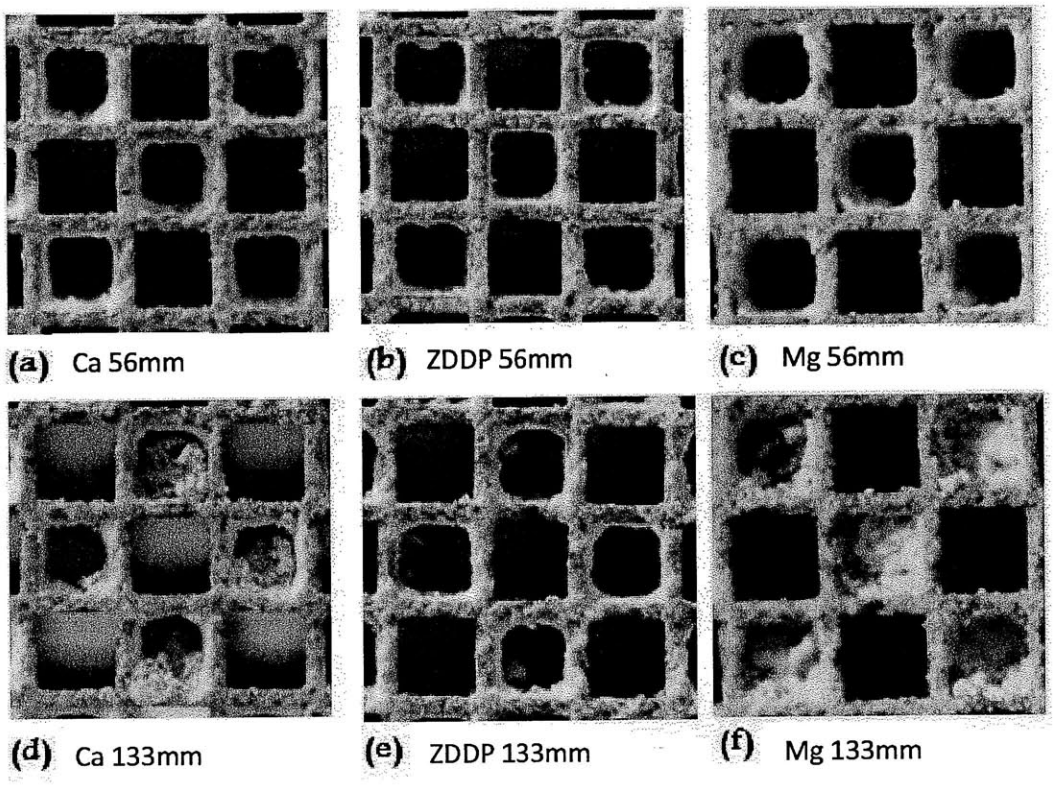

Figure 7.1: Ash accumulation 57 mm from DPF face for (a) DPF containing 29 g/L Ca ash, (b) DPF containing 28 g/L ZDDP ash, (c) DPF containing 24 g/L Mg ash, and 133 mm from DPF face for (d) DPF containing 29 g/L Ca ash, (e) DPF containing 28 g/L ZDDP ash, (f) DPF containing 24 g/L Mg ash all generated via periodic generation. Images for the Ca and ZDDP test cases taken from [50].

Figure 7.1 (a-c) displays slight differences in ash morphology and layer thickness for the three single additive cases. The ash layer for the magnesium case (c) seems to be loosely packed together and almost aerated in nature while that for calcium (a) seems to be tightly packed together along the channel walls. Figure 7.1 (d-f) displays distinct difference in end plug characteristics between the three test cases. The end plugs for the magnesium test case (f) seems to be loosely packed and longer than the other two test cases. The ZDDP ash plugs (e) seem to be the shorter in length with distinct agglomerated particles forming the deposits and most likely more dense.

The calcium based ash also seemed to form the "stickiest" deposits. The ZDDP and magnesium based ash had various layer thicknesses and plug characteristics but could all be easily tapped out of the filter samples. The calcium ash deposits were the hardest to remove.

The measured ash layer thickness along the DPF centerline is shown in figure 7.2 for the three single additive lubricant formations. The ash layer thickness for the three cases slightly differed ranging from 0.11mm for the magnesium-based ash to 0.18mm for the calcium-based ash. The error for these

measurements was determined by taking into consideration both the ash layer thickness variability and clean channel variability. The error for these data points are approximately ±0.03mm (Mg), ±0.015mm (ZDDP) and ±0.02mm (Ca) respectively. Due to the low axial resolution of the measurement technique (dependent on DPF sample size) the ash layer profiles near the start of the end plug are not accurately know therefore making it difficult to obtain high resolution measurements in ash plug length.

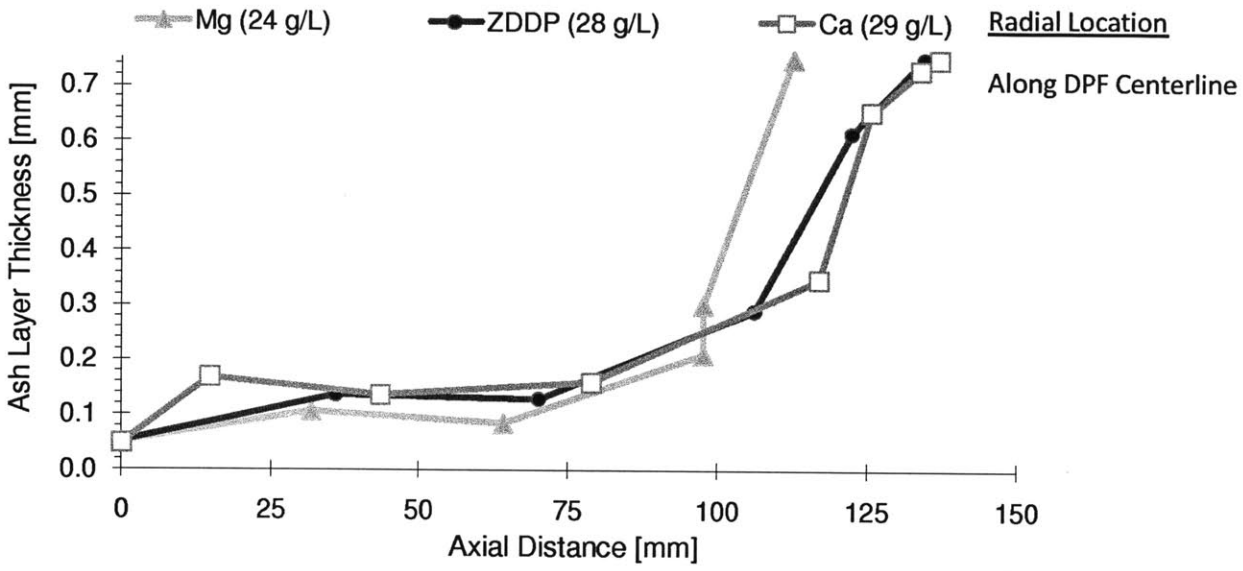

Figure 7.2: Ash layer thickness profiles measured along DPF centerline for DPFs containing ash generated by base oil + Ca detergent, base oil + ZDDP and base oil + Mg detergent. Ca and ZDDP data taken from [50].

Graphs similar to figure 7.2 will be presented throughout this section in which the ash end plug is completely formed when the layer thickness reaches the maximum of half of the clean channel height, 0.75mm. It can be seen from figure 7.2 that the magnesium-based ash has both the thinnest ash layer as well as the longest end plug. The magnesium based ash also has the most non-characteristically consistent end plug lengths ranging from 25 – 65 mm which is distinguished by the various profile increases at the earliest axial distance. The ZDDP and Ca based ashes have very similar layer thickness profiles with the calcium case having a slightly larger thickness and shorter average end plug. These characteristics for the calcium-based ash are likely linked to the high observed "stickiness" which would reduce the transport rate of ash particles contained in the cake layer to the end plug.

Figure 7.3 presents similar ash distribution profiles measured in the radial direction, 36 mm from the DPF centerline for the three test cases. The error for these data points are approximately ±0.025mm (Mg), ±0.012mm (ZDDP) and ±0.012mm (Ca) respectively. The ash layer profile trends for the samples

36mm off the DPF centerline are very similar to those noticed along the centerline in figure 7.2. This confirms the characteristically consistent ash distribution of the accelerated ash loading.

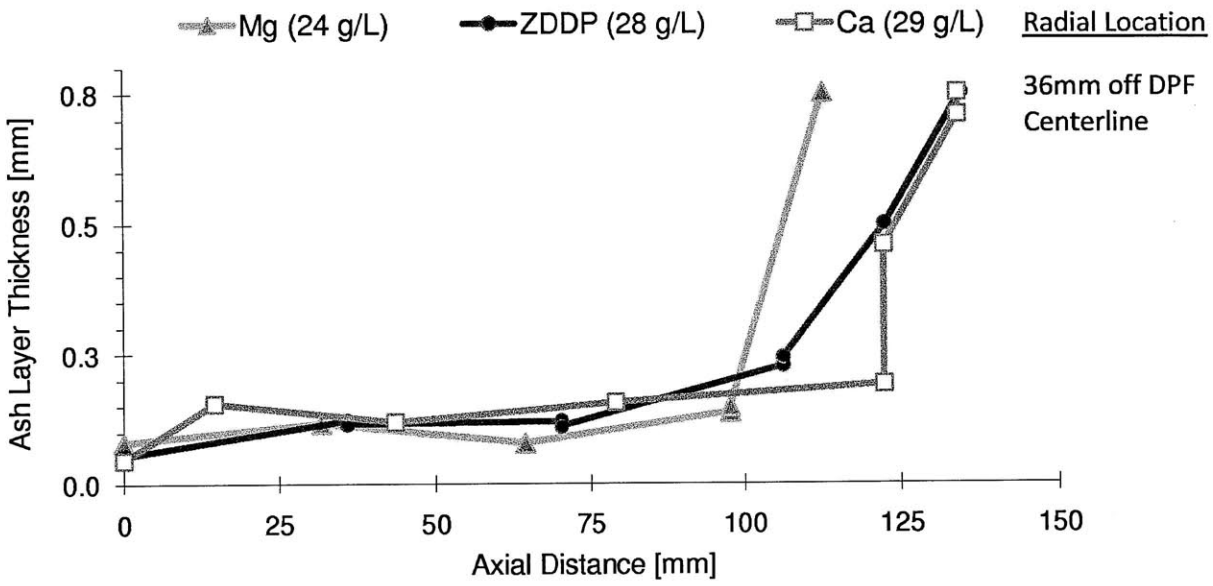

Figure 7.3: Ash Layer thickness profiles measured 36mm from DPF centerline for DPFs containing ash generated from base oil + Ca detergent, base oil + Mg based detergent, and base oil + ZDDP. Data from Ca and ZDDP test cases taken from [50].

Figures 7.4, 7.5 and 7.6 show the full ash distribution profiles within the DPF channels for three different radial locations with the magnesium-, calcium- and ZDDP-based ash respectively.

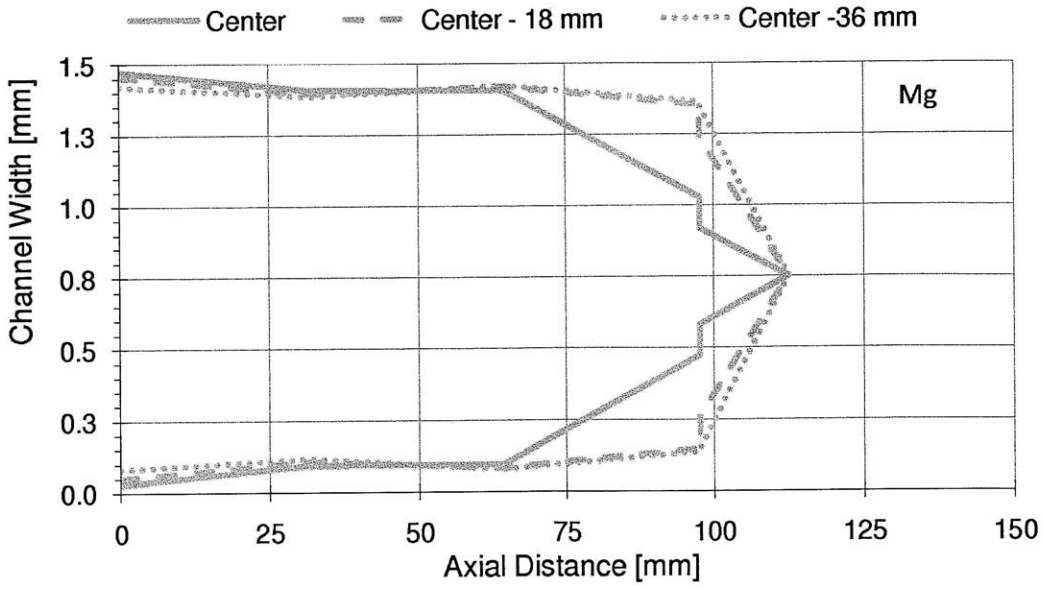

Figure 7.4: Single channel ash distribution profiles for a DPF containing 24 g/L ash generated using base oil containing only a Mg-based detergent.

It can be seen in figure 7.4 that the magnesium based ash distribution profile has the thinnest ash layer and longest, most non-characteristically consistent end plugs of the three test cases compared. There is little radial difference in the ash cake layer but the end plug length variance is much more pronounced.

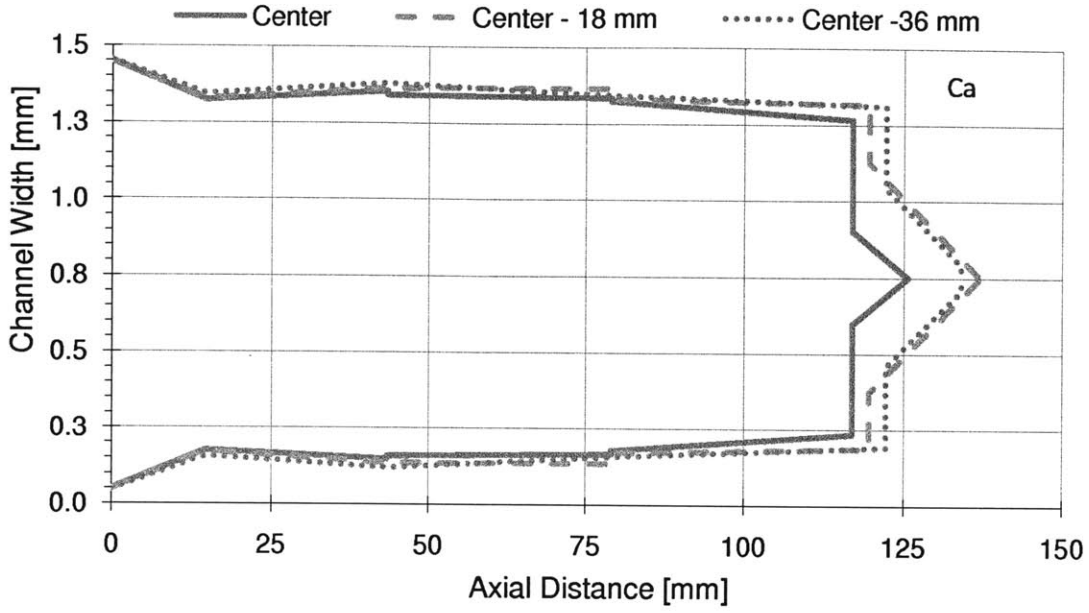

Figure 7.5: Single channel ash distribution profiles for a DPF containing 29 g/L ash generated using base oil containing only a Ca-based detergent. Data taken from [50].

It can be seen from figure 7.5 that the ash plug formation of the calcium-based ash is shorter but more characteristically consistent that the magnesium-based ash (fig. 7.4) and much more pronounced and characteristically consistent compared to the ZDDP-based ash (fig. 7.6). The same filter also displays little radial difference in both the ash cake layer thickness as well as end plug characteristics. The calcium-based ash layer thickness is slightly larger than both the magnesium- and ZDDP- based ashes with a unique large build-up of ash at approximately 15mm front he inlet face.

Figure 7.6 displays the much less pronounced and non-uniform nature of the ZDDP-based ash end plugs. There is little difference in the ash layer thickness and eng plug characteristics in the radial direction. With this being said, all of the test cases has the thickest ash layer along the DPF centerline and decreased in the radial direction away from the center of the filter. Similarly, the ash end plug was the longest at the DPF centerline and decreased in length in the radial direction.

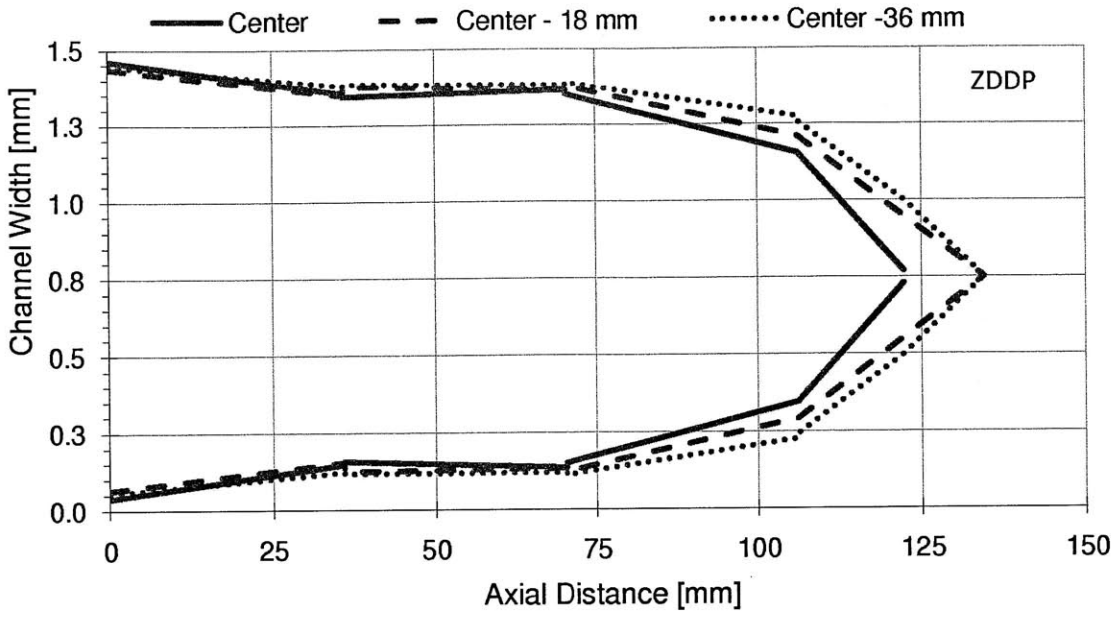

Figure 7.6: Single channel ash distribution profiles for a DPF containing 28 g/L ash generated using base oil containing only a ZDDP additive. Data taken from [50].

Figures 7.7 and 7.8 show the channel open area profiles computed from the ash thickness and clean channel measurements for these three filters along the centerline and 36mm off centerline respectively.

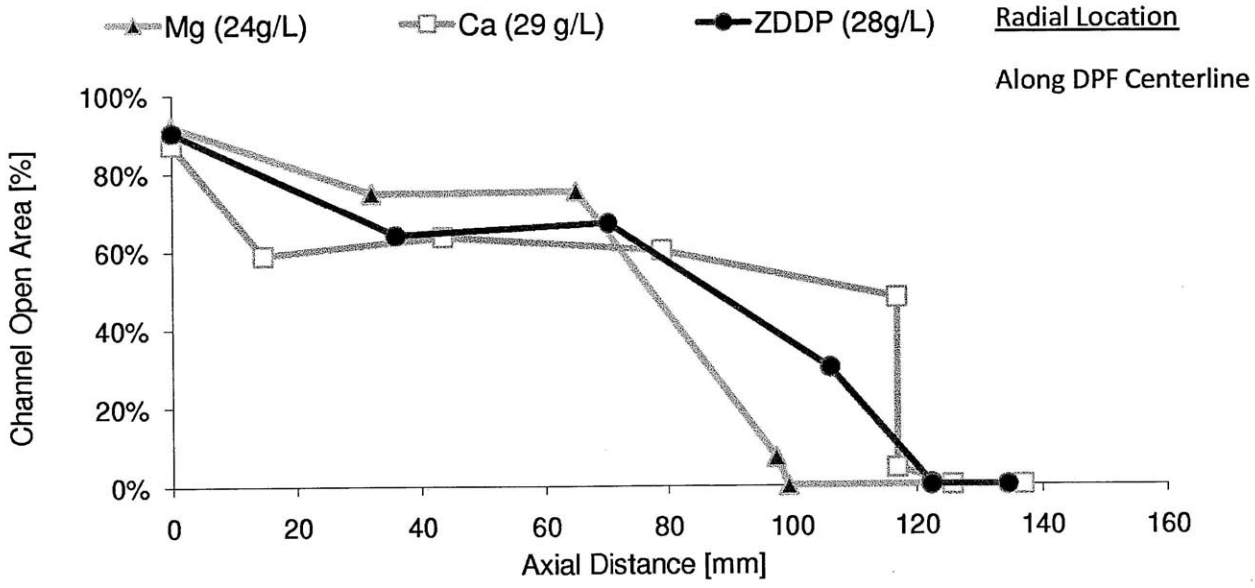

Figure 7. 7: Channel open area profiles measured along the DPF centerline for DPFs containing ash generated from base oil + Mg detergent, base oil + Ca detergent, and base oil + ZDDP. Data for Ca and ZDDP cases taken from [50].

From the ash cake layer only, the calcium-based ash displays the highest reduction in available channel area. Because the magnesium-based ash has the longest end plugs, it has the largest average area

reduction of approximately 50% compared to 40% for the calcium-based ash and 35% for the ZDDP-based ash. Another interesting note is how the open channel area profiles for the calcium- and ZDDP-based ash are relatively characteristically consistent in the radial direction whereas there is a larger difference for the magnesium based ash.

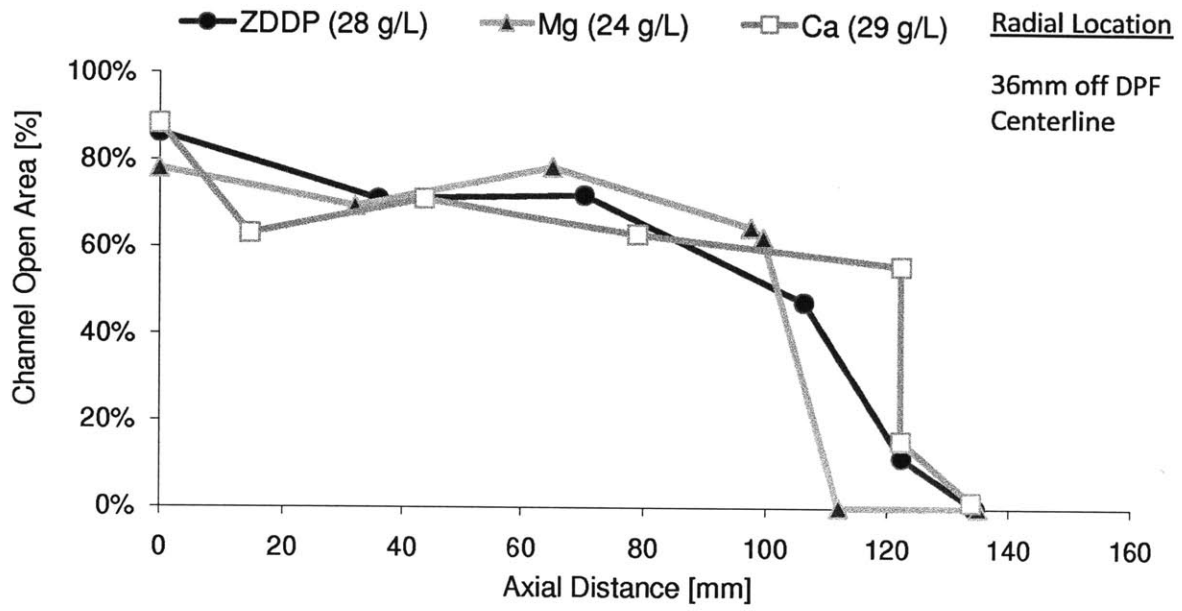

Figure 7.8: Channel open area profiles measured 36mm off the centerline of the DPFs containing ash generated from base oil + Mg detergent, base oil + Ca detergent, and base oil + ZDDP. Data for Ca and ZDDP cases taken from [50].

7.1.2 Multi-Additive Lubricant Formulations

The filters loaded with ash derived from multi-additive lubricants were subjected to the post-mortem analysis following the ash loading and performance evaluation phases of the tests. Similarly to the ash derived from single additives, the ash generated from these three test cases displayed clear visual differences in composition and morphology both in the cake layer and in the end plug. A direct comparison of two filter samples from the same positions within each of the three DPFs is shown in figure 7.9. Figure 7.9 (a-c) display images at 57mm from the DPF inlet face to depict visual difference in the ash cake layer deposited along the channel walls. Figure 7.9 (d-f) display images 133mm from the DPF inlet face to depict visual difference in ash plug length, uniformity and morphology.

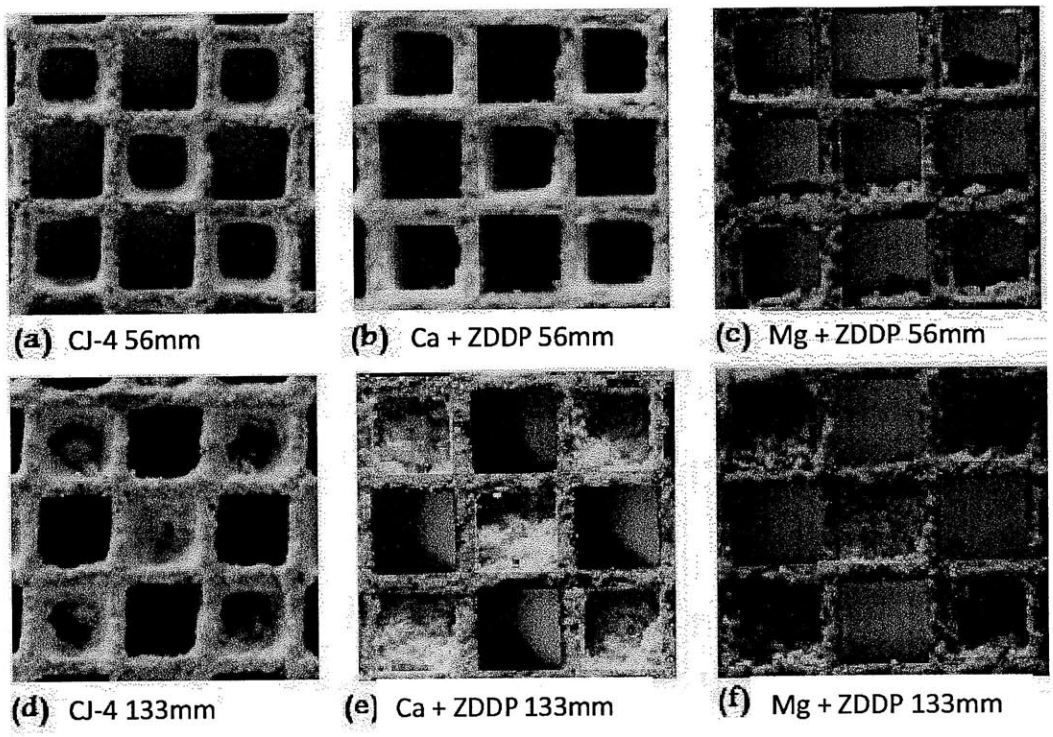

Figure 7. 9: Ash accumulation 57 mm from DPF face for (a) DPF containing 42 g/L CJ-4 ash, (b) DPF containing 25 g/L Ca + ZDDP ash, (c) DPF containing 23 g/L Mg + ZDDP ash, and 133 mm from DPF face for (d) DPF containing 42 g/L CJ-4 ash, (e) DPF containing 25 g/L Ca + ZDDP ash, (f) DPF containing 23 g/L Mg + ZDDP ash. Images for CJ-4 case taken from [50].

Figure 7.9 (a-c) displays slight differences in ash morphology and layer thickness for the three multi-additive cases. The ash layer for the Mg plus ZDDP case (c) seems to be loosely packed together and aerated in nature similar to the single magnesium additive case. On the other hand, the Ca plus ZDDP case (b) and the CJ-4 case (a) seem to tightly adhere along the channel walls. Figure 7.1 (d-f) displays distinct difference in end plug characteristics between the three test cases. The end plugs for the Mg plus ZDDP test case (f) seem to be more predominant and loosely packed compared to the other two test cases. In general the visual observations of the additive combination ash cases tend to take on a blend of the characteristics noticed in the single additive case with those of the calcium- and magnesium-based detergent being the most predominant and overpowering. The addition of the ZDDP additive seems to generate more agglomerated ash particles when compared to the ash not containing the ZDDP additive.

Similarly to the single additive cases, ash which contained calcium (CJ-4 and Ca plus ZDDP) seemed to form the "stickiest" deposits and were the most difficult to remove while the Mg plus ZDDP ash was easily tapped out.

The measured ash layer thickness along the DPF centerline is shown in figure 7.10 for the three multi-additive lubricant formations. The ash layer thickness for the three cases differed little from 0.14mm for the CJ-4 case to 0.10 mm for the Ca plus ZDDP case and 0.08mm for the Mg plus ZDDP ash. It is important to note that the ash load of the CJ-4 test case, 42 g/L, is much higher than both the Ca plus ZDDP and Mg plus ZDDP test cases, 25 g/L and 23 g/L. Taking this into consideration, some of the measurements might not necessarily be directly comparable. The errors calculated for these test points take into account the variability of both ash layer thickness and clean channel dimensions. The respective data point errors are approximately ±0.02mm for CJ-4 and Ca plus ZDDP test cases and ±0.015 for the Mg plus ZDDP test case.

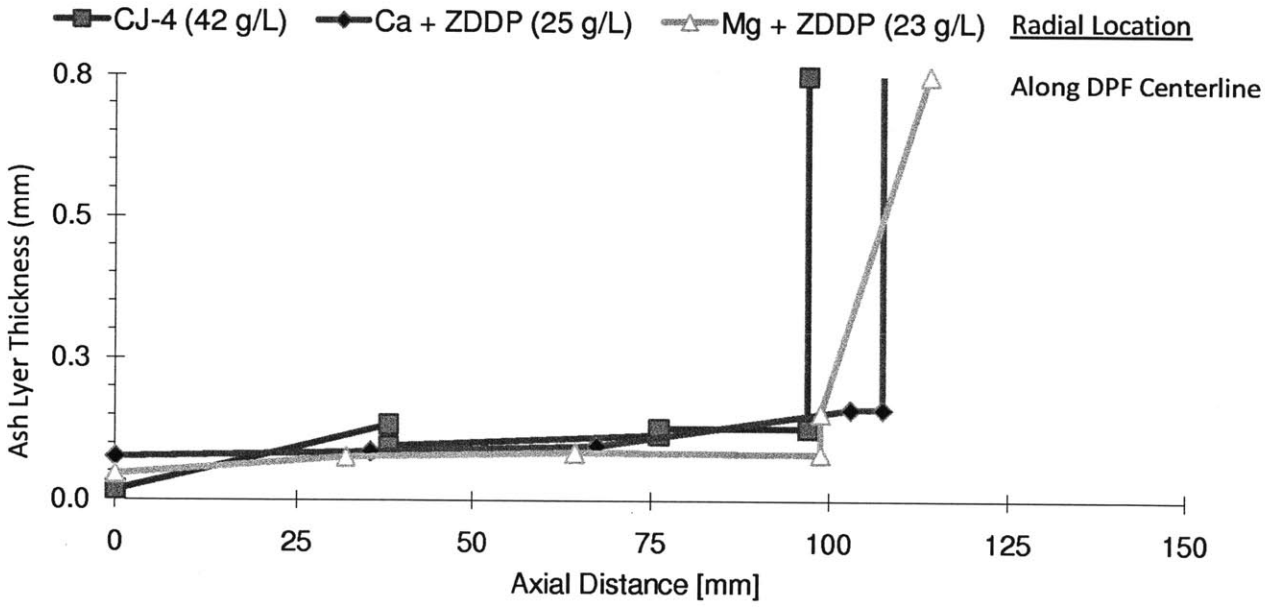

Figure 7.10: Ash layer thickness profiles measured along DPF centerline for DPFs containing ash generated from fully formulated CJ-4, base oil + Ca & ZDDP and base oil + Mg & ZDDP. CJ-4 data taken from [50].

It can be seen from figure 7.10 that the CJ-4 and Ca plus ZDDP ash contain a more characteristically consistent end plug formation and increase in plug length, 1.7cm and 0.8cm respectively, compared to the Mg plus ZDDP test case. Similar to the single additive test case, the Mg plus ZDDP test case displays the thinnest ash layer and longer average end plugs than the Ca plus ZDDP test case.

Figure 7.11 presents similar ash distribution profiles measured at the radial direction, 36 mm from the DPF centerline for the three test cases. The error for these data points are approximately ±0.012mm (Mg + ZDDP), ±0.014mm (Ca + ZDDP) and ±0.010mm (CJ-4) respectively. The ash layer profile trends for

the samples 36mm off the DPF centerline are very similar to those noticed along the centerline in figure 7.9. This again confirms the characteristically consistent ash distribution of the accelerated ash loading.

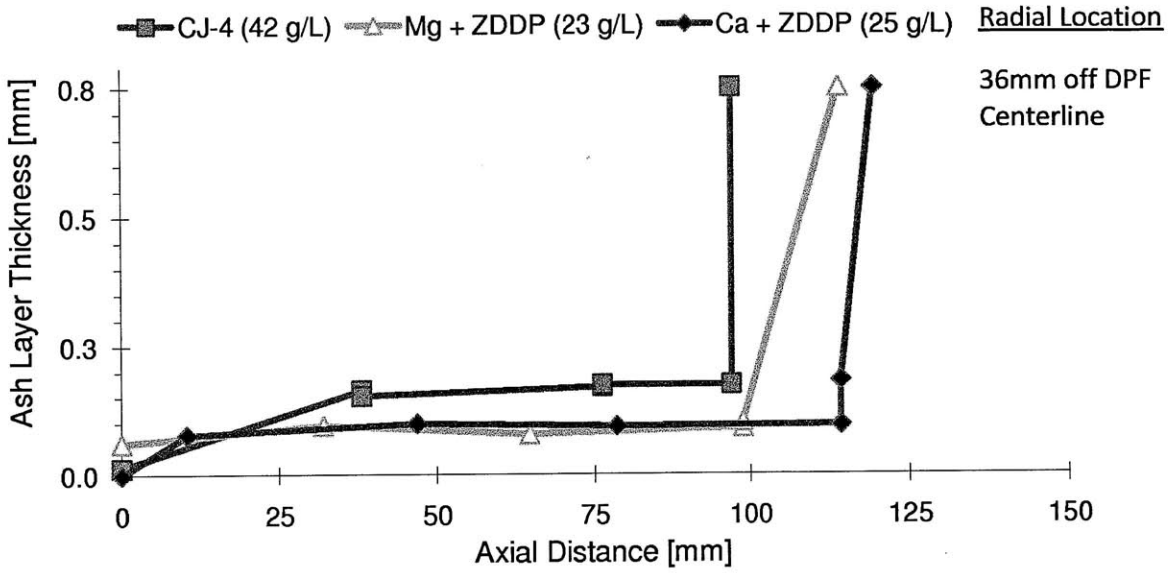

Figure 7. 11: Ash layer thickness profiles measured 36 mm off centerline for DPFs containing ash generated from fully formulated CJ-4, base oil + Ca & ZDDP and base oil + Mg & ZDDP. CJ-4 data taken from [50].

To go in a bit more detail, figures 7.12, 7.13 and 7.14 show the full ash distribution profiles for three different radial locations for the CJ-4, calcium plus ZDDP, and magnesium plus ZDDP-based ash respectively.

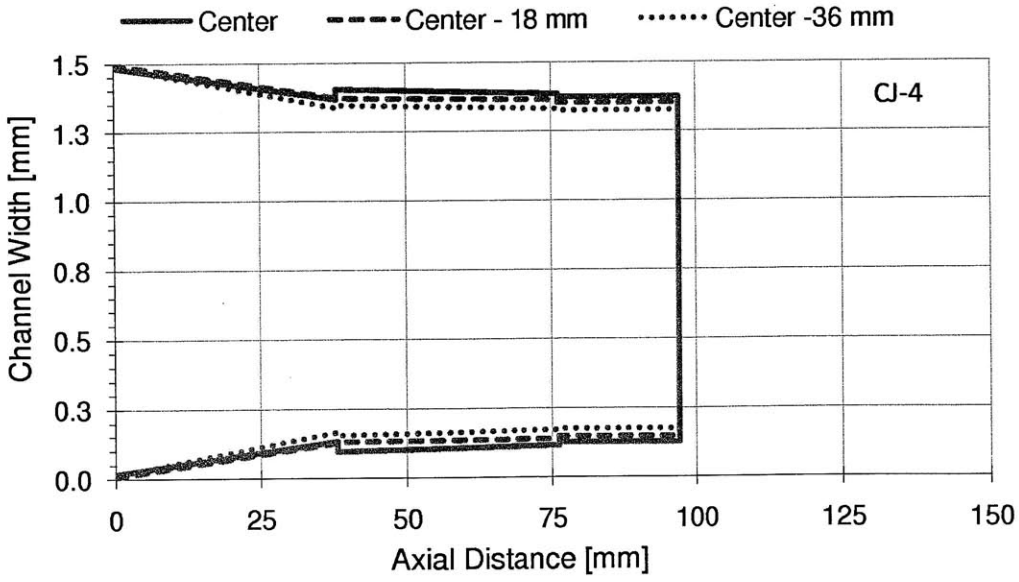

Figure 7.12: Single channel ash distribution profiles for a DPF containing 42 g/L ash generated using fully formulated CJ-4. Data taken from [50].

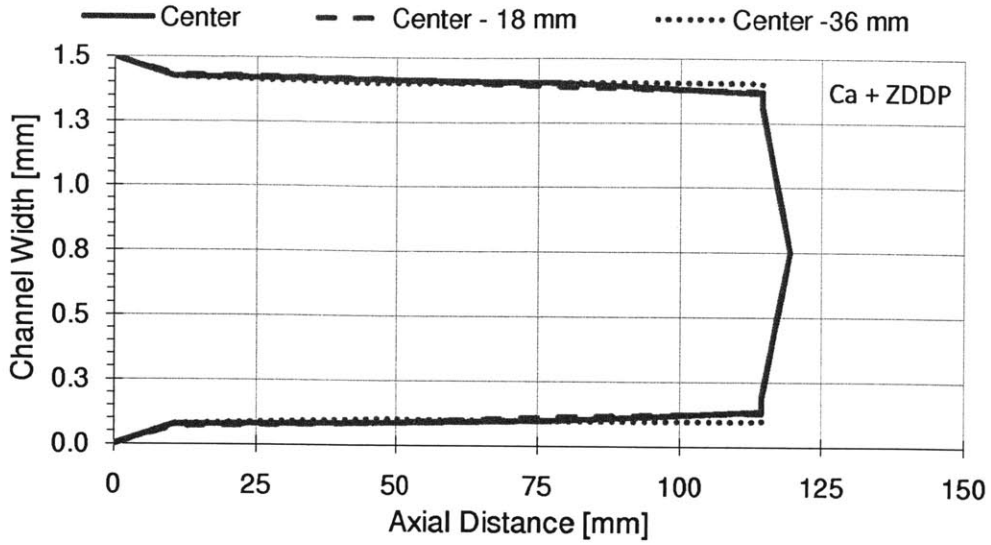

Figure 7.13: Single channel ash distribution profiles for a DPF containing 25 g/L ash generated using base oil + Ca & ZDDP.

It can be seen from figure 7.12 that out of all of the multi-additive tests, the CJ-4 case has the longest and most characteristically consistent end plug. It is important to remember that the CJ-4 test was ash loaded to 42 g/L which is the likely cause of this characteristic. The ash end plug for the Ca + ZDDP ash seen in figure 7.13 is much more uniform but shorter on average than the end plugs of the Mg + ZDDP ash seen in figure 7.13. It is also very interesting to note how the multi-additive cases have little to no variation in the radial direction along the filter which was not the case for the single additive tests.

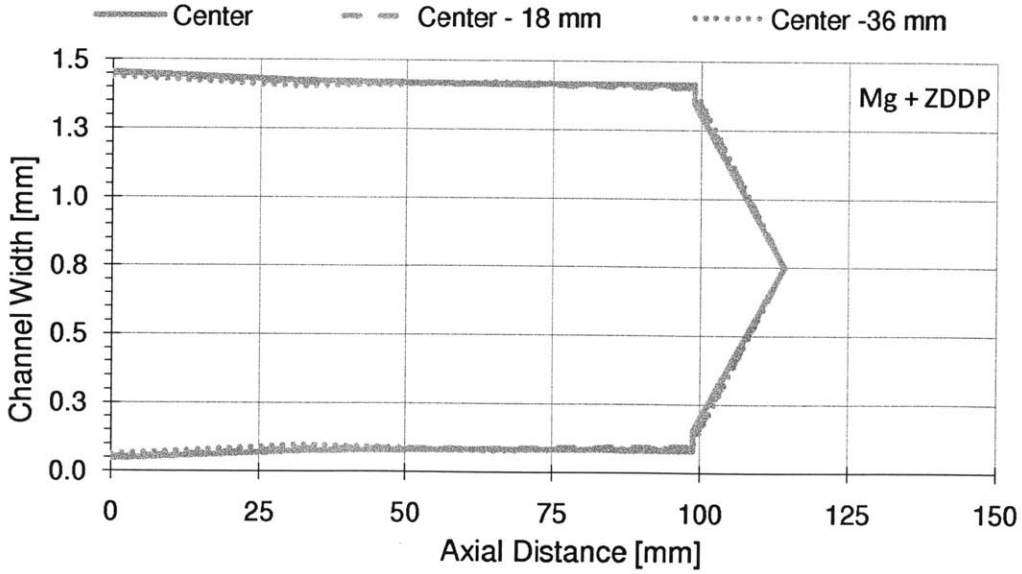

Figure 7.14: Single channel ash distribution profiles for a DPF containing 24 g/L ash generated using base oil + Mg & ZDDP.

Figures 7.15 and 7.16 show the channel open area profiles computed from the ash thickness and clean channel measurements for these three filters along the centerline and 36mm off centerline respectively.

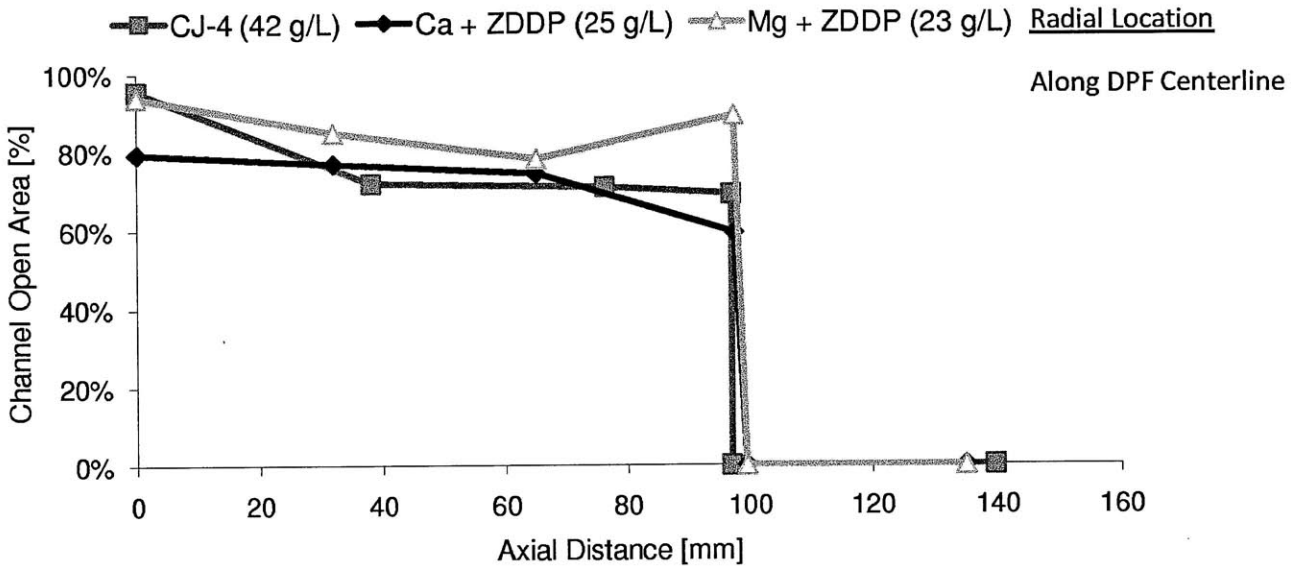

Figure 7.15: Channel open area profiles measured along the DPF centerline for DPFs containing ash generated from CJ-4, base oil + Mg & ZDDP, and base oil + Ca & ZDDP. Data for CJ-4 case taken from [50].

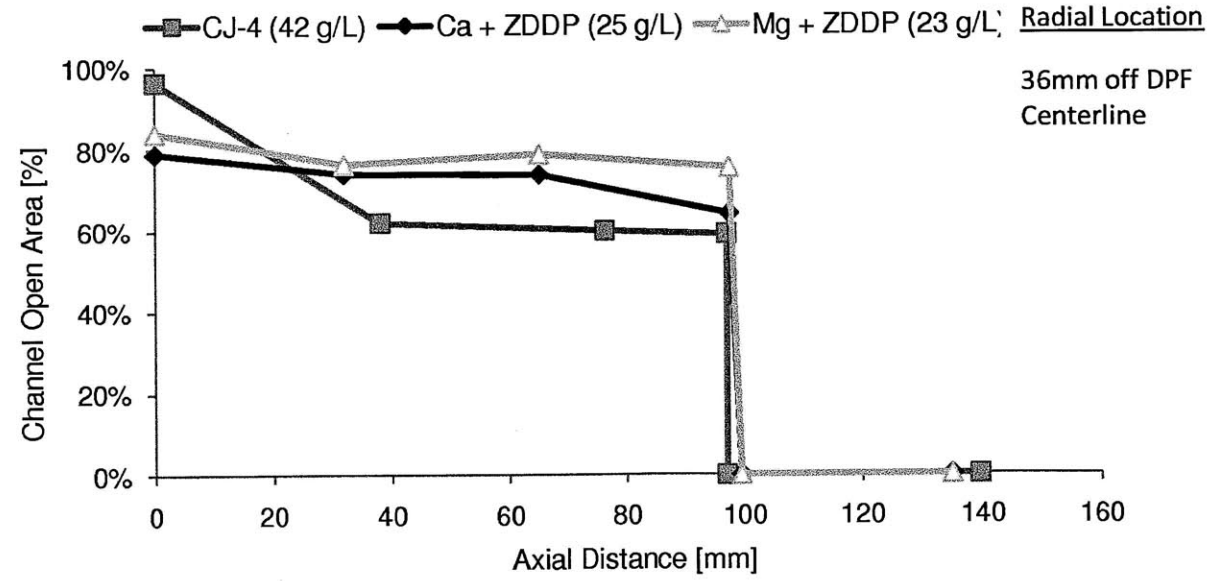

Figure 7. 16: Channel open area profiles measured 36mm off the DPF centerline for DPFs containing ash generated from CJ-4, base oil + Mg & ZDDP, and base oil + Ca & ZDDP. Data for CJ-4 case taken from [50].

These figures describe the characteristics mentioned previously in the thickness profile analyses. The CJ-4 case has the quickest reduction in open channel area likely due to the high amount of ash accumulation at 42 g/L. The calcium plus ZDDP based ash displays the largest open area decrease at the

early axial lengths because it has comparatively the largest layer thickness from 0 to 20 mm from the filter inlet face.

Figures 7.17 and 7.18 compare the bi-additive lubricant ash layer thickness profiles with the profiles of those test conducted on the corresponding single additive lubricants.

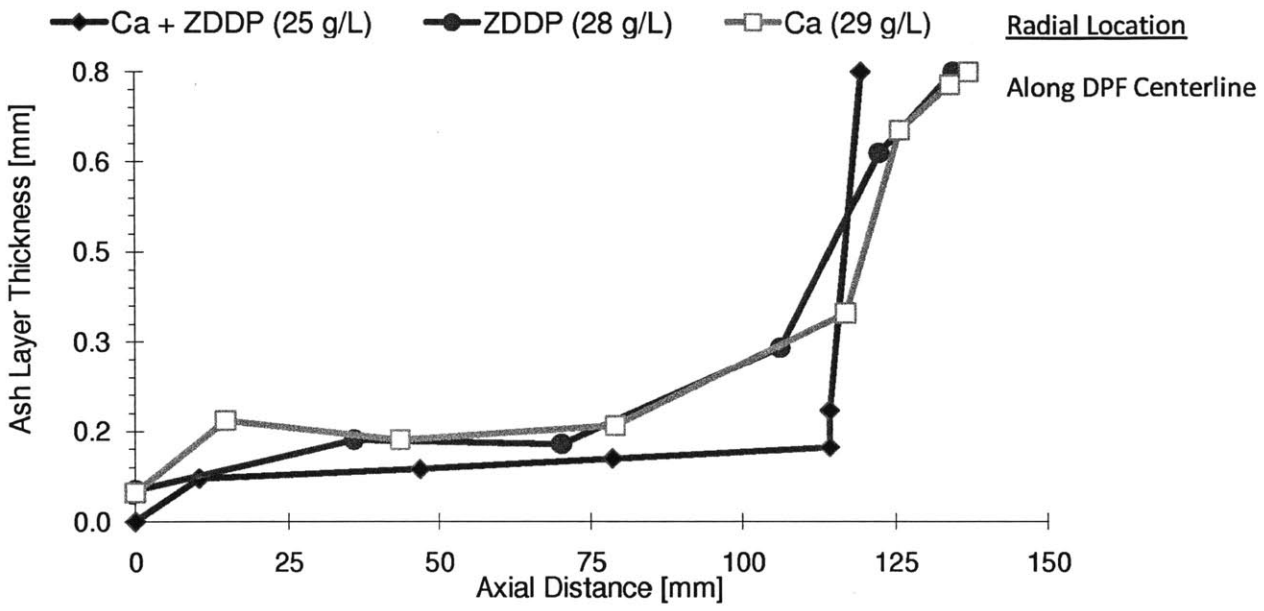

Figure 7. 17: Ash layer thickness profiles measured along DPF centerline for DPFs containing ash generated by base oil + Ca detergent, base oil + ZDDP and base oil + Ca & ZDDP. Base + Ca and Base + ZDDP data taken from [50].

It is interesting to note that when ZDDP is added to the Ca- and Mg-detergents, the ash layer and end plug formation becomes much more characteristically consistent than the profiles of the detergents alone. The synergistic effects are noticeable with the more characteristically consistent end plug length, and smaller ash layer thickness. For figure 7.17, this is likely due to the ZDDP's addition altering the "stickiness" of the Ca-based ash deposits. The reader may also notice that as additives are combined, the profiles beings to closer resemble the profile of the CJ-4 test case which contain all of the tested additives.

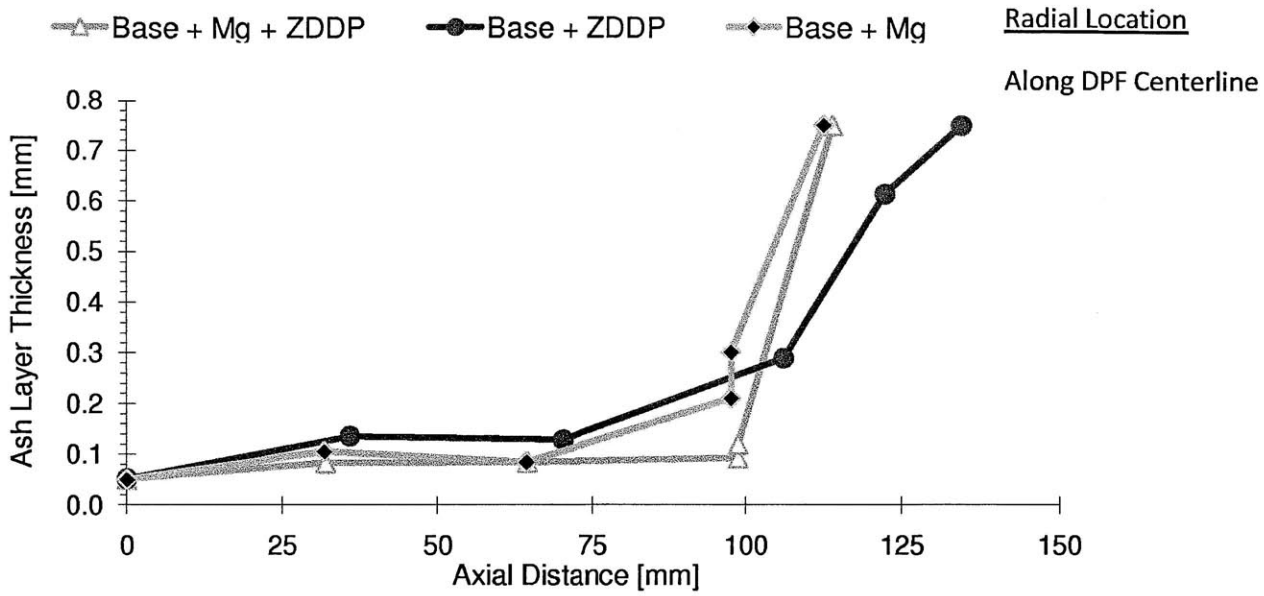

Figure 7. 18: Ash Layer thickness profiles measured along DPF centerline for filters containing ash generated from base oil + Mg & ZDDP, base oil + Mg based detergent, and base oil + ZDDP. Data for ZDDP test case taken from [50].

Figure 7.19 presents the ash layer profiles of two filters loaded with the magnesium + ZDDP ash at 12 and 23 g/L respectively. This figure displays that end plug formation begins to start at approximately 12 g/L ash load as previously seen in past data. It should also be noted that past 12 g/L, there is a slight increase in ash layer thickness with a larger deposition and ash transport toward the ash end plug.

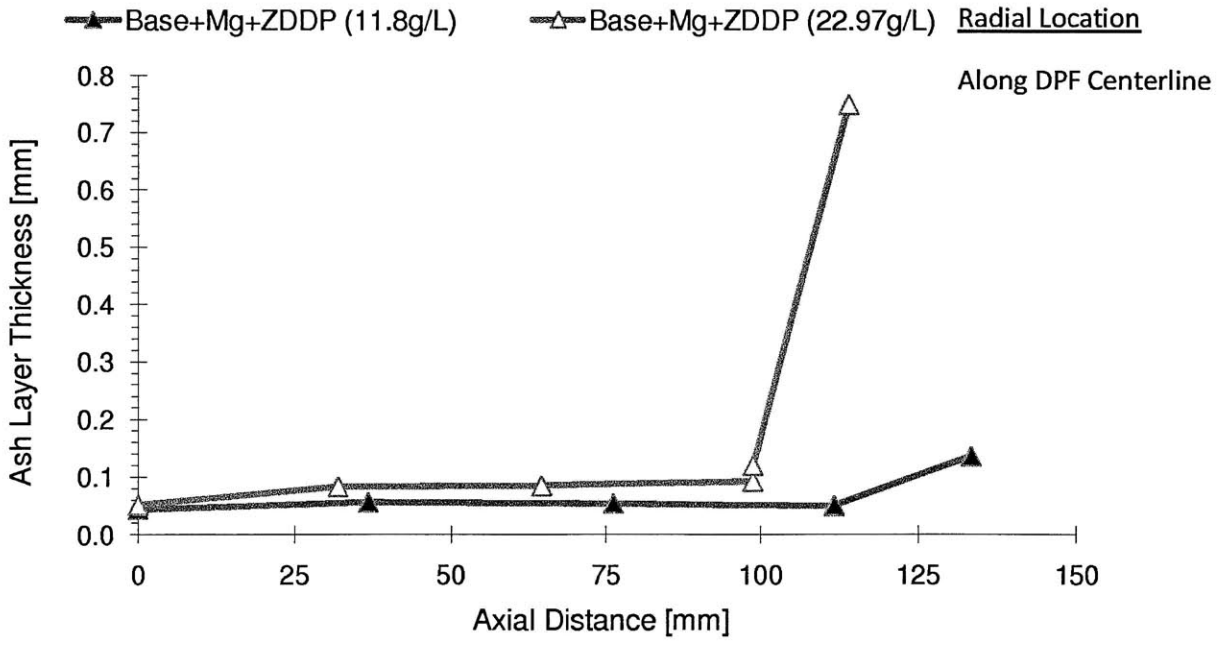

Figure 7.19: Ash Layer thickness profiles measured along DPF centerline for filters containing ash generated from base oil + Mg & ZDDP at 12 g/L and 23 g/L.

7.2 Ash Packing Density

Ash packing density measurements were also carried out using the measured ash distribution and the known weight of the ash deposit in the various filter samples. In past experiments it was seen that the packing density varied little in the axial direction along the length of the channels with a slight decrease in the vicinity of the ash end plug. It was also seen that there was little variation in the radial direction for a given axial location [50]. These same characteristics were noticed for the test cases performed in this research.

As noted in chapter 5, the packing density for the sample 57 mm from the front face ("B" Samples) of the DPF are most representative of the ash cake layer. Similarly, the packing density for the samples 133 mm from the front filter face ("D" Samples) are the most representative of the ash end plugs. Figure 7.20 presents a direct comparison of the ash layer packing densities for the compared filters.

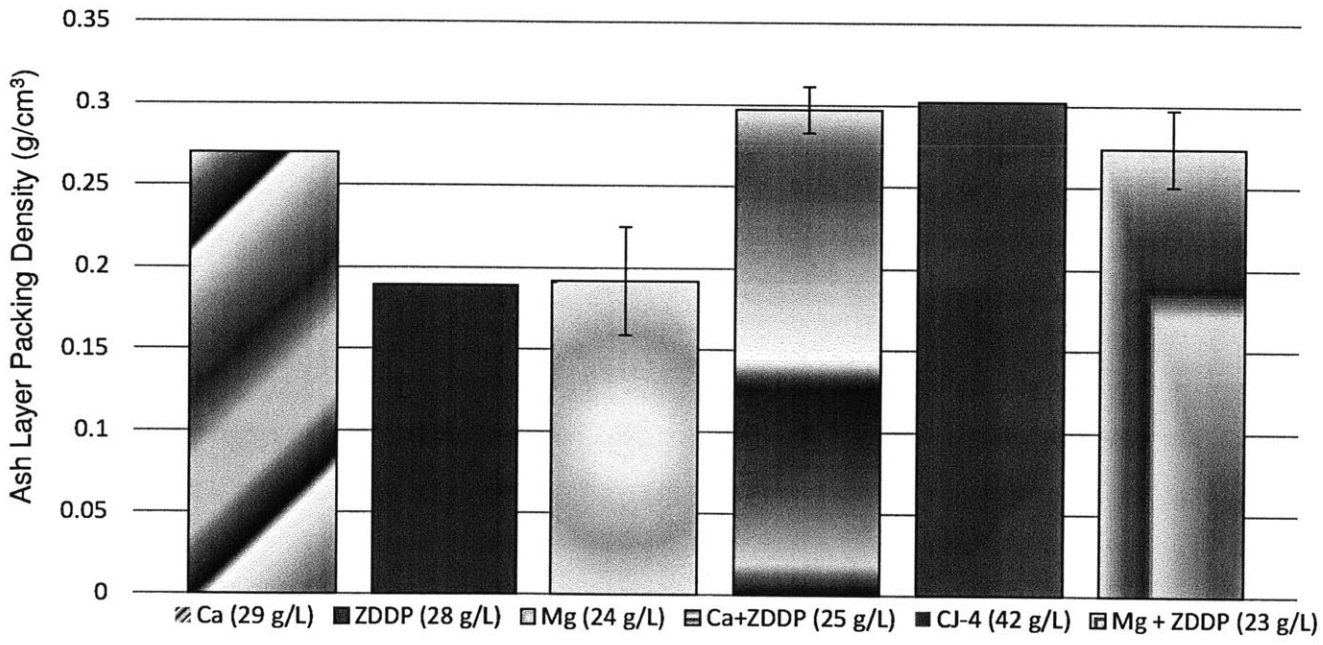

Figure 7.20: Ash layer packing density measurements for the compared test cases. Data taken from base + Ca, base + ZDDP and CJ-4 taken from [50].

The ash layer packing densities described in figure 7.20 were calculated by averaging the observed packing densities from the "B" samples 57mm from the inlet filter face. The standard deviations determined for the test cases conducted in this study are present; those from past values were not

located. As seen in figure 7.20, the ash layer packing densities for the performed and past experiments range between 0.19 and 0.30 g/cm^3.

Of the single additive based lubricants, the ash derived from the calcium detergent displays the highest layer packing density whereas the magnesium & ZDDP based ashes display substantially lower and similar packing densities. This corresponds substantially well with the pressure drop trends notices in figure 6.4 noting that the packing density may have a dominant effect on the resultant pressure drop of the ash layer.

From the combination lubricants, the formulation of the calcium-based detergent and ZDDP along with the fully formulated CJ-4 oil display the highest layer packing densities followed by the magnesium-based detergent and ZDDP. These packing density trends also correlate with the pressure drop trends seen in figure 6.6, but it is interesting to note the combination formulations have a much lower maximum packing density difference from test to test compared with the single additive formulations.

Figure 7.21 displays the ash plug packing densities for the compared test cases. For every test case conducted, the ash plug packing density was lower than the cake layer packing density. It can be seen from figure 7.21 that the single additive test cases display very similar plug packing densities to one another and are only slightly higher than the combination lubrication formulations. This is circumstantial evidence that the ash transport and deposition mechanisms play a key role in controlling the packing characteristics of the ash end plugs. It was previously noted that the ash deposited in a layer along the channel walls experiences higher filtration velocities compared to the ash accumulated in the end plugs[50].

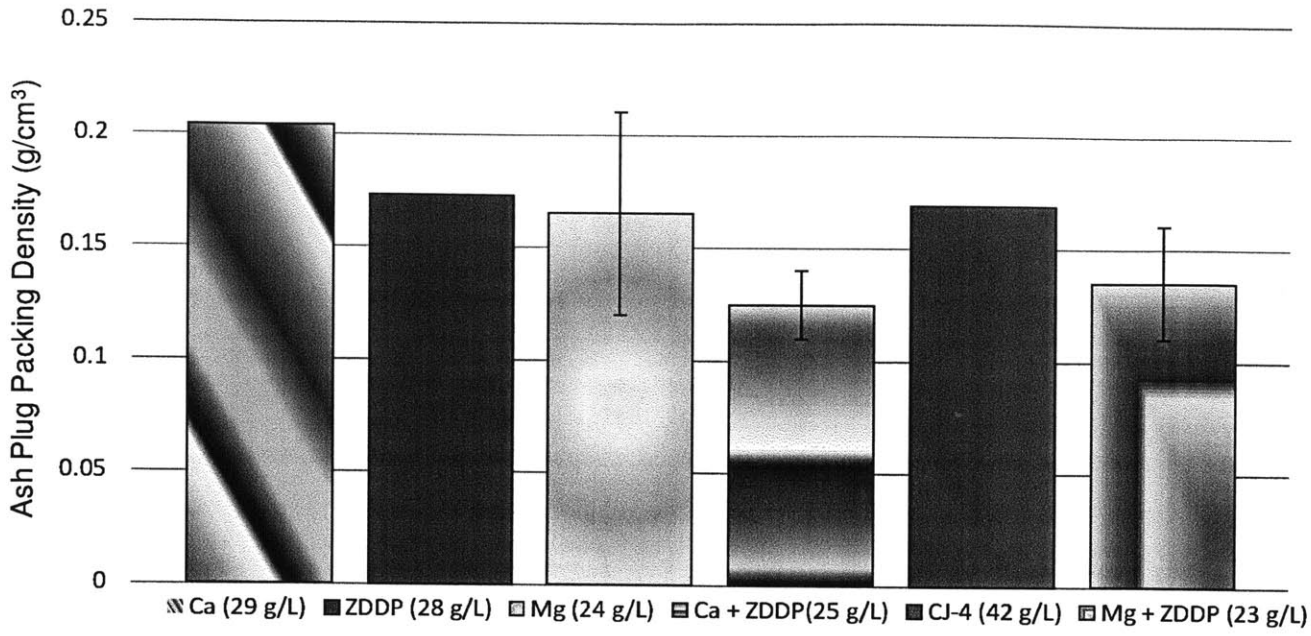

Figure 7. 21: Ash plug packing density measurements for the compared test cases. Data taken from base + Ca, base + ZDDP and CJ-4 taken from [50].

7.3 Ash Composition

To determine the composition of the ash derived from the unique lubrication oil formulations used in this research, XRD analysis was conducted on the ash derived from the magnesium plus ZDDP oil, calcium plus ZDDP oil and base oil plus magnesium-based detergent. This analysis was also conducted in the past by Sappok. on the ash derived from base oil + calcium and base oil + ZDDP formulations.

The XRD spectrum for the base oil + Mg ash is shown in figure 7.22. There were a number of compounds located in the ash and some of the predominant peaks have been highlighted. By using the relative intensity values (RIR) for each of the discovered compounds, the mass percentage of each compound present was determined. The majority of this ash derived from solely the magnesium-based detergent was composed of magnesium oxide (MgO). Along with magnesium oxide, a small percentage of magnesium zinc phosphate ($Mg_{1.8}Zn_{1.2}(PO_4)_2$) was also found as well as traces of cordierite. The cordierite traces were due to a small amount of DPF wall substrate being present in the ash sample material.

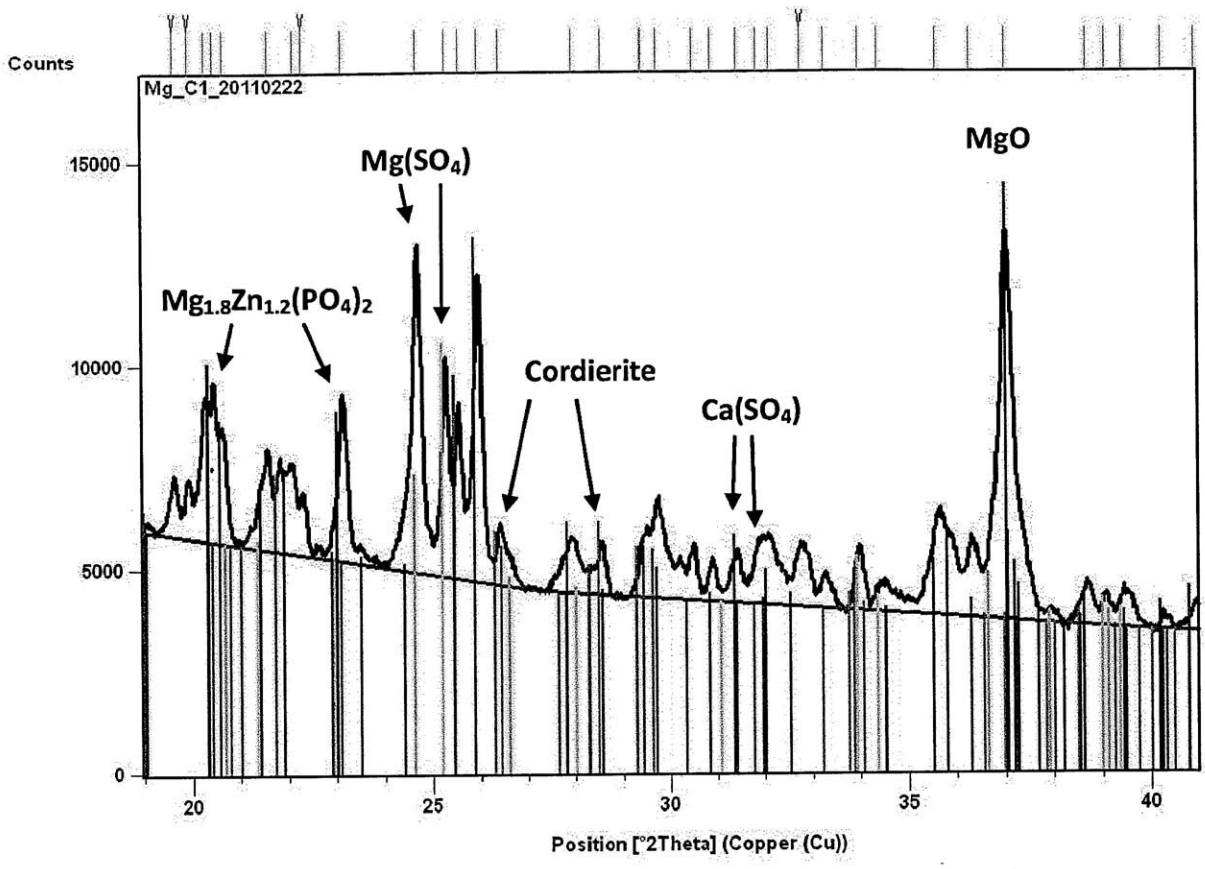

Figure 7.22: Ash compositional analysis via XRD for ash generated from oil containing only magnesium detergent.

The primary compounds found in the ash derived from the magnesium detergent were magnesium oxide (MgO) and a form of magnesium zinc phosphate ($Mg_{1.8}Zn_{1.2}(PO_4)_2$). There were trace amounts of other compounds found in the ash but only in small percentages. Table 7.1 presents the found compounds with their relative mass percentages for both the entire ash sample, as well as a simplified ash composition. The simplified ash composition was determined by proportionally distributing the trace compound mass percentages to the more prevalent compounds present. Once this simplified ash composition was determined, the ash theoretical density was determined using the theoretical density of the individual compounds as well as their corresponding mass percentages. Once the theoretical density of the ash was determined, the porosity was calculated using the measured packing density measurements and the relationship stated in equation 3.10 in chapter 3.

Comp	Name	Mass %	Density (g/cm^3)	Notes
Mg O	Magnesium Oxide	64	3.58	
$Mg(SO_4)$	Magnesium Sulfate	5.0	2.66	Anhydrous
$Mg_2(Al_4Si_5O_{18})$	Cordierite	12	2.65	Range 2.55 - 2.75
$Mg_{1.8}Zn_{1.2}(PO_4)_2$	Magnesium Zinc Phosphate	14	3.60	$MgZn_2(PO_4)_2$
$Ca(SO_4)$	Calcium Sulfate	5.0	2.96	Anhydrous
Mg O	Magnesium Oxide	82	3.58	Simplified
$Mg_{1.8}Zn_{1.2}(PO_4)_2$	Magnesium Zinc Phosphate	18	3.60	Composition
	Theoretical Density	3.58	g/cm^3	
	Layer Packing Density	0.192	g/cm^3	
	Porosity	94.6 %		

Table 7. 1: Tabular results of XRD and porosity analysis for ash derived from magnesium-based detergent.

A similar analysis was conducted by Sappok on the ash derived from both the calcium-based detergent and the ZDDP additives independently. The author noted that the calcium detergent produced ash composed primarily of calcium sulfate ($CaSO_4$) with smaller traces of calcium carbonate ($CaCO_3$). The composition of the ash derived from the ZDDP additive was primarily two forms of zinc phosphate ($Zn_3(PO4_4)_2$ and $Zn_2P_2O_7$). To determine the theoretical densities of the this ash, the author assumed a 100% mass percentage of $CaSO_4$ for the calcium derived ash and a 50/50 mass percentage of $Zn_3(PO4_4)_2$ and $Zn_2P_2O_7$ for the ZDDP derived ash.

This XRD analysis and porosity computation was conducted for the combination lubricant oils consisting of ZDDP plus magnesium detergent as well as ZDDP plus calcium detergent. Figure 7.23 presents the XRD spectrum results for the ZDDP plus magnesium detergent derived ash. There were a number of compounds located in the ash and some of the predominant peaks have been highlighted. The majority of the ash was found to be a form of magnesium zinc phosphate ($Mg_{1.8}Zn_{1.2}(PO_4)_2$), which interestingly enough was found in trace amounts within the ash derived solely from the magnesium-based detergent. The other primarily ash constituents were a form of calcium zinc phosphate ($CaZn_2(PO_4)_2$) and calcium aluminum phosphate ($Ca_9Al(PO_4)_2$). This is interesting because no calcium was present in the lubrication oil which makes it hard to determine the reason for its presence. One possible explanation is that residual ash from the previous tests could have been trapped within the accelerated ash loading system and was subsequently deposited into the filter being loaded with magnesium plus ZDDP ash. This is likely due to the fact that parts of the test set-up were disassembled and repaired during the magnesium plus ZDDP experiment which may have loosened some of the ash generated during past experiments stuck within the system to be deposited into the filter being loaded. It may be beneficial to run this XRD analysis again to determine whether the presence of these calcium-based compounded is

repeatable or an outlier in the ash sample tested. Regarding the confidence of the porosity calculation, the theoretical densities of the calcium-based compounds compared to the the magnesium zinc phosphate differ only slightly with a maximum difference of 0.60 g/cm^3 for the compound with the smallest mass percentage of 20%. If the ash sample contained 100% magnesium zinc phosphate without any presence of the calcium-based compounds, the porosity was calculated to be 92.4% compared to a porosity of 92.1% including the calcium-based compounds. Because these porosities are so similar, the presence of the undesired calcium-based compounds do not greatly affect the porosity calculation of the ash sample. The presence of aluminum can likely be attributed to the filter substrate's wash coat which is primarily composed of aluminum and/or tin.

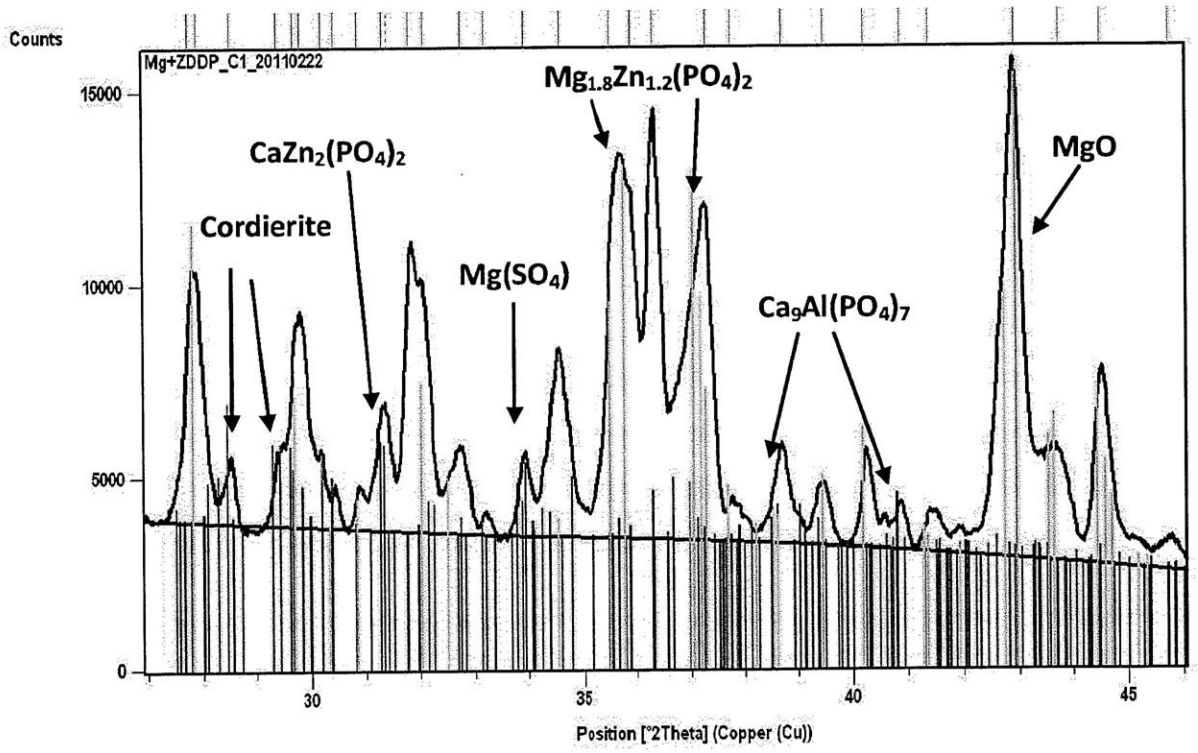

Figure 7.23: Ash compositional analysis via XRD for ash generated from oil containing ZDDP + magnesium detergent.

Similar to the method described for the magnesium-based detergent ash, a simplified ash composition was determined by proportionally distributing the trace compounds' mass percentages to the primary ash constituents. Once the simplified ash composition was determined, the theoretical density of the ash was determined using the weighted mass percentage and theoretical densities for each of the ash compounds present. Table 7.2 presents these results as well as the porosity calculation from equation 3.10.

Comp	Name	Mass %	Density (g/cm^3)	Notes
Mg O	Magnesium Oxide	7.0	3.58	
$Mg(SO_4)$	Magnesium Sulfate	8.0	2.66	Anhydrous
$Mg_2(Al_4\ Si_5O_{18})$	Cordierite	7.0	2.65	Range 2.55 - 2.75
$Mg_{1.8}Zn_{1.2}(PO_4)_2$	Magnesium Zinc Phosphate	30	3.60	$MgZn_2(PO_4)_2$
$Ca(SO_4)$	Calcium Sulfate	9.0	2.96	Anhydrous
$Ca_9Al(PO_4)_7$	Calcium Aluminum Phosphate	16	3.05	
$CaZn_2(PO_4)_2$	Calcium Zinc Phosphate	23	3.65	
$Ca_9Al(PO_4)_7$	Calcium Aluminum Phosphate	23	3.05	Simplified Composition
$CaZn_2(PO_4)_2$	Calcium Zinc Phosphate	33	3.65	
$Mg_{1.8}Zn_{1.2}(PO_4)2$	Magnesium Zinc Phosphate	44	3.60	
	Theoretical Density	3.49	g/cm^3	
	Layer Packing Density	0.274	g/cm^3	
	Porosity	92.1%		

Table 7.2: Tabular results of XRD and porosity analysis for ash derived from ZDDP + Mg detergent.

Figure 7.24 presents the XRD spectrum results for the ZDDP + calcium detergent derived ash. There were a number of compounds located in the ash and some of the predominant peaks have been highlighted. The ash was primarily composed of calcium sulfate ($CaSO_4$) a form of calcium aluminum phosphate ($Ca_9Al(PO_4)_7$) and a form of calcium zinc phosphate ($CaZn_2(PO_4)_2$). Other compounds were found but only in trace amounts. The presence of a calcium-aluminum compound is interesting and likely due to a portion of the wash coat being bonded with some calcium phosphate and changing phase.

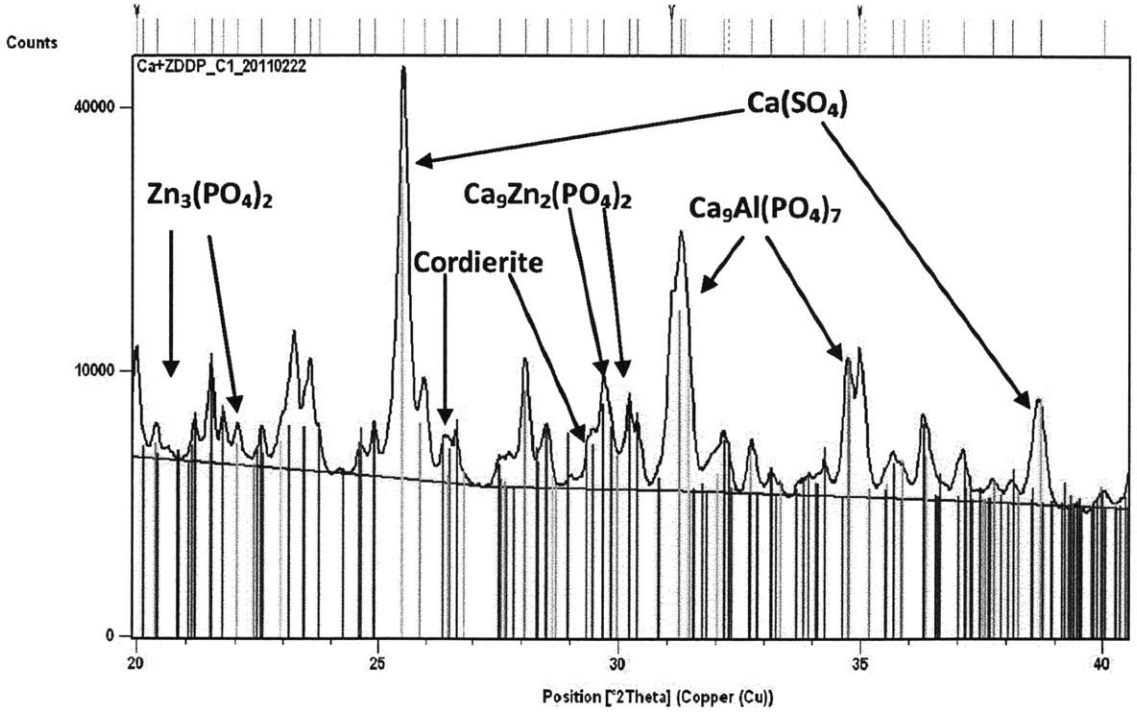

Figure 7. 24: Ash compositional analysis via XRD for ash generated from oil containing ZDDP + calcium detergent.

Similar to the method described for the previously analyzed ashes, a simplified ash composition was determined by proportionally distributing the trace compounds' mass percentages to the primary ash constituents. Once the simplified ash composition was determined, the theoretical density of the ash was determined using the weighted mass percentage and theoretical densities for each of the ash compounds present. Table 7.3 presents these results as well as the porosity calculation from equation 3.10.

Comp	Name	Mass %	Density (g/cm^3)	Notes
$Mg_2(Al_4Si_5O_{18})$	Cordierite	8.0%	2.65	Range 2.55 - 2.75
$Ca(SO_4)$	Calcium Sulfate	40%	2.96	Anhydrous
$Ca_9Al(PO_4)_7$	Calcium Aluminum Phosphate	29%	3.05	
$CaZn_2(PO_4)_2$	Calcium Zinc Phosphate	18%	3.65	
SiO_2	Silicon Oxide	1.0%		
$Zn_3(PO_4)_2$	Zinc Phosphate	4.0%	3.84	
$Ca(SO_4)$	Calcium Sulfate	46%	2.96	Simplified Composition
$Ca_9Al(PO_4)_7$	Calcium Aluminum Phosphate	33%	3.05	
$CaZn_2(PO_4)_2$	Calcium Zinc Phosphate	21%	3.65	
	Theoretical Density	3.13	g/cm^3	
	Layer Packing Density	0.297	g/cm^3	
	Porosity	91%		

Table 7.3: Tabular results of XRD and porosity analysis for ash derived from ZDDP + Ca detergent.

Along with the results of the above described lubricant oil formulations, a similar analysis was conducted on the ash derived from fully formulated CJ-4 oil by Sappok in 2009.

7.4 Summary of Measured and Computed Ash Properties

A summary of the measured ash properties from the post-mortem analysis is present in table 7.4 below.

Lubricant	Regeneration	Ash Load	Ash Layer Thickness	Wall Density	Plug Density	Simplified Theoretical Density	Ash Porosity
		[g/L]	[cm]	[g/cm^3]	[g/cm^3]	[g/cm^3]	[%]
Base + Ca [50]	Periodic	29	0.015	0.270	0.204	3.00	90.9
Base + Mg	Periodic	24	0.009	0.192	0.165	3.58	94.6
Base + ZDDP [50]	Periodic	28	0.013	0.189	0.173	3.90	95.1
CJ-4 [50]	Periodic	42	0.013	0.299	0.170	3.40	91.1
Ca + ZDDP	Periodic	25	0.011	0.297	0.125	3.133	90.5
Mg + ZDDP	Periodic	23	0.009	0.274	0.135	3.49	92.1

Table 7.4: Summary of the measured ash properties for ash generated from lubrication oil containing single and multiple additives with periodic generation. Data taken from [50] where specified.

Based on the measured packing density values and proportionally weighted densities of the primary ash composition determined via XRD (simplified theoretical density), the ash porosities ranged from 91% to 95% with the ash derived from the calcium-based detergent being the least porous, and the ash derived

from the ZDDP-based detergent being the most porous. In general, the properties of the calcium based ash (base plus Ca and Ca plus ZDDP) are very similar to those of the fully formulated CJ-4 ash. This provides further evidence that the calcium-based detergent exerts the greatest influence on ash morphology and properties as well as the resulting pressure drop. It is also interesting to note that the magnesium plus ZDDP ash displays a porosity that is lower than both the magnesium and ZDDP ashes alone pointing to the possibility of some unpredictable synergistic effects of the resultant ash which occurs when the two additives are mixed. This is likely due to the magnesium and ZDDP based ash having both higher theoretical densities based off the identified compounds as well as lower packing densities. These two factors result in a higher porosity for the magnesium and ZDDP ash compared to the magnesium plus ZDDP ash.

Table 7.5 provides additional parameters related to the DPF geometries computed from the ash distribution measurements and properties listed in table 7.4.

Lubricant	Regeneration	Ash Load	Average Hydraulic Diameter	Average End Plug Length	Available Filtration Area per Channel	Change in Filtration Area
		[g/L]	[cm]	[cm]	[cm^2]	[%]
Base + Ca [50]	Periodic	29	0.117	2.8	4.30	-49.6
Base + Mg	Periodic	24	0.129	4.8	4.30	-49.6
Base + ZDDP [50]	Periodic	28	0.121	3.9	3.69	-56.8
CJ-4 [50]	Periodic	42	0.121	4.8	3.69	-56.8
Ca + ZDDP	Periodic	25	0.125	3.1	4.48	-47.5
Mg + ZDDP	Periodic	23	0.130	3.9	4.33	-49.2

Table 7.5: Summary of the average filter properties for ash generated from lubrication oil containing single and multiple additives with periodic generation. Data taken from [50] where specified.

7.5 Ash-Compositional Effects on Pressure Drop

Using the zero dimension pressure drop model described in chapter 3, the post-mortem ash characteristics and the fully ash loaded space velocity measurements, the pressure drop attributed to the flow through the ash and substrate layers (porous media) as well as the wall velocity can be determined. Figure 7.25 plots the porous media pressure drop as a function of wall velocity for the cases compared throughout this research.

As previously mentioned, the ash distribution measurements obtained from the post-mortem analysis were used to compute the average velocity of the exhaust gas through the filter wall, which is dependent on the exhaust gas flow rate and available filtration area. Using the equations described in

chapter 3, pressure drop due to gas flow through the porous media layer was determined and plotted as a function of wall velocity creating figure 7.25. The slopes of the pressure drop curves in figure 7.25 are directly proportional to the quantity (w/k) relating to the flow resistance of the porous media (layer thickness divided by permeability). The porous media layer refers to the combination of the substrate and the ash layer. Therefore the permeability determined is not just of the ash layer but also the substrate whose flow resistance may have been impacted by ash particles within its pores. It is also important to note that the exhaust gas used for all the pressure drop determinations was ambient air at room temperature. Because these exhaust gas parameters were constant, the various ash characteristics were the only possible contributor to the differences in pressure drop ensuring the ability to compare the determined permeability measurements.

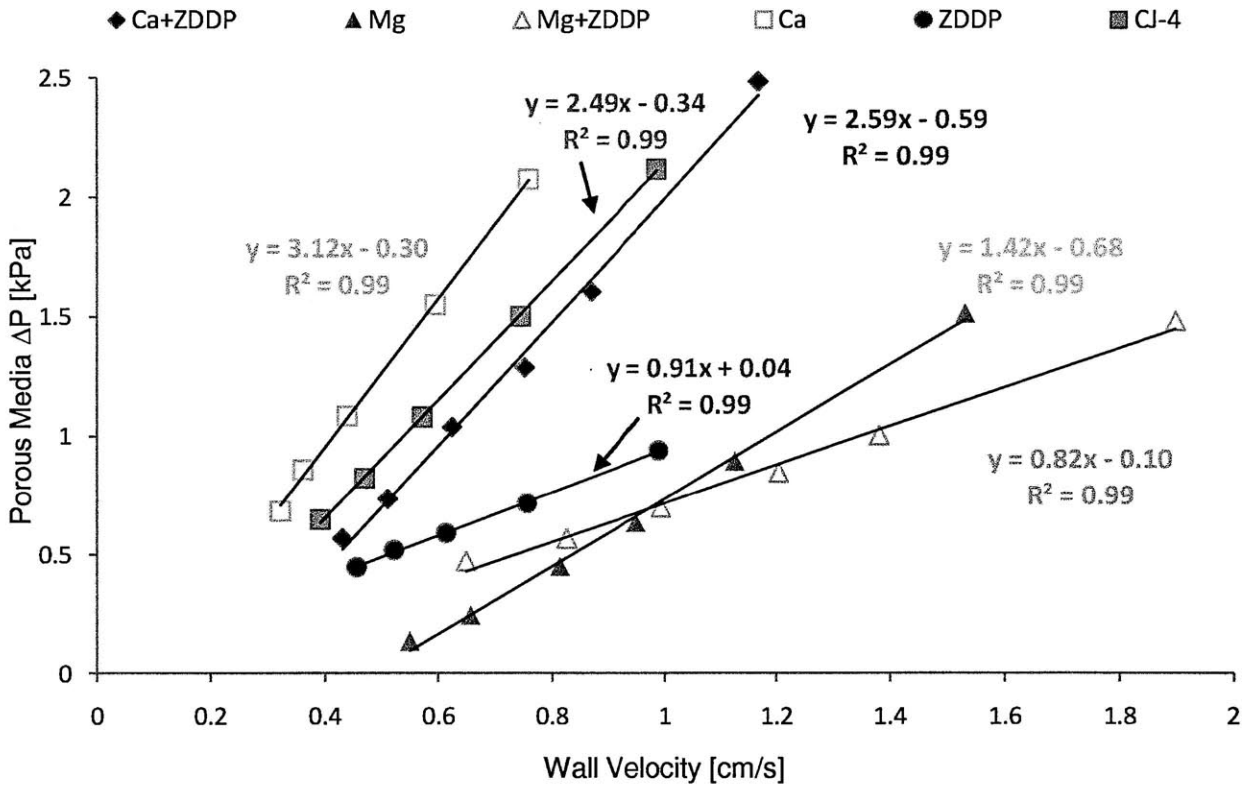

Figure 7. 25: Pressure drop through the ash layer and DPF substrate as a function of wall velocity for ash loaded DPFs with varying lubricant-derived ash chemistries. Data for Base + Ca, Base + ZDDP and CJ-4 taken from [50].

Table 7.4 presents the average layer thickness data for each of the compared test cases all being relatively close in magnitude from 0.009 mm to 0.013 mm. Taking this into consideration along with the fact that the pressure drop slopes in figure 7.25 are substantially different, the determined ash permeability values were expected to be vary greatly. Since all of the substrates were composed of the

same material, comparing the slopes is a semi-quantitative method of comparing permeability values. Table 7.6 present the each of the test cases' permeability values relative to that of fully formulated CJ-4 ash.

Lubricant	Permeability Relative to CJ-4
Base + Ca	0.8
Base + ZDDP	2.74
Base + Mg	1.75
Ca + ZDDP	0.96
Mg + ZDDP	3.05
CJ-4	1

Table 7.6: Ash permeability values relative to CJ-4 for each of the test cases compared. Data for base + Ca, base + ZDDP and CJ-4 taken from [50].

By observing the values in table 7.6, it can be seen that of the ash derived from single additives, ZDDP and magnesium are much more permeable than ash from the CJ-4 oil. On the other hand, the ash derived from the calcium-based detergent displays a permeability measurement very similar to that of ash derived from fully-formulated CJ-4 oil. Of the ash derived from combinations of additives, the formulation composed of the magnesium-based detergent plus ZDDP displays the highest comparative permeability of all the test cases compared, including the ashes derived from the magnesium-based detergent and ZDDP independently. This further confirms that synergistic effects occur as additives are combined which may not necessarily be predictable in a proportional manner based off individual additive test results. This is likely due to the different compounds that are formed from the additive combination ash cases which were not found in the single additive ash produced. It was also noticed that as ZDDP is added to the calcium-based detergent, the resultant permeability closely resembles the permeability of the CJ-4 ash. This synergistic effect is a bit more predictable taking into consideration the determined permeability, porosity and pressure drop values of the calcium-based detergent and ZDDP independently. By comparing all of the relative permeability values, the ash derived from the calcium-based detergent seems to portray the lowest permeability values whereas the magnesium-based detergent and ZDDP additives produce ashes which are much more permeable. These determinations support both the packing density and pressure drop values previously mentioned.

7.6 Scanning Electron Microscopy Analysis

Scanning electron microscopy (SEM) images were taken of the ash layers for each of the test cases within this experiment. In general the areas of interest were the ash layer itself, the ash-substrate interface, as well as ash particles and agglomerates. All of the images taken were performed at the

Massachusetts Institute of Technology's Center for Material Science and Engineering using a JOEL 5910 general purpose SEM with a Bruker Elemental Dispersive X-ray (EDX) system for elemental analysis and mapping.

To construct the samples necessary for the SEM imaging, small filter specimens were taken from the "B" location approximately 57mm downstream from the inlet filter face. These samples were approximately 2.5 cm in length and 8 cells x 5 cells in size resulting in approximately 20 loaded filter channels for observation. Once these samples were cut to size, they were impregnated with epoxy and the desired observation face was ground and polished resulting in an extremely smooth surface. Once the polishing was complete, the sample observation face was coated with 9 nm of carbon resulting in a fully prepared sample ready for imaging. Figure 7.26 depicts an example of a typical sample used in this analysis. It can be seen from this image that the channel cross sections were the areas of interest.

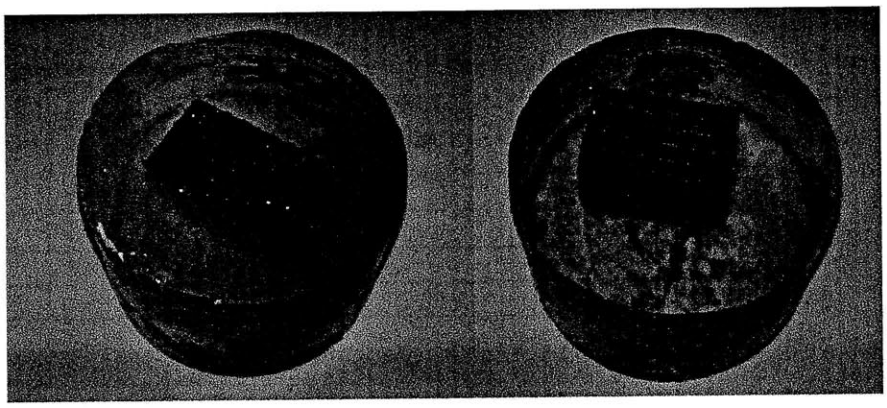

Figure 7.26: Examples of SEM samples displaying the image surface.

Figure 7.27 displays some of the ash layer images as well as the corresponding mapping. The qualitative results from all of the images taken, regardless of ash composition, corresponded for all of the samples observed:

- The extent of ash depth filtration into the substrate was minimal consisting of only the surface pores.
- Comparing the various single-element EDX maps corresponds with the compounds found through XRD.
- Ash particles follow a bimodal distribution consisting of primary particles and agglomerates.
- The cross section of the ash layer within a channel is relatively smooth and even with slightly more ash collecting in the channel corners.
    - At a high ash load, the open channel cross-sectional area is circular instead of square in nature.
- No Boron was found using the EDX mapping.

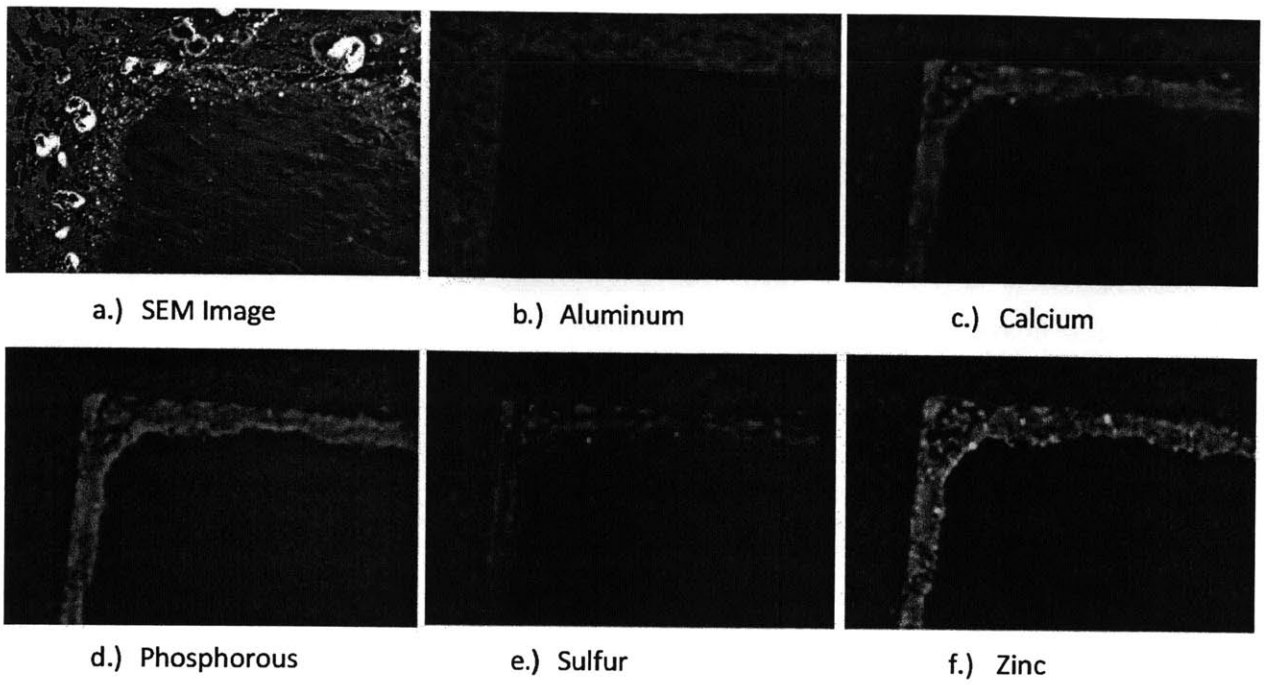

Figure 7.27: SEM (A) and EDX (B-F) images for the ash layer of the Ca + ZDDP test case.

Figure 2.27 displays the ash layer SEM and a portion of the EDX images taken. The EDX image for aluminum (Al) clearly defines the substrate layer due to the fact that aluminum is one of the primary elements found in cordierite and not present in the ash layer. By comparatively looking at the EDX images for calcium (Ca), phosphorous (P), sulfur (S) and zinc (Zn) one can note that the elements are simultaneously present in the same locations. This leads to the assumption that calcium zinc phosphates, calcium zinc sulfates, calcium sulfates & phosphate as well as zinc sulfates & phosphates are possibly present in the ash layer which was confirmed with the XRD analysis previously described. All of the SEM & EDX images taken for each test case can be found in the appendix figures A-10 through A-12.

Figure 7.28 presents closer images that look at the ash-substrate interface to determine the extent of depth filtration. It can be seen from this image that the ash only seems to penetrate the surface pores of the substrate. In cases where there are larger surface pores, like that seen in figure 7.28, the ash has the ability to penetrate deeper into the substrate but in general the ash does not travel deep within the substrate matrix. The extent of depth filtration seen in all of interface images was on the order of 25μm.

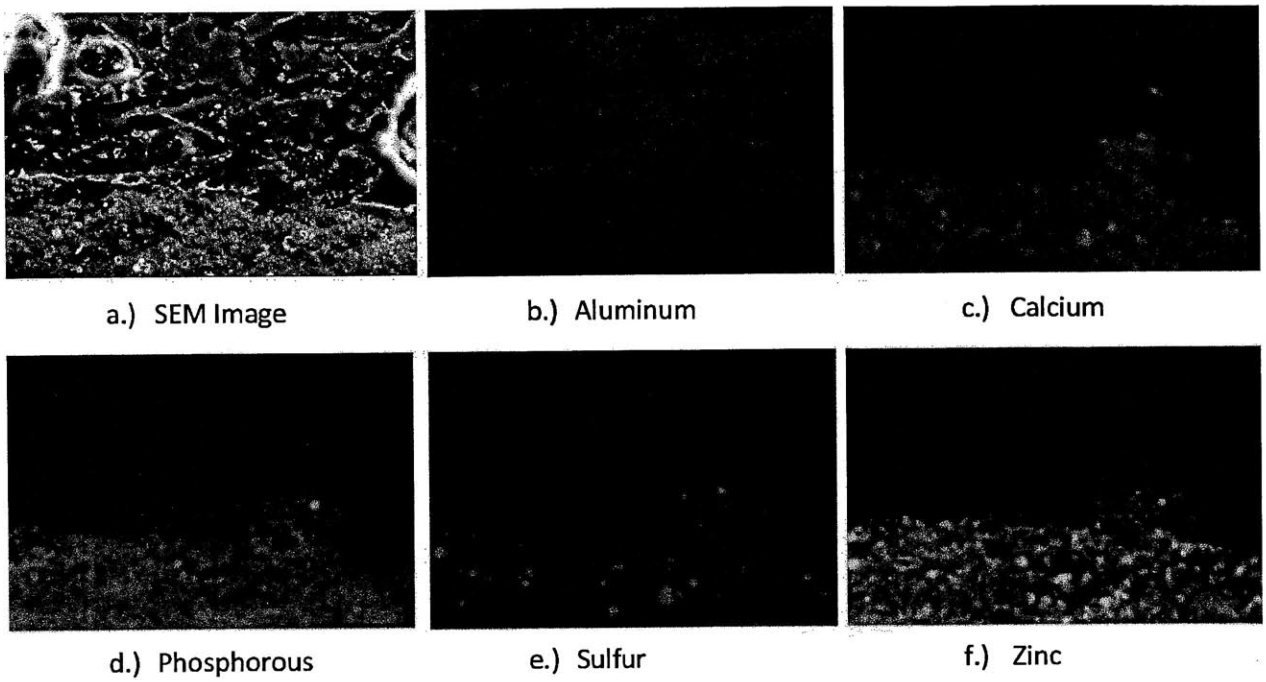

Figure 7.28: SEM (A) and EDX (B-F) images for the ash-substrate interface for the Ca + ZDDP test case.

7.7 Field Core Sample Analysis

A portion of the post-mortem analysis was performed on an obtained field sample. The field sample consisted of a removed DPF core section from a long-haul truck. Figure 7.29 displays the field core sample and table 7.7 provides the available information regarding the sample. The back 1 inch of the core sample was removed by the provider prior to shipping. This outlet 1 inch contained the ceramic end plugs of the inlet channels as well as some amount of ash end plug. Because of the limited quantity of the filter provided, only a few ash layer thickness measurements along with the ash plug packing density determination were performed.

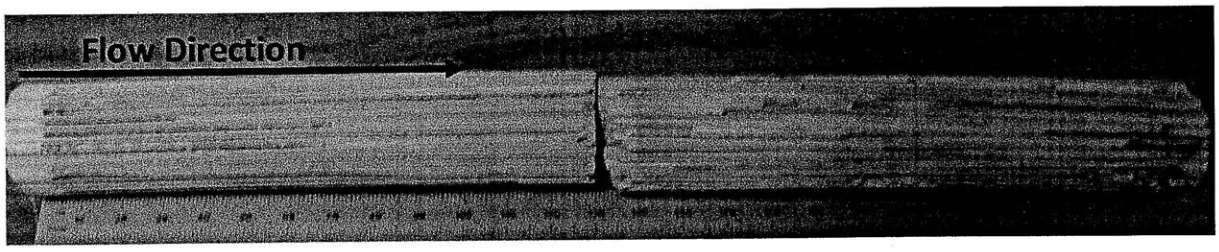

Figure 7.29: Picture of the field core sample obtained for post-mortem analysis.

The downstream most portion of the field sample had been removed by the manufacturer prior to obtaining the sample. This removed portion was approximately 2.5 cm in length and contained the

ceramic end plugs of the inlet cells. With this being said, a substantial amount of ash plug was still provided enabling a packing density measurement.

Figure 7.30 graphically depicts how the field sample was sectioned as well as the relative axial distances.

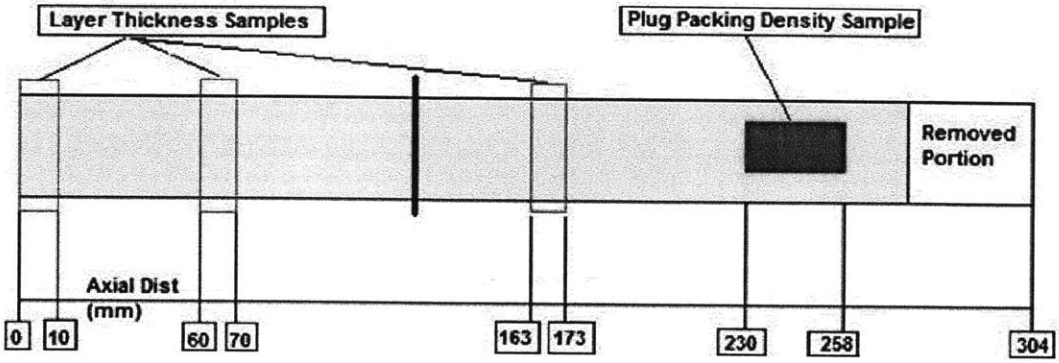

Figure 7.30: Field sample sectioning depiction with appropriate axial distances in mm from filter inlet face.

Engine Type	Filter Type	Lubrication	Filter Aging
Medium Duty	Cordierite Pt-catalyst	CJ-4	480k miles

Table 7. 7: Amplifying information on field DPF sample obtained and analyzed.

Three 10mm long samples were removed and ash layer thickness measurements were taken on both sides. One segment was taken towards the end of the sample which was used for ash plug packing density measurements. No samples were taken between the axial distances 173mm to 230mm because the provided core sample seemed to be cracked and any further cutting would likely break the sample into unworkable pieces.

The ash layer thickness determinations were made using the same graphical technique previously described. The end plug length was determined by probing the appropriate channels of the cracked segment (173mm → 230mm) with a small metal wire to determine the plug's length from the back of the sample. The ash layer profile for the core sample can be seen in figure 7.31. The average ash layer thickness was approximately 0.033mm which is roughly 20% to 30% of the layer thicknesses seen in the lab experiments discussed in chapter 7.1. It is important to note that a majority of the ash contained along the cake layer of this sample was likely inadvertently removed during shipping. Because of this, these results may not be able to be directly compared to those of the lab generated test cases described throughout this research. The end plugs of this sample were measure to be approximately 71mm in length which is approximately one and half times larger than the end plug length seen in the lab generated CJ-4 case at 42 g/L. For a valid comparison these end plug lengths must be normalized by their respective filter lengths. Doing this results in comparable end plug to filter length ratios of 0.23

and 0.31 for the field and CJ-4 samples respectively. Although the ash load was not known for the field sample, one could deduce that it was on the order of 42 g/L due to the relative similar ash end plug to filter length ratios.

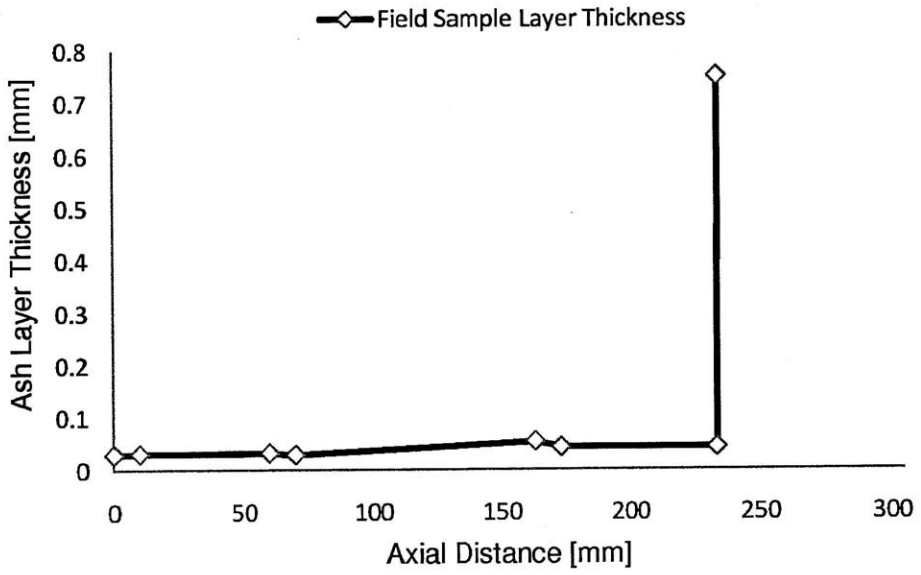

Figure 7.31: Ash Layer profile for the obtained field sample.

The ash plug packing density was determined in a slightly different manner than the lab generated test cases previously discussed. Because there were only a few measurements to be taken for the field sample, it was necessary to measure the dimensions and weights of each individual plug to provide enough data points for a confident average plug packing density value with a reasonable standard deviation. The first step of the process was to precisely cut a plug filled filter specimen from the core sample. It was noticed that not all of the expected filter channels had ash end plugs which was likely due to their inadvertent removal during the shipping process. This is likely due to the removal of the back 1 inch of the filter by the providing source which contained the ceramic inlet channel end plugs which ensure that the ash does not exit the filter on the outlet end of those channels. Due to the small number of ash end plugs in the sample, each plug was individually numbered and measured for length. Figure 7.32 presents a picture of the end plug sample with each plug labeled with its appropriate number.

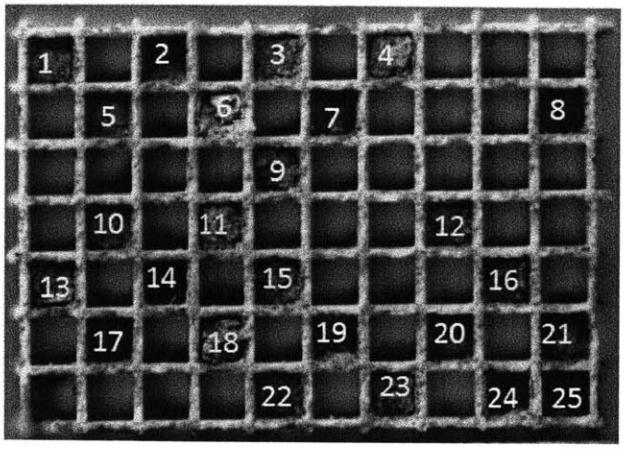

Figure 7.32: Ash plugs present in sample used for packing density measurements with each plug numerically labeled.

To determine the ash plug packing density measurements, each individual plug's length was measured. To determine these plug lengths accurately, each plug was probed with a thin metal wire and the probe distance was subtracted from the length of the entire sample containing the end plugs. Each plug was removed from the sample by extending the metal wire through the length of the sample and then tapping out the residual ash. The sample was weighed at various intervals of plug removal.

Based on the assumption that the ash plug takes up the total frontal area of the channel along the entire sample length, the plug packing density of the field sample was determined to be 0.352 g/cm^3. This value is approximately 1.73 to 2.8 times the values seen through the compared lab generated filters and specifically approximately 2 times that of the CJ-4 test 42 g/L. The difference in field and lab plug packing density measurements are likely due to both the elevated ash load of the field sample as well as the exhaust flow and thermal history of the field ash- loaded filter.

(This page intentionally left blank)

8.0 CONCLUSIONS

The results of this work regarding how the ash derived from specific lubricant additives adversely affect diesel particulate filters are among the few of its kind. Past studies have shown that ash comprises 50% of the collected particulate matter within a DPF after only 35,000 miles of on road use [50]. Because of this it is important to understand how ash negatively affects diesel aftertreatment performance over a minimum DPF service life of 150,000 miles. A large number of studies have been conducted on fully-formulated CJ-4 lubricant oil and its resultant ash effects, but the underlying understanding as to why it acts in this manner is still unknown. Lubricant chemistry and exhaust conditions have been found to play a significant role in how ash affects the pressure drop across a DPF. By conducting experiments on single lubricant additives as well as simple combinations, the individual and synergistic effects of the additives contained in CJ-4 lubricant can be studied and analyzed. The results of this study provide practical information to aid lubricant formulators, engine manufactures and aftertreatment designers to mitigate the adverse effects of ash accumulation within a DPF.

8.1 Lubricant Chemistry Effects on Pressure Drop

After the performance evaluation phase was completed a pressure drop profile was generated for each of the test cases and compared. Each of the profiles followed the same general trend with a steep pressure drop increase from 0 g/L to approximately 3 g/L of ash load due to depth filtration followed by a shallower linear rise due to the buildup of an ash cake layer. Through analysis of the pressure drop profiles, the pressure drop due to "depth filtration" or substrate surface pore coverage accounts for roughly 50-75% of the total measured pressure drop for all the compared test cases. This highlights the fact that "depth filtration" reduction is a major objective in the optimization of DPF use. The pressure drop slopes due to the ash cake layer build up differed between the test cases ranging from 0.002 $\frac{kPa}{g/L}$ to 0.05 $\frac{kPa}{g/L}$. Because of this, ash of various chemistries that build up along the channel walls have a very different effect on pressure drop which confirms that lubricant chemistry factors into DPF performance.

Of the single additive test cases, the calcium ash had a pressure drop one and a half to two times larger than the magnesium and ZDDP cases for a given ash load. Throughout the cake layer build up the calcium test case produced the largest profile slope representing that the accumulation of the calcium-detergent ash has the largest effect on pressure drop on a per gram basis. This is likely due to the calcium ash layer having the highest packing density and lowest theoretical density based off the determined composition. These two factors paired with one another result in a porosity value roughly

4% lower than both the magnesium and ZDDP ash. Through the Kozeny-Carman relationship described in equation 3.9, the porous media permeability and thus pressure drop due to the flow across the porous layer is extremely sensitive to porosity.

Of the multiple additive test cases, the calcium plus ZDDP test case had the largest pressure drop for a given ash load followed by the CJ-4 lubricant and lastly the magnesium plus ZDDP lubricant. This correlates well with the determination that the calcium based additive has the largest effect on pressure drop regardless of what other additives are included. The calcium plus ZDDP lubricant formulation had the highest concentration of the calcium based detergent and displayed the largest pressure drop. The magnesium detergent plus the ZDDP additive had no calcium detergent present and displayed under half the pressure drop for a given ash load compared to the calcium plus ZDDP test case. All three additive combination test cases had similar packing densities as well as theoretical densities. The resultant porosities differed by one percent. Although the Kozeny-Carman relationship is sensitive to porosity, particle diameter is also an input variable to determine the porous layer permeability. Although it was beyond the scope of this work, the particle diameter range for the test cases compared should be analyzed to further understand the resultant pressure drop differences.

8.1.1 Conclusions on Lubricant Chemistry Effects on Pressure Drop

In general it seems that the calcium based detergent has the largest effect on DPF pressure drop on a mass basis. This is likely due to the relatively low porosity of calcium-based ash penetrating or covering the surface pores of the substrate causing an increased flow resistance. The addition of other additives to the calcium based lubricant produces some advantageous synergistic effects from a pressure drop perspective by increasing the ash's porosity or possibly affecting the particle diameter but its presence alone has a large impact on DPF performance. The magnesium based detergent on the other hand has a much lower impact on DPF pressure drop and although more expensive, should be studied in more detail as a possible replacement for its calcium counterpart due to their similar functions as lubricant detergents.

8.2 Combined Soot and Ash Effects on DPF Pressure Drop

After the test cases were fully loaded with their respective ash (> 22 g/L), soot was deposited on top of the ash layer to observe the combined effects of soot and ash on the performance of a DPF. Of the performed test cases, the presence of the ash derived from lubricants not containing a calcium detergent had a beneficial effect on DPF performance from a pressure drop perspective compared to a clean DPF. This was due to the prevention of soot depth filtration by the ash cake layer which had only a

slight effect on the DPF pressure drop alone. Although the calcium test case also prevented soot depth filtration, the high pressure drop increase of the ash layer alone did not provide a beneficial effect compared to a clean DPF. All of the combined ash soot profiles seemed relatively constant for each of the single additive test cases except for the magnesium case at soot loads greater than 2.5 g/L. This is likely attributed to the substantially larger end plug length of the magnesium case between the other cases. Although the calcium and magnesium cases had the same available filtration area, past research as determined that the end plug length has been found to largely affect the DPF performance of soot loaded on top of ash layers [50]. Because of the magnesium ash is more prone to transport from the ash cake layer to the end plug, the end plug length of the magnesium test case is larger compared to the other lubricant formulations and thus has a greater negative effect on combined soot and ash performance characteristics.

8.3 Ash Transport and Deposition

For all of the test cases the general deposition and transport mechanisms remained constant although the extent of each differed between lubricant chemistry. During the initial stages of loading, from 0 g/L to approximately 3 g/L, the majority of the ash is deposited in the surface pores of the substrate. At ash loads between approximately 3 g/L to 10 g/L, an ash cake layer begins to build up along the walls of the filter channel. At ash loads above approximately 10 g/L, the ash cake layer seems to reach a critical thickness and deposits begin to transport to the back of the filter creating what is referred to as an end plug. As this end plug is formed and growing in length at loads above approximately 10 g/L, the ash layers along the channel walls still grow slightly at a much slower rate compared to that seen between 3-10 g/L. The ash layer thickness, profile and eng plug length differ substantially between lubricants of various chemistries.

Of all the performed tests, the magnesium and magnesium plus ZDDP ash displayed ash layer thickness between 18-40% smaller than the other tests cases. The largest ash layer thickness was seen for the calcium ash. Although the average layer thicknesses, the values fall within the standard deviations of one another resulting in comparable ash layer thicknesses. There was little difference in ash layer thicknesses in the radial direction for each test case. There were large differences noticed in the characteristics of the ash end plugs. The magnesium, ZDDP and magnesium plus ZDDP ash displayed end plug lengths 36-42% larger than the ash derived from lubricant containing the calcium detergent. The magnesium ash displayed the largest and most non- characteristically consistent end plug lengths with an approximate 37% decrease in length off the DPF centerline.

When comparing the simple additive combinations of Ca + ZDDP and Mg + ZDDP with their corresponding single additive tests some interesting characteristics were noticed. The addition of ZDDP to the magnesium-based detergent seems to create a much more characteristically consistent, yet still transport prone, ash which results with an characteristically consistent ash layer along the DPF with a thickness similar to that of magnesium and a more uniform ash end plug length in-between that of magnesium and ZDDP. Similar characteristics were seen with the addition of ZDDP to the calcium-base detergent.

By comparing the ash layer and end plug characteristics of the magnesium plus ZDDP case at two ash loads, 12 g/L and 23 g/L, some insight into the ash transport process is gained. At just under 12g/L of ash, end plugs begin to form at the outlet end of the filter. The ash layer thickness of the 12 g/L case is roughly 60% of that of the 23 g/L case. This leads to the observation that as the end plug grows in length past ash loads of 12 g/L, the ash layer thickness slightly builds as well.

8.3.1 Conclusions on Ash Deposition and Transport

The fundamental depositions process of "depth filtration" and surface pore coverage followed by the buildup of an ash cake layer was consistent for all test cases. The ash derived from the magnesium based detergent is likely more prone to transport displaying a smaller average layer thickness and longer average end plug length. This ash is likely to have a lower critical shear stress and bonding energy compared to the calcium derived ash. It should be noted that the magnesium ash was the only ash primarily composed of an oxide and not a sulfate or phosphate. With this being said it may be a possibility that ash composed of oxides are more prone to transport within a DPF due to their specific compound shape or bonding energy.

8.4 Ash Packing Characteristics

The ash packing characteristics differed between each test case which was expected considering the differences in pressure drop profiles and transport. For the single additive test cases, the calcium ash displayed a 30% increase in packing density compared to the magnesium and ZDDP test cases. This correlates well with the pressure drop profiles for the respective test cases being that the ash packed less densely is less restrictive to air flow resulting in a lower pressure drop. The differences in packing density are likely attributed to the bonding energies of the ash compounds as well as their respective physical shapes. For all of the test cases, the ash end plugs were less dense than their respective ash cake layers. With this being said, the ash plug densities follow a similar trend with the calcium plugs being roughly 15% denser than the ZDDP and magnesium plugs. This relates to the transport trends

noticed and mentioned in the previous section. Although the calcium ash is the least likely to transport, when it transports to the end plug it tightly packs together in a dense fashion. On the other hand, the magnesium ash is most likely to transport but does so in a less dense fashion resulting in a longer end plug for a given mass of ash.

For the additive combination lubricant formulations, the ash layer packing densities were much closer in magnitude to one another differing only 10%. The magnesium plus ZDDP test case produced an ash layer packing density much higher than expected likely due to the difference in bonding energy and packing characteristics between magnesium oxide, which was the primary constituent of the magnesium ash, and magnesium zinc phosphate, which is the primary constituent of the magnesium plus ZDDP case. Although the ash layer packing density of the magnesium plus ZDDP case is close to that of the calcium plus ZDDP and CJ-4 cases, the pressure drop trends differ greatly resulting in probable porosity and particle size differences between the ash deposits. The ash plug packing density was the greatest in the CJ-4 test case which was likely due to the fact that it was at an elevated ash load of 42 g/L. This observation was also seen in the post mortem analysis of the field sample which noted that the plug packing density is likely to increase as the ash load reaches elevated values.

8.4.1 Conclusions on Ash Packing Characteristics

For all of the test cases, the ash end plug was packed less densely than its respective ash cake layer. The calcium containing test cases as well as the magnesium plus ZDDP test case displayed the highest packing densities. These packing characteristics likely relate to the particle size and shapes of the compounds calcium sulfate, calcium zinc phosphate and magnesium zinc phosphate. On the other hand, the magnesium oxide and zinc phosphates did not pack densely together along the ash cake layer which can likely be attributed to their respective particle shapes. It was also noticed through field sample analysis that the filter thermal history and flow characteristics likely influence the ash layer and end plug packing densities.

8.5 Ash Composition and Morphology Results and Conclusions

Using XRD analysis, the ash derived from each test lubricant differed in composition which in turn affects the ash's porosity and resultant permeability. The ash derived from the magnesium-based detergent was primary composed of magnesium oxide (MgO) with a small percentage of magnesium zinc phosphate ($Mg_{1.8}Zn_{1.2}(PO_4)_2$). This produced a proportionally combined, primary compound-derived density, or "simplified theoretical density", of 3.58 g/cm^3 and a resultant porosity of 94.6%. The ash derived from the calcium-based detergent was primarily composed of calcium sulfate ($CaSO_4$) and

calcium carbonate ($CaCO_3$) which produced a simplified theoretical density of 3.0 g/cm^3 and resultant porosity of 90.9%. The ZDDP based ash was primarily composed of two forms of zinc phosphate ($Zn_3(PO4_4)_2$ & $Zn_2P_2O_7$) which produced a simplified theoretical density of 3.9 g/cm^3 and resultant porosity of 95.1%. The pressure drop model described in chapter 3 is very sensitive to porosity so although all measured porosities are above 90%, a one or two percent difference will greatly impact the total pressure drop calculated. The porosities of the base + Mg and base + ZDDP test cases are much higher than that of the base + Ca case which correlates well with the pressure drop trends described previously.

The primary compound found with the Mg + ZDDP test case was zinc phosphate ($Mg_{1.8}Zn_{1.2}(PO_4)_2$), and trace amounts of calcium zinc phosphate ($CaZn_2(PO_4)_2$) and calcium aluminum phosphate ($Ca_9Al(PO_4)_2$). This produced a simplified theoretical density of 3.49 g/cm^3 and resultant porosity of 92.1%. The ash derived from the Ca + ZDDP test case was primarily composed of calcium sulfate ($CaSO_4$), a form of calcium aluminum phosphate ($Ca_9Al(PO_4)_7$) and a form of calcium zinc phosphate ($CaZn_2(PO_4)_2$). This resulted in a simplified theoretical density of 3.13 g/cm^3 and resultant porosity of 90.5%. The fully formulated CJ-4 found respective percentages of the aforementioned compounds relating to a simplified theoretical density of 3.4 g/cm^3 and resultant porosity of 91.1%. The porosity of the Mg + ZDDP ash was the highest of the multi-additive lubricants which agrees with the compared pressure drop trends. The compounds found within the Mg + ZDDP ash should be studied in depth to possible account for the unexpected packing density increase compared to the base + Mg and base + ZDDP test cases.

The relative permeability to CJ-4 ash was determined for each of the lubricants tested. Of the single additive test cases, the base + ZDDP had the highest permeability compared to CJ-4. This partially explains how the base + ZDDP ash had the lowest pressure drop trend although a lower porosity and thicker ash layer compared to the base + Mg test case. The base + Ca ash layer had the lowest permeability compared to the CJ-4 ash layer. This paired with the lowest porosity and highest packing density explains why it would result in a very high pressure drop profile.

Of the additive combinations, the Mg + ZDDP test case had the highest permeability compared to the CJ-4 ash. This partially explains how the pressure drop trend is extremely low although the packing density is relatively high. The Ca + ZDDP ash's permeability closely resembles that of the CJ-4 which agree with the corresponding pressure drop profiles.

The SEM images of each of the test cases resulted in the same qualitative observations:

- The extent of ash depth filtration into the substrate was minimal consisting of only the surface pores.
- Comparing the various single-element EDX maps corresponds with the compounds found through XRD.
- Ash particles follow a bimodal distribution consisting of primary particles and agglomerates.
- The cross section of the ash layer within a channel is relatively smooth and even with slightly more ash collecting in the channel corners.
    - At a high ash load, the open channel cross-sectional area is circular instead of square in nature.
- No Boron was found using the EDX mapping.

8.6 Practical Applications

The major goal of this research to further the fundamental understanding of how lubricant derived ash affects DPF performance is meant to provide lubricant formulators and filter manufacturers information to mitigate its negative effects. From a lubrication formulation perspective, it seems as though magnesium-based detergents should be explored as a direct replacement for calcium-based based detergents. Although more expensive, magnesium-based ash affects DPF pressure drop much less than calcium-based ash as well as having favorable transport characteristics. When combined with other additives, the magnesium formulation seems to have favorable packing characteristics as well as roughly half the pressure drop of its calcium counterpart. An economic study should be conducted to determine the cost-benefit analysis of using the more expensive magnesium detergent for more favorable affects over the DPF's lifecycle.

It could also be investigated to have a specified time-based loading cycle for DPFs using different lubricant formulations at different aspects of the filter's life. During the initial stages of loading, a more expensive magnesium-based lubrication oil could be used to mitigate the pressure drop due to "depth filtration". Once the substrate surface pores were covered with the more porous magnesium ash layer, a cheaper calcium formulation could be used during the ash cake layer build up. Although from a pressure drop perspective this would not be better then strictly using magnesium-based oil, if the cost of the magnesium additive was too high it may be beneficial to use it only at the initial stages of filter loading. Being that the pressure drop due to "depth filtration" comprises nearly 50-75% of the total lifetime filter pressure drop, it would be beneficial to mitigate that aspect of filter loading if possible.

The most desirable transport characteristics were noticed in the magnesium ash test case. One possibility for this observation could be attributed to the fact that the magnesium ash was primarily composed of an oxide and not a sulfate or phosphate. If lubrication formulators could influence the formation of oxides vice sulfates and phosphates during lubrication combustion, more desirable transport characteristics could be noticed over the course of the DPF lifespan.

8.7 Future Work Considerations

Although many qualitative results were found through this research, the underlying mechanisms for their presence and differences are yet to be determined. There are a number of possible future work opportunities which would help determine why the results found in this research exist. One aspect which should be explored are some possible advanced diagnostics on ash layers to help determine:

1. The critical shear stress of the ash layers derived from various lubricant chemistries
2. Available porous volume within the ash layers of the various chemistries
3. Exhaust flow and thermal histories of ash layers and their resultant effects

The first possibly noted above would provide more insight on the observed ash transport and packing characteristics noted previously in this section. Ash transport directly affects pressure drop as well as the available filtration area. If this could be understood in more detail, it would greatly influence the optimization of advanced diesel aftertreatment systems.

The second point noted above would provide further understanding into the synergistic effects of soot and ash layer interaction. It is inevitable that over the lifetime of a DPF that a soot layer would be deposited on top of an existing ash layer. If the understanding of the synergistic effects of this could be explained, the resultant pressure drop effects would therefore be further understood.

By comparison of the lab and field samples, some differences have been noted. This is likely due to the dynamic exhaust flow and thermal history of the DPF. Although this area is very broad, it should be explored in more detail to better understand the fundamental aspects of a field DPF's life.

The results obtained through this study provide considerable insight into how the ash derived from specific lubricant chemistries adversely affect the performance of a diesel particulate filter and why. Although a great deal of progress has been made there is still much room for further understanding. With this being said, this work not only provides further fundamental understanding but also identifies

practical results to aid lubrication formulators and aftertreatment designers to better optimize the diesel aftertreatment system to accommodate lubricant derived ash accumulation.

(This page intentionally left blank)

9 REFERENCES

[1] Heywood, J.B., Internal Combustion Engine Fundamentals, McGraw-Hill, Inc., New York, 1988.

[2] Diesel Technology Forum, "Where is Diesel: Cars, Trucks, SUVs, <http://www.dieselforum.org/where-is-diesel/cars-trucks-suvs/>, 2005.

[3] Schindler, K-P., 1997. "Why Do We Need The Diesel?", SAE 972684, 1997.

[4] DieselNet Technology Guide, "Case for the Diesel", Revision 2000-10, DieselNet. <http://www.dieselnet.com/tech/diesel_case.html>, 2000.

[5] Energy Information Administration, Doc. No. DOE/EIA-X063, "Diesel Fuel Prices: What Consumers Should Know", United States Department of Energy, 2007.

[6] Charles River Associates, "Diesel Technology and the American Economy," Diesel Technology Forum Report no. D02378-00, 2000.

[7] National Center for Environmental Assessment Office of Research and Development, Doc. No. EPA/600/8-90/057F, "Health Assessment Document for Diesel Engine Exhaust", US Environmental Protection Agency, 2002.

[8] American Lung Association of California, "Health Effects of Diesel Exhaust", <http://oehha.ca.gov/public_info/facts/pdf/diesel4-02.pdf>.

[9] Environmental Protection Agency, "Health Assessment Document for Diesel Emissions (Draft)", Environmental Protection Agency, Washington, DC, February 1998.

[10] Klanner, W., "Car Emissions and Euro 5 Consumers View," ADAC Workshop, Brussels, <http://www.fiafoundation.com/>, 2005.

[11] Office of Transportation and Air Quality, "Heavy Duty Engine and Vehicle Standards and Highway Diesel Fuel Sulfur Requirements," US Environmental Protection Agency (EPA) <http://www.epa.gov/otaq/regs/hd2007/frm/f00057.pdf>, 2000.

[12] US Environmental Protection Agency, Doc. No. 40 CFR Parts 9, 69, et al, "Control of Emissions of Air Pollution From Nonroad Diesel Engines and Fuel; Final Rule", US Environmental Protection Agency, 2004.

[13] Ramanathan, V., and Carmichael, G., "Global and Regional Climate Changes Due to Black Carbon," Nature Geosciences, vol. 1, April 2008. <www.nature.com/ngeo/journal/v1/n4/pdf/ngeo156.pdf>.

[14] Volkswagen ,"NAIAS Detroit 2007: Volkswagen continues BLUETEC offensive", Volkswagen, 2007.

[15] PSA Peugeot Citroën, "Air Quality: Complying with Standards", PSA Peugeot Citroën <http://www.sustainability.psa-peugeot-citroen.com/environment/air-quality/indicators.htm>.

[16] Mogaka, Z.N., Wong, V.W., and Shahed, S.M., "Performance and Regeneration Characteristics of a Cellular Ceramic Diesel Particulate Trap," SAE 820272, 1982.

[17] Salvat O., P. Marez and G. Belot, 2000. "Passanger Car Serial Application of a Particulate Filter System on a Common Rail Direct Injection Diesel Engine", SAE 2000-01-0473, 2000.

[18] Sappok, A., and Wong, V., "Detailed Chemical and Physical Characterization of Ash Species in Diesel Exhaust Entering Aftertreatment Systems", SAE 2007-01-0318, 2007.

[19] Ishizawa, T., Yamane, H., Satoj, H., Sekiguchi, K., Arai, M., Yoshimoto, N. and Inoue, T., "Investigation into Ash Loading and Its Relationship to DPF Regeneration Method". SAE 2009-01-2882.

[20] Bodek, B., and Wong, V., "The Effects of Sulfated Ash, Phosphorus and Sulfur on Diesel Aftertreatment Systems – A Review", SAE 2007-01-1922, 2007.

[21] Konstandopoulos, A., Zarvalis, D., Kladopoulou, E., and Dolios, I.: "A Multi-Reactor Assembly for Screening of Diesel Particulate Filters," SAE 2006-01-0874.

[22] Manufacturers of Emission Controls Association (MECA): "Diesel Particulate Filter Maintenance: Current Practices and Experience," Washington D.C., 2005.

[23] Boschert, T., 2002. "The Lubricant Contribution to Future Low Emission Engine Design", Diesel Particulate and NOx Emissions Course (University of Leeds), Ann Arbor, MI, October 2002.

[24] ASTM International. "D 874-06: Standard Test Method for Sulfated Ash from Lubrication Oils and Additives."

[25] McGeehan, J.A. "Diesel Engines Have a Future and That Future is Clean." SAE 2004-01-1956, 2004.

[26] McGeehan, J.A. el al. "API CJ-4: Diesel Oil Category for Both Legacy Engines and Low Emission Engines Using Diesel Particulate Filters." SAE 2006-01-3439, 2006.

[27] Hoshino, T., et al, "New Four-Stroke Diesel Engine Oil Standards for Japanese Market: JASO DH-2 and DL-1". SAE 2005-01-3718, 2005.

[28] The Lubrizol Corporation, "European Engine Oil Technology: ACES E6-08", Lubrizol, <http://www.lubrizol.com/EuropeanEngineOils/E608.html>.

[29] Rizvi, Syed Q.A., Lubricant Additives Chemistry and Applications: Chapter 4. Detergents, CRC Press, 2003.

[30] American Petroleum Institute, Doc. No. API 1509 Appendix E, "API Base Oil Interchangeability Guidelines for Passenger Car Motor Oils and Diesel Engine Oils", Revised January 2011.

[31] Sappok, A., Santiago, M., Vianna, T. and Wong V., "Characteristics and Effects of Ash Accumulation on Diesel Particulate Filter Performance: Rapidly Aged and Field Aged Results", SAE 2009-01-1086, 2009.

[32] Process for making overbased calcium sulfonate detergents using calcium oxide and a less than stoichiometric amount of water. U.S. Patent 6,015,778. (1/18/2000, AJ Rolfes and SE Jaynes).

[33] Magnesium low rate number sulfonates. U.S. Patent 5,922,655. (7/13/99, D Moulin, JA Cleverley and CH Bovington).

[34] Method of preparing overbased barium sulfonates. U.S. Patent 3,959,164 (5/25/76, AR SABOL)

[35] Overbased alkali metal sulfonates, U.S. Patent 4,867,891 (9/19/89, MW Hunt).

[36] Gergel, WC., Lubricant Additive Chemistry., Presented at the International Symposium on Technical Organic Additives and Environment, Interlaken, Switzerland, May 24-35, 1984.

[37] Rizvi, Syed Q.A., Lubricant Additives Chemistry and Applications: Chapter 5. Dispersants, CRC Press, 2003.

[38] Kruez, KL., "Diesel Engine Chemistry as Applied to Lubricant Problems". Lubrication 56:77-88, 1970.

[39] McDonald, Randolph A., Lubricant Additives Chemistry and Applications: Chapter 2. Zinc Dithiophosphates, CRC Press, 2003.

[40] Bridgewater, AJ., Dever, JR., Sexton, MD., "Mechanisms of Antioxidant Action, Part 2. Reactions of zinc bis[O,O'-dialkyl(aryl)phosphorodithioates] and related compounds with hydroperoxides". J Chem Soc Perkin II, 1006-1016, 1980.

[41] Givens, W., Buck, W., Jackson, A., Klador, A., Hertzberg, A., Moehrmann, W., Mueller-Lunz, S., Pelz, N., and Wenniger, G., "Lube Formation Effects on Transfer of Elements to Exhaust After-Treatment System Components", SAE 2003-01-3109. 2003.

[42] Bardasz, E., Cowling, S., Panesar, A., Durham, J., and Tadrous, T., "Effects of Lubricant Derived Chemistries on Performance of the Catalyzed Diesel Particulate Filters", SAE 2005-01-2168, 2005.

[43] Britton, N., Sutton, M., Otterholm, B., Tengstrom, P., Frennfelt, C., Walker, A., and Murray, I., "Investigations into Lubricant Blocking of Diesel Particulate Filters", SAE 2004-01-3013, 2004.

[44] Warner, J., Johnson, J., Bagley, S., and Huynh, C., "Effects of Catalyzed Particulate Filter on Emissions from a Diesel Engine: Chemical Characterization Data and Particulate Emissions Measured with Thermal Optical and Gravimetric Methods", SAE 2003-01-0049, 2003.

[45] Manni, M., Pedicillo, A., and Bazzano, F., "A Study of Lubricating Oil Impact on Diesel Particulate Filters by Means of Accelerated Engine Tests", SAE 2006-01-3416, 2006.

[46] Aravelli, K., and Heibel, A., "Improved Lifetime Pressure Drop Management for Robust Cordierite (RC) Filters with Asymmetric Cell Technology (ACT)", SAE 2007-01-0920, 2007.

[47] Sappok, A., Rodriguez, R., and Wong, V., "Characteristics and Effects of Lubricant Additive Chemistry on Ash Properties Impacting Diesel Particulate Filter Service Life", SAE 2010-01-1213, 2010.

[48] Takeuchi, Y., Hirano, S., Kanauchi, M., Ohkubo, H., Nakazato, M., Sutherland, M., and Van Dam, W., "The Impact on Diesel Engine Lubricants on Deposit Formation in Diesel Particulate Filters", SAE 2003-01-1870, 2003.

[49] Bardasz, E., Mackne, D., Britton, N., Kleinschek, G., Olofsson, K., Murray, I., and Walker, A., "Investigations of the Interactions between Lubricant-Derived Species and Aftertreatment Systems on a State-of-the-Art Heavy Duty Diesel Engine", SAE 2003-01-1963, 2003.

[50] Sappok, A., "The Nature of Lubricant-Derived Ash-Related Emissions and Their Impact on Diesel Aftertreatment System Performance," PhD Dissertation, Massachusetts Institute of Technology, 2009.

[51] Aravelli, K., Jamison, J., Robbinson, K., Gunasekaran, N., and Heibel, A., "Improved Lifetime Pressure Drop Management for DuraTrap RC Filters with Asymmetric Cell Technology (ACT)," Diesel Engine Efficiency and Emissions Reduction Conference, Detroit, MI, 2006.

[52] DieselNet Technology Guide, "Wall-Flow Monoliths", Revision 2005-09a, DieselNet. < http://www.dieselnet.com/tech/dpf_wall-flow.html>, 2005.

[53] DieselNet Technology Guide, "Cellular Monolith Substrates", Revision 1998-08c, DieselNet. < http://www.dieselnet.com/tech/cat_substrate.html#pressure>, 2005.

[54] Merkel, G.A., Cutler, W.A., Warren, C.J., 2001. "Thermal Durability of Wall-Flow Ceramic Diesel Particulate Filters", SAE Technical Paper 2001-01-0190

[55] Mao, F., C.G. Li, 2005. "Performance Validation of an Advanced Diesel Particulate Filter With High Catalyst Loading Capacity", SAE Technical Paper 2005-01-3696

[56] Miyakawa, N., H. Maeno and H. Takahashi, 2003. "Characteristics and Evaluation of Porous Silicon Nitride DPF", SAE Technical Paper 2003-01-0386

[57] Konstandopoulos, A., Kostoglou, M., Skaperdas, E., Papaioannou, E., Zarvalis, D., and Klaopoulou, E., "Fundamental Studies of Diesel Particulate Filters: Transient Loading, Regeneration and Aging", SAE 2000-01-1016, 2000.

[58] Young, D., Hickman, D., Bhatia, G., and Gunasekaran, N., "Ash Storage Concept for Diesel Particulate Filters", SAE 2004-01-0948, 2004.

[59] McGeehan, J., Yeh, S., Couch, M., Hinz, A., Otterholm, B., Walker, A., and Blakeman, P., "On the Road to 2010 Emissions: Field Test Results and Analysis with DPF-SCR System and Ultra Low Sulfur Diesel Fuel", SAE 2005-01-3716, 2005.

[60] Kimura, K., Lynskey, M., Corrigan, E., Hickman, D., Wang, J., Fang, H., and Chatterjee, S., "Real World Study of Diesel Particulate Filter Ash Accumulation in Heavy-Duty diesel Trucks", SAE 2006-01-3257. 2006

[61] Harlé, V., Pitois, C., Rocher, L., and Garcia, F., "Latest Development and Registration of Fuel Borne Catalyst for DPF Regeneration", SAE 2008-01-0331, 2008.

[62] Konstandopoulos, A., Zarvalis, D., Kladopoulou, E., and Dolios, I., "A Multi-Reactor Assembly for Screening of Diesel Particulate Filters", SAE 2006-01-0874, 2006.

[63] Gaiser, G., and Mucha, P., "Prediction of Pressure Drop in Diesel Particulate Filters Considering Ash Deposit and Partial Regenerations", SAE 2004-01-0158, 2004.

[64] Lee, K., Zhu, J., Ciatti, S., Yozgatligil, A., and Choi, M., "Sizes, Graphitic Structures and Fractal Geometry of Light-Duty Diesel Engine Particulates", SAE 2003-01-3169, 2003.

[65] Lee, K., and Zhu, J., "Effects of Exhaust System Components on Particulate Morphology in a Light-Duty Diesel Engine", SAE 2005-01-0184, 2005.

[66] Konstandopoulos, A., Kostoglou, M., Skaperdas, E., Papaioannou, E., Zarvalis, D., and Klaopoulou, E., "Fundamental Studies of Diesel Particulate Filters: Transient Loading, Regeneration and Aging", SAE 2000-01-1016, 2000.

[67] Kladoppoulou, E., Yang, S., Johnson, J., Parker, G., and Konstandopoulos, A., "A Study Describing the Performance of Diesel Particulate Filters During Loading and Regeneration ~ A Lumped Parameter Model for Control Applications", 2003-01-0842, 2003.

[68] Konstandopoulos, A., Skaperdas, E., and Masoudi, M., "Microstructural Properties of Soot Deposit in Diesel Particulate Traps", SAE 2002-01-1015, 2002.

[69] Houi, D and Lenormand, R., "Particle Deposition on a Filter Medium," Kinetics of Aggregation and Gelation, Elsevier Science Publishers, B.V., 1984.

[70] Tassopoulos, M., O'Brien, J., and Rosner, D., "Simulation of Microstructure/Mechanism Relationships in Particle Deposition." AICHe Journal, Vol. 35, No. 6, June 1989

[71] Tasspopulos, M., "Relationships Between Particle Deposition Mechanism, Deposit Microstructure and Effective Transport Properties," PhD Dissertation, Yale University, 1991.

[72] Konstandopoulos, A., Kostoglou, M., Housiad, P., Vlachos, N., and Zarvalis, D., "Multichannel Simulation of Soot Oxidation in Diesel Particulate Filters," SAE 2003-01-0839. 2003.

[73] Karin, P., Cui, L., Rubio, P., Tsuruta, T., and Hanamura, K., "Microscopic Visualization of PM Trapping and Regeneration in Micro-Structural Pores of a DPF Wall", SAE 2009-01-1476, 2009.

[74] Sutton, M., Britton, N., Otterholf, B., Tengström, P., Frennfelt, C., Walker, A., and Murray, I., "Investigations into Lubricant Blocking of Diesel Particulate Filters," SAE 2004-01-3013, 2004.

[75] Totten, G., Handbook of Lubrication and Tribology: Application and Maintenance, CRC Press, Boca Raton, FL, 2006.

[76] Institute of Mechanical Engineers, "Correcting Mass Measurement of Diesel Particulate Filters at Non-Ambient Temperatures", SAE 18-223-D1-9 , 2009.

10 APPENDIX

Run 1		
CL (°C)	Edge (°C)	Mass (kg)
680.5	534	7.2479333
648.5	478.5	7.2485333
616	459	7.2487333
480.5	319.5	7.2498667
409.5	271.5	7.2497333
282	175	7.2504
220.5	151	7.2512
175.5	138.5	7.2518667

Run 2		
CL (°C)	Edge (°C)	Mass (kg)
618	425.5	7.2486
589.5	395	7.2490667
498.5	334	7.2498
454.5	297.5	7.25
379	255.5	7.2505333
313.5	179.5	7.2512667
150.5	123	7.2523667
145	104.5	7.253

Run 3		
CL (°C)	Edge (°C)	Mass (kg)
684	505.5	7.2487333
613.5	424.5	7.2496
527	356.5	7.2503333
427	280.5	7.2506
373.5	243.5	7.2512
246.5	166.5	7.252
208.5	147	7.2527333
78.5	85	7.2534

Table A- 1. Table of results from the mass v. temp variability analysis.

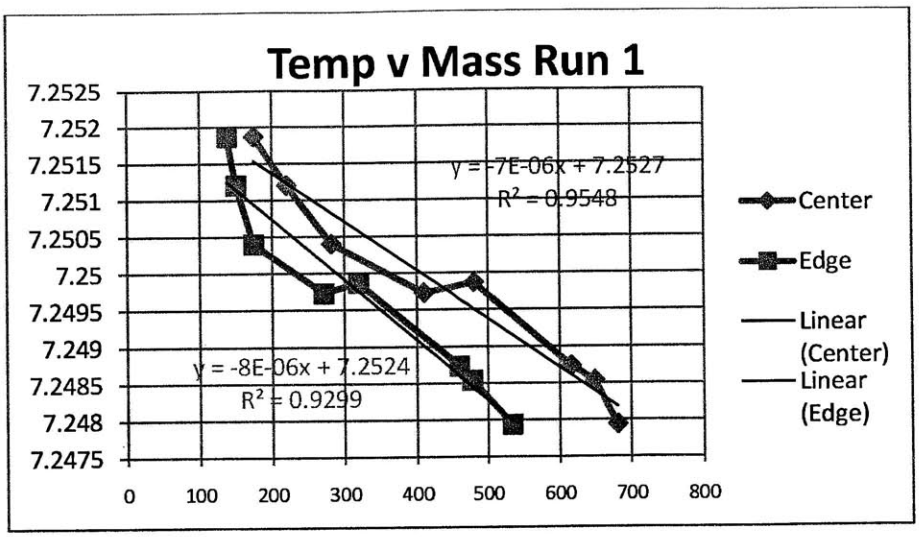

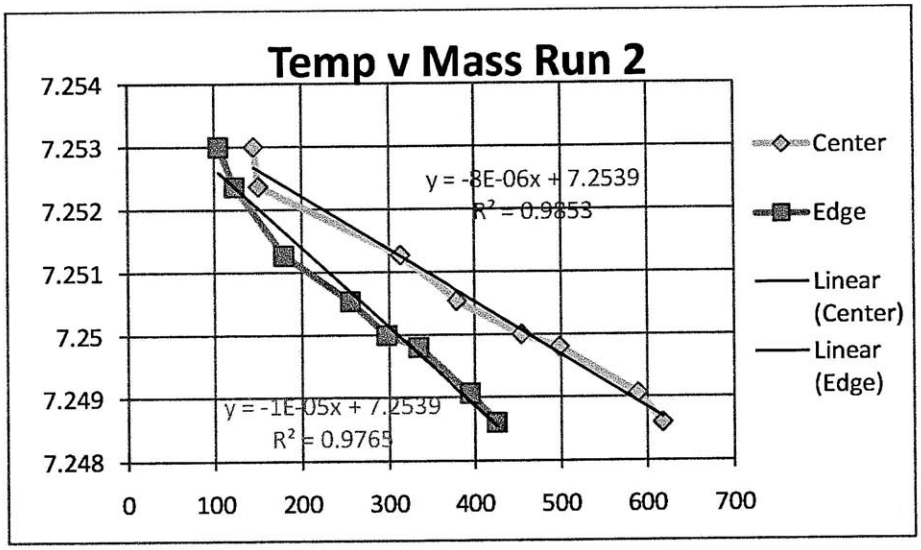

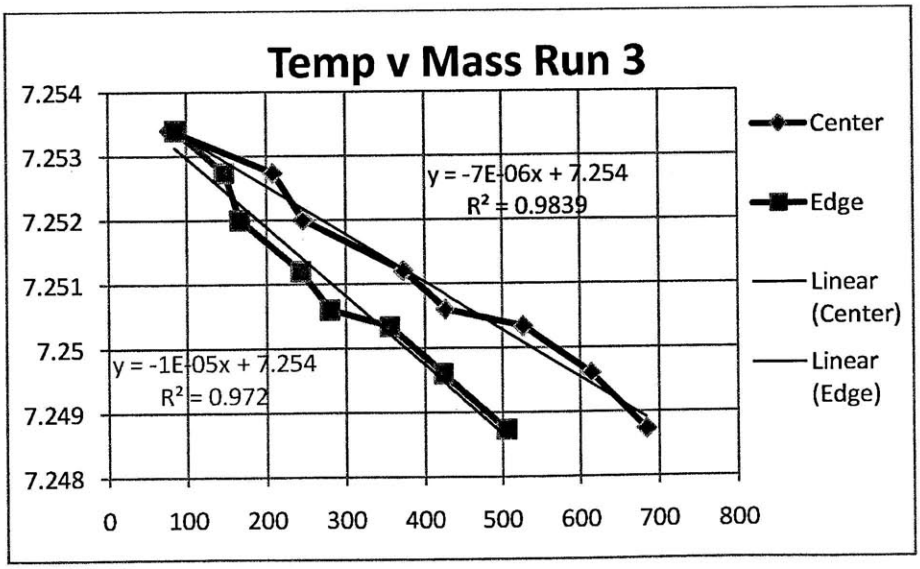

Figure A- 13. Mass v. Temp Variability graphs

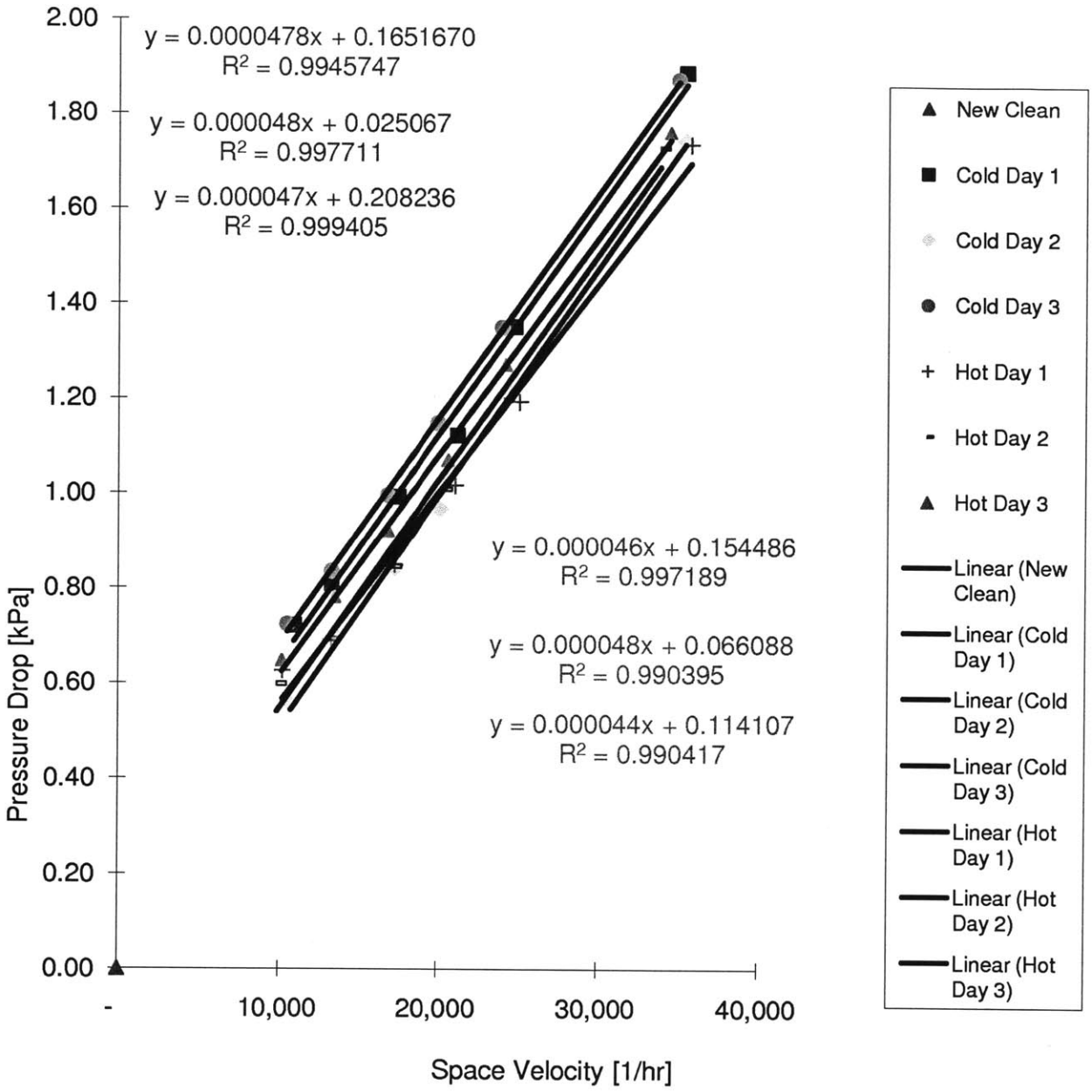

Figure A- 2. Space velocity graphs for pressure drop variability study conducted on filter with 22.7 g/L ash.

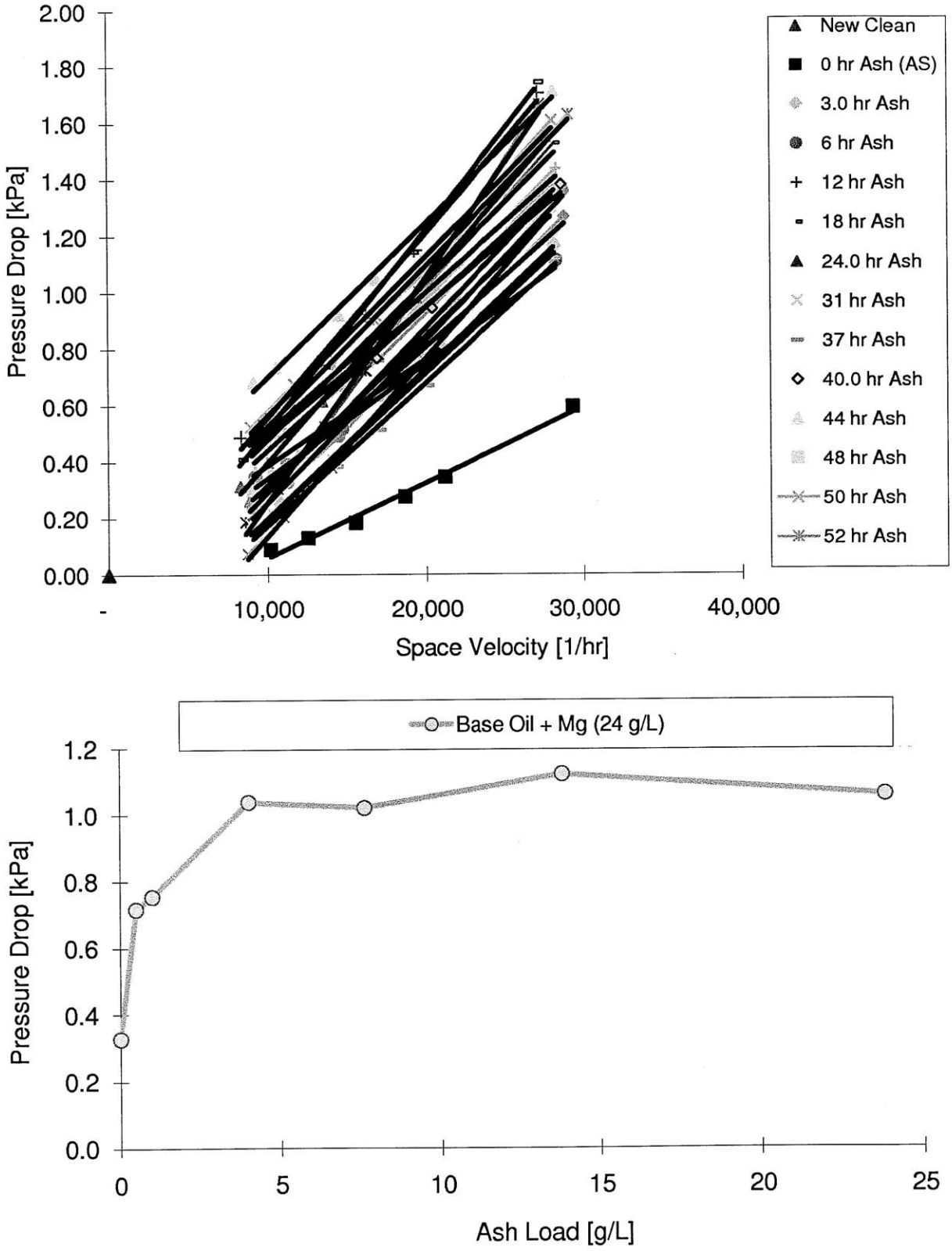

Figure A- 3. Space velocity and pressure drop graphs for ash loading of base + Mg test case.

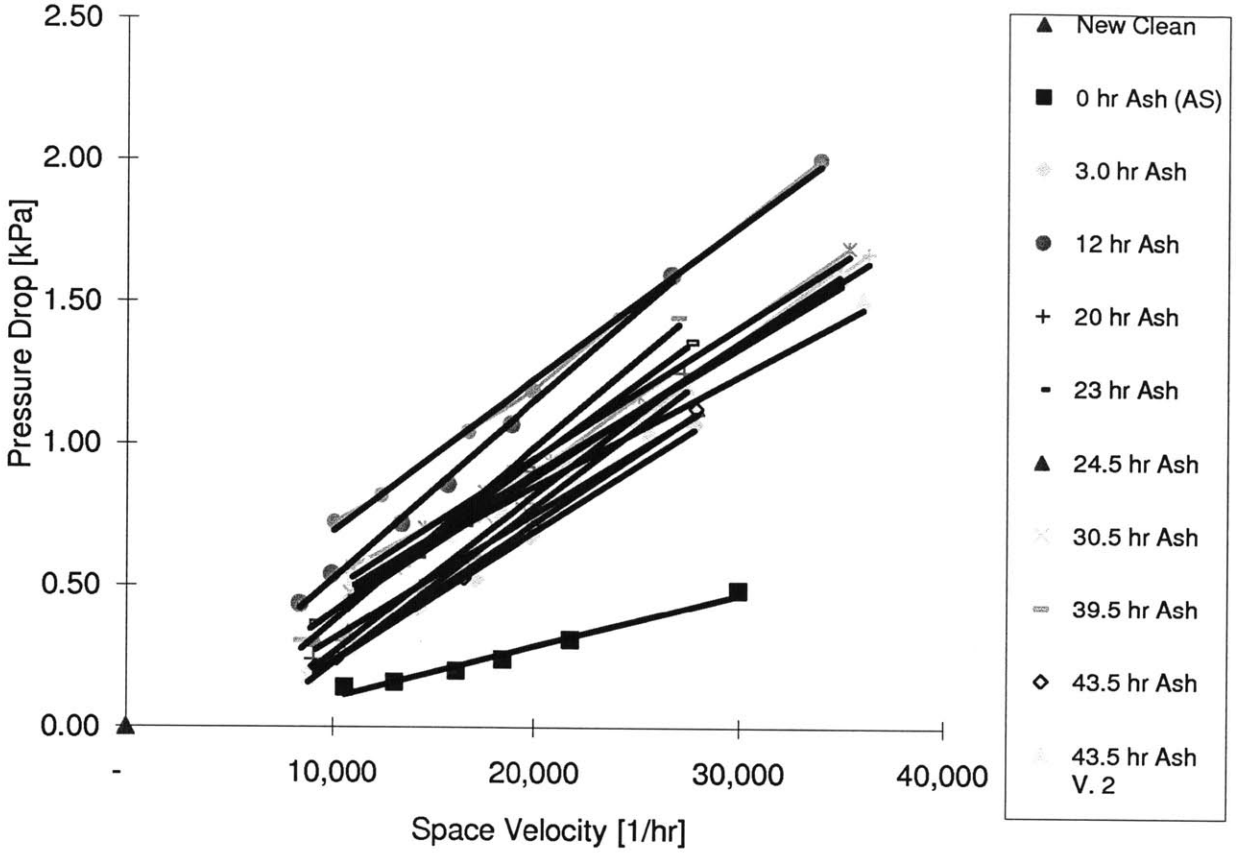

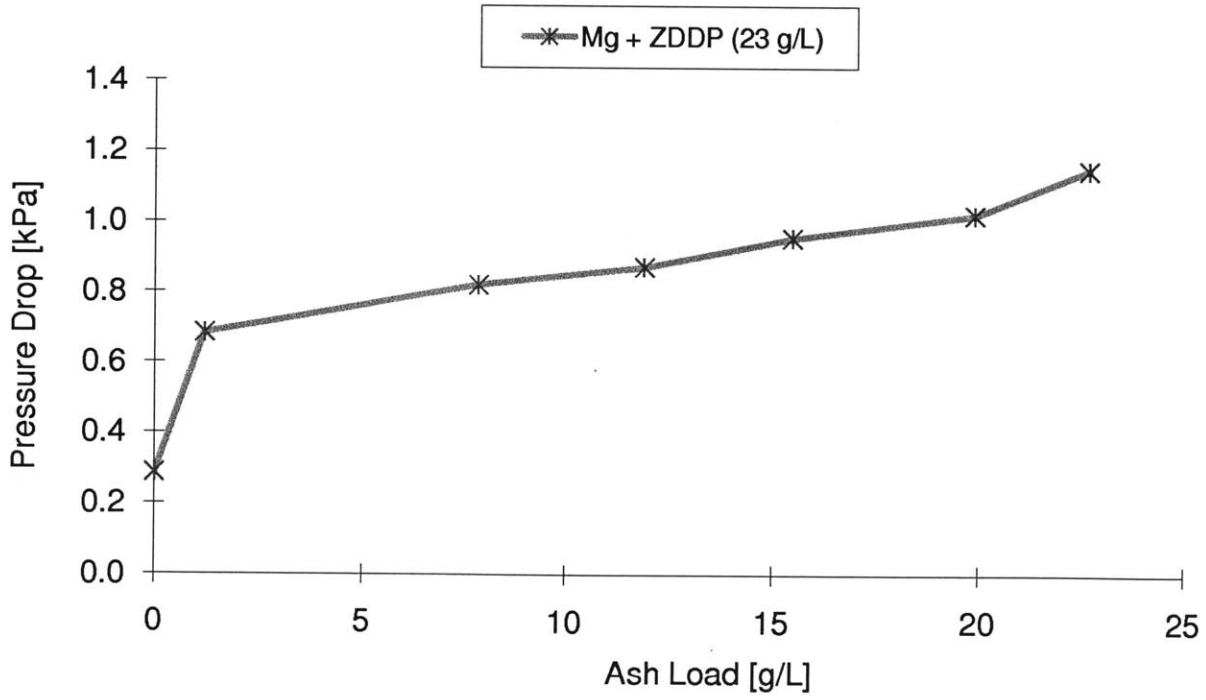

Figure A- 4. Space velocity and pressure drop graphs for ash loading of Mg + ZDDP test case.

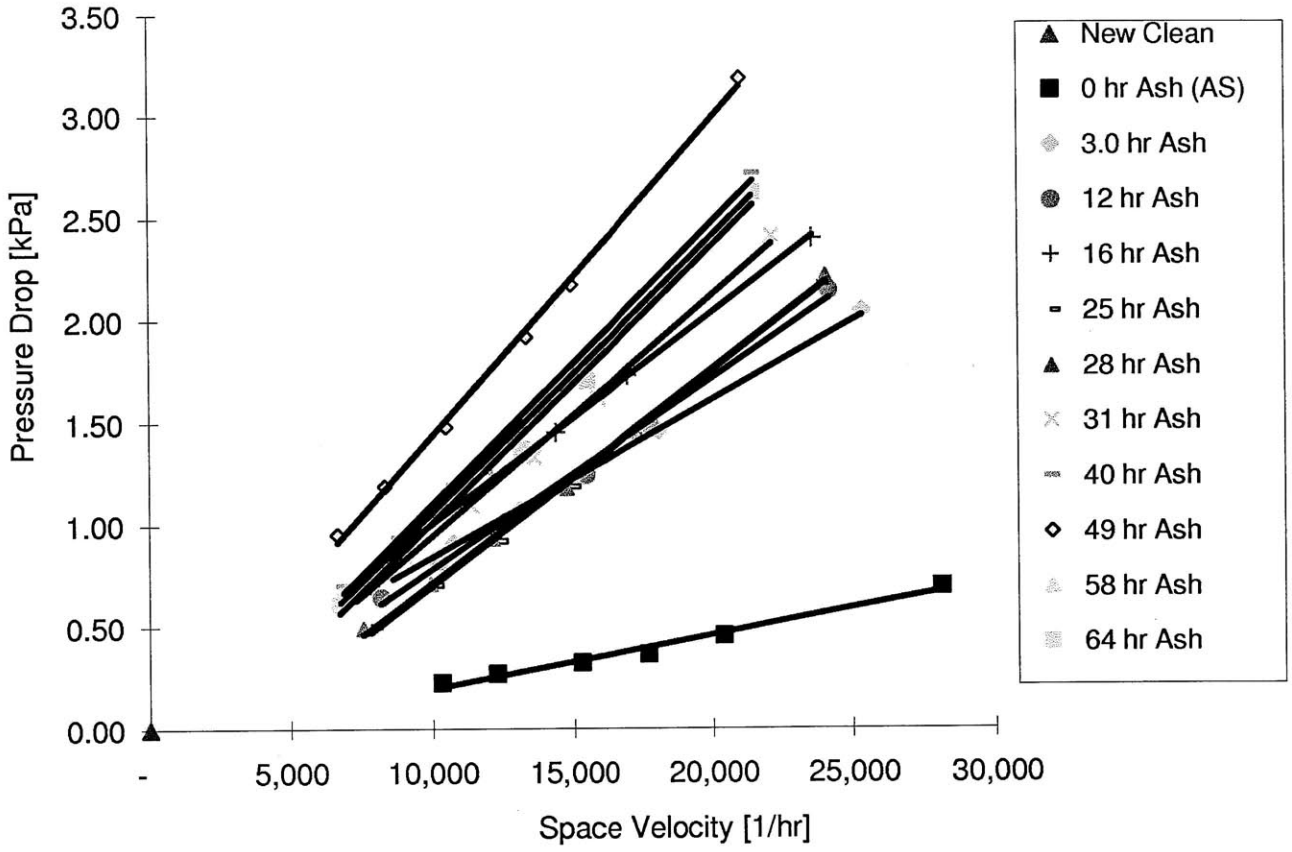

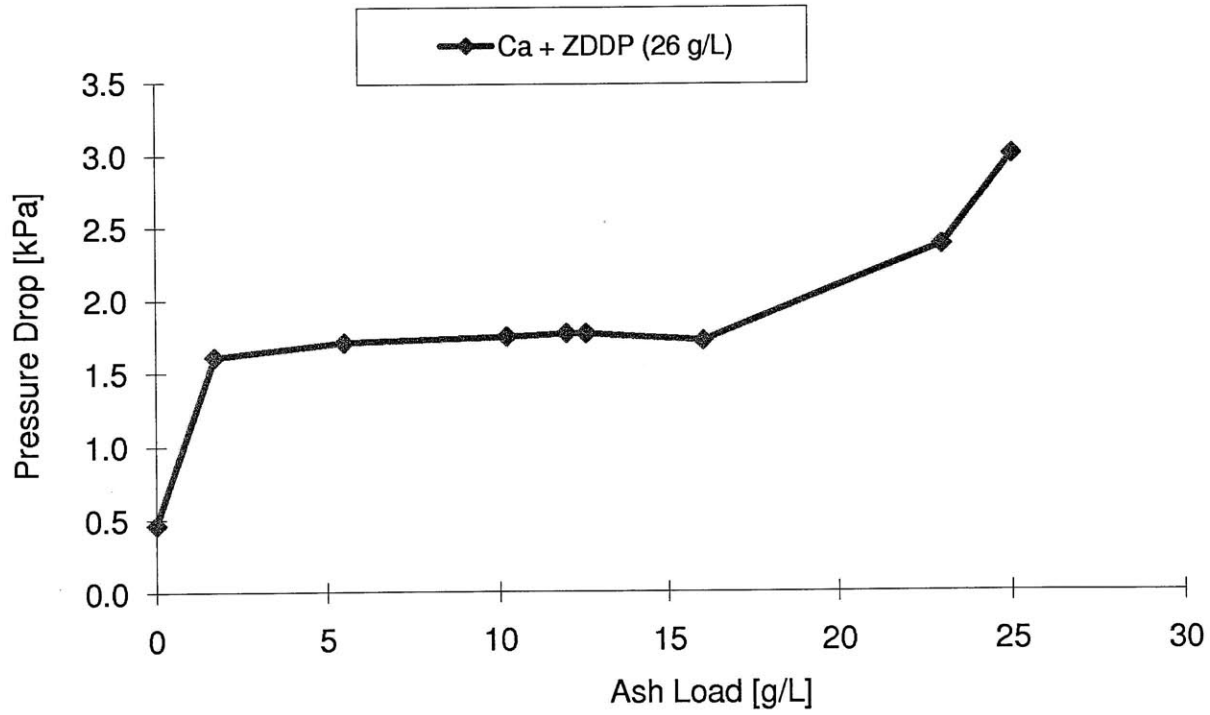

Figure A- 5. Space velocity and pressure drop graphs for ash loading of Ca + ZDDP test case.

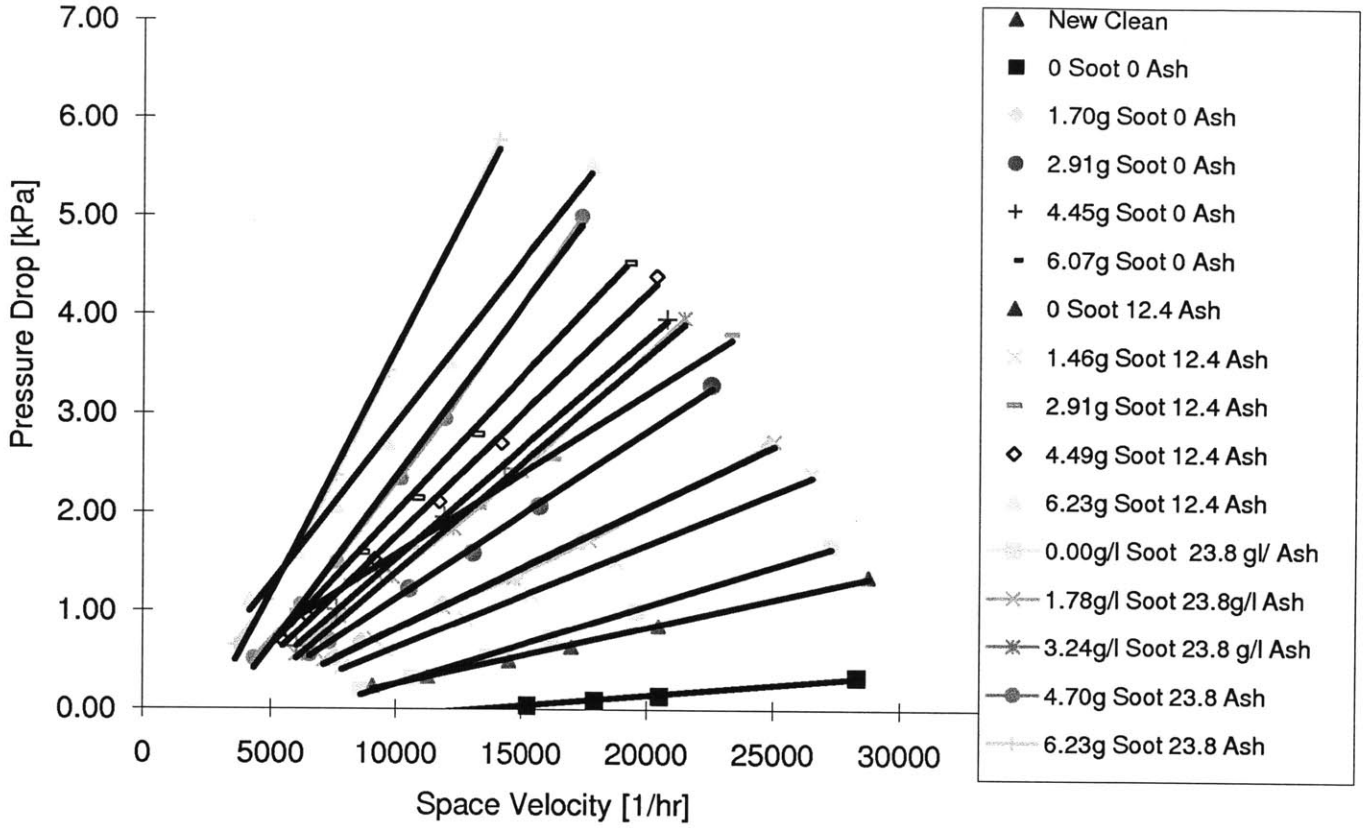

Figure A- 6. Space velocity and pressure drop graphs for soot loading of base + Mg test case.

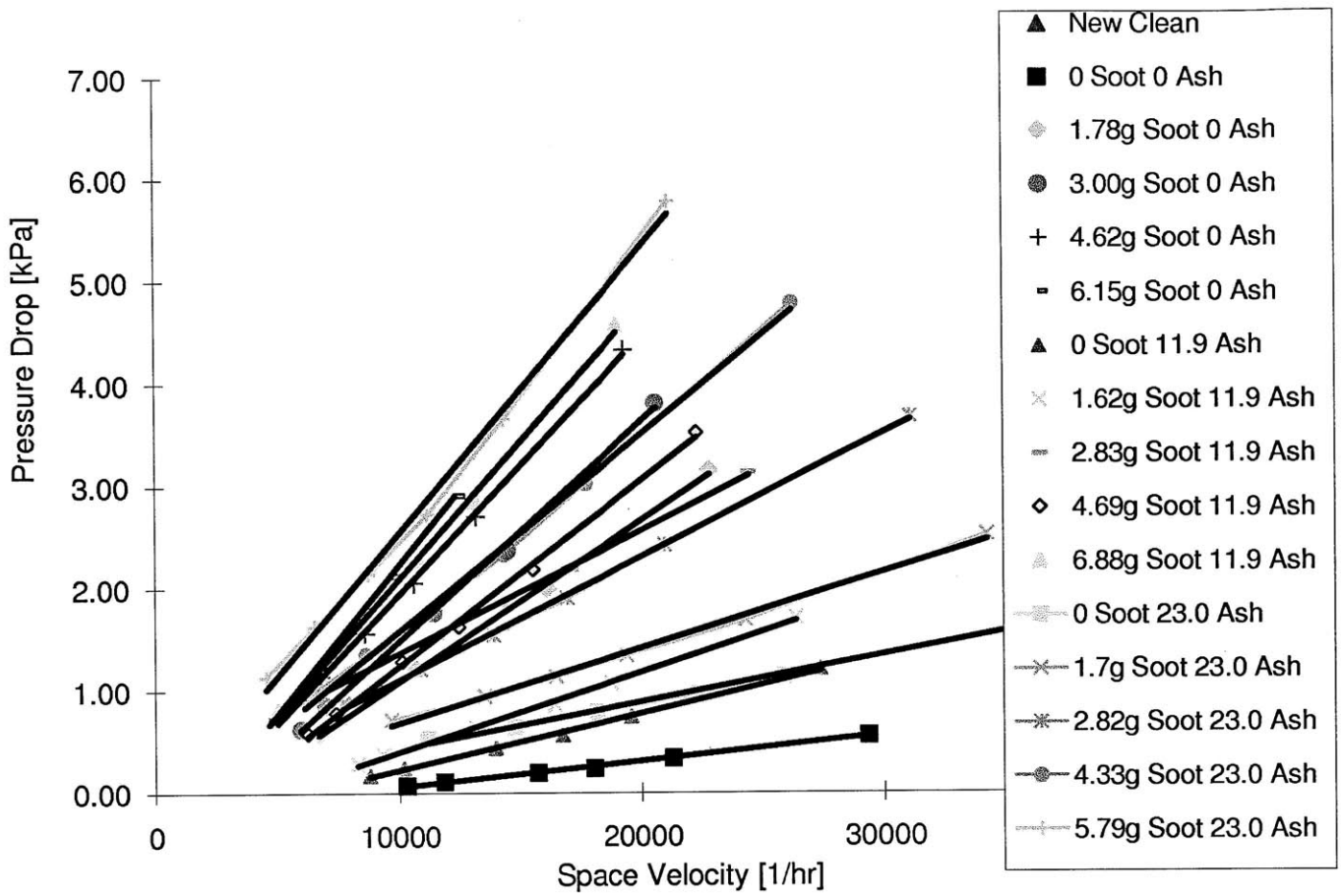

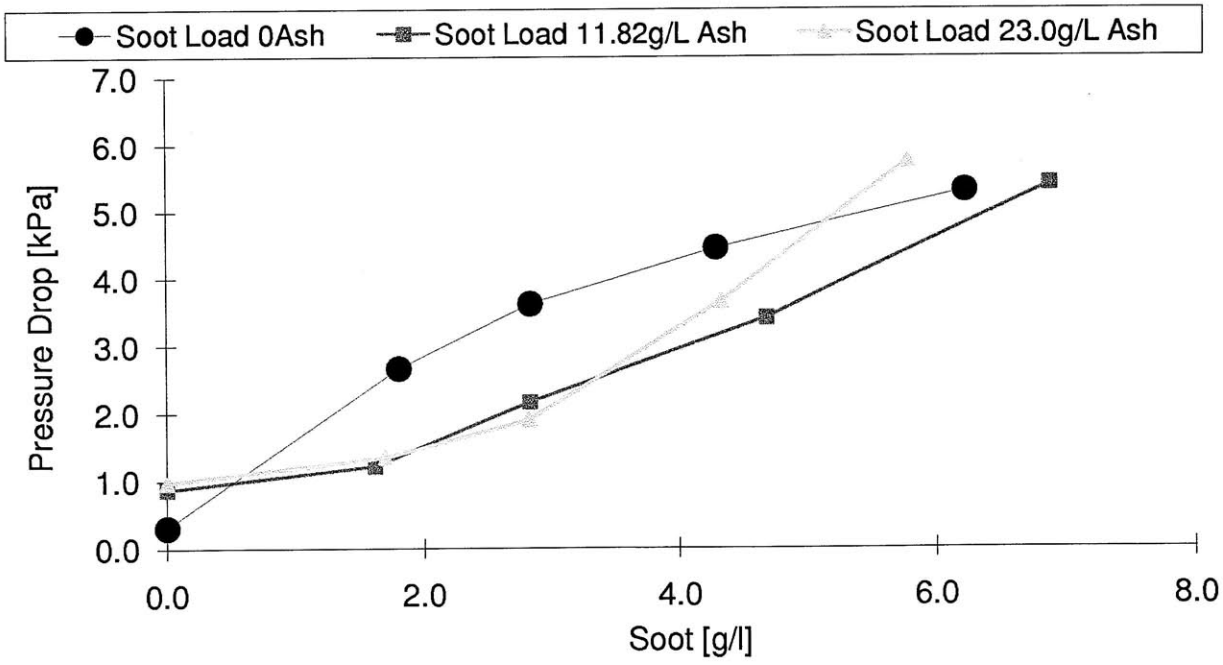

Figure A-7. Space velocity and pressure drop graphs for soot loading of Mg + ZDDP test case.

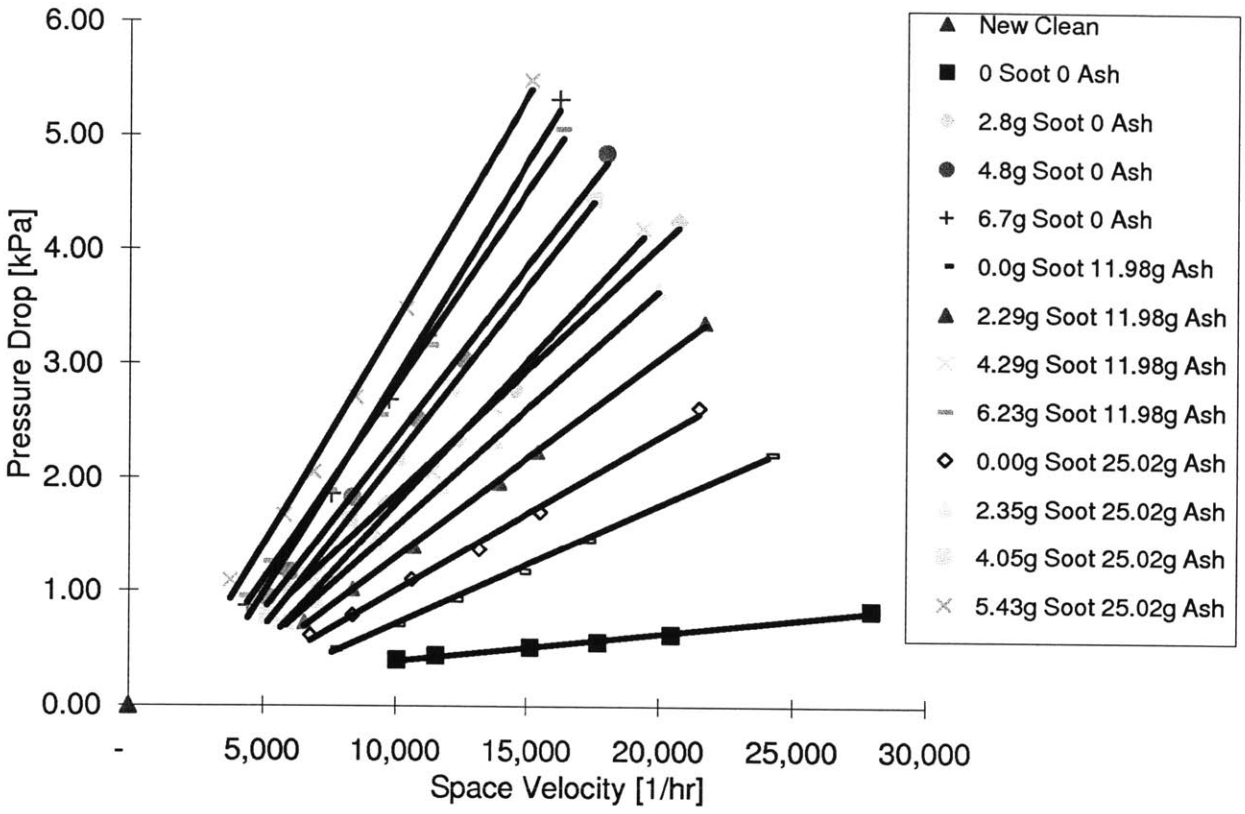

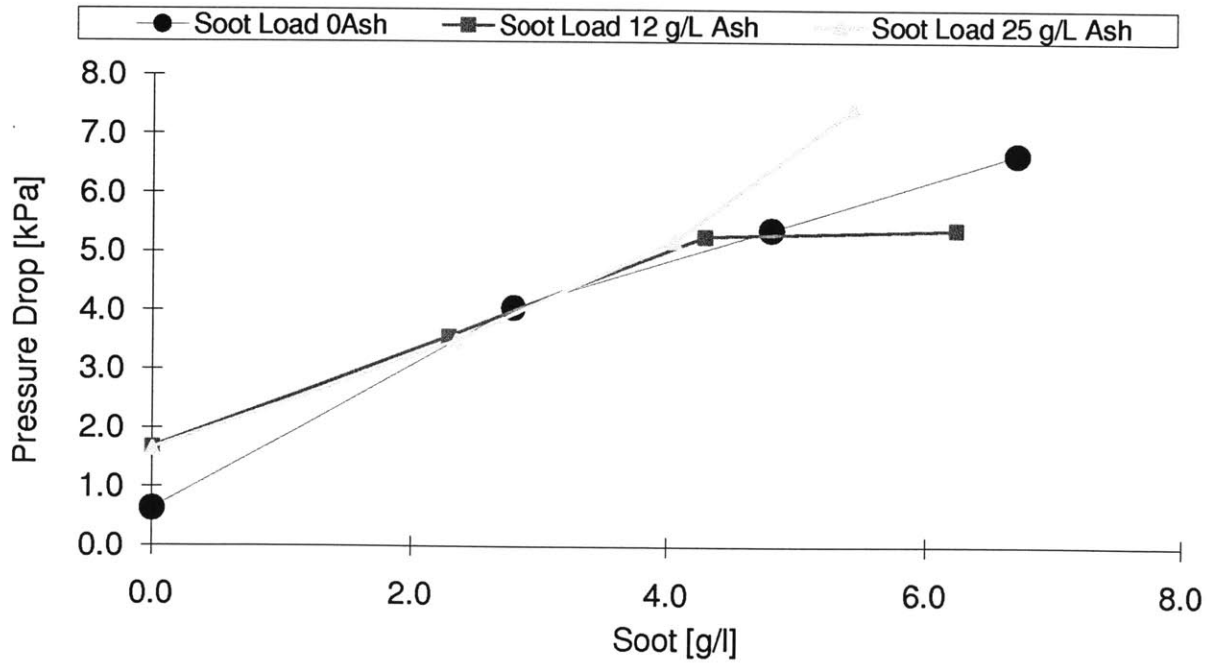

Figure A- 8. Space velocity and pressure drop graphs for soot loading of Ca + ZDDP test case.

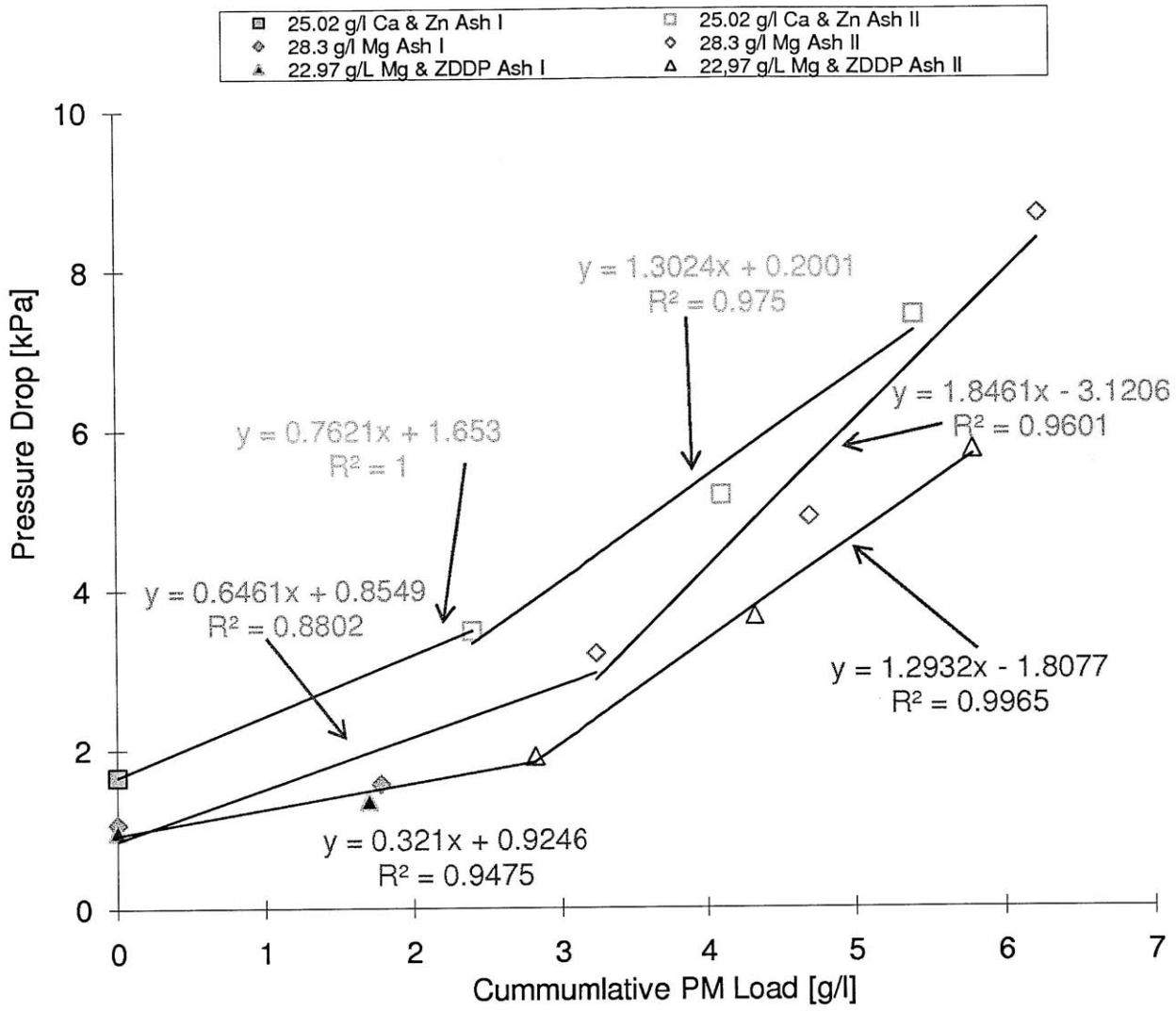

Figure A- 9. RPS used in the determination of RPS for test cases conducted in this research.

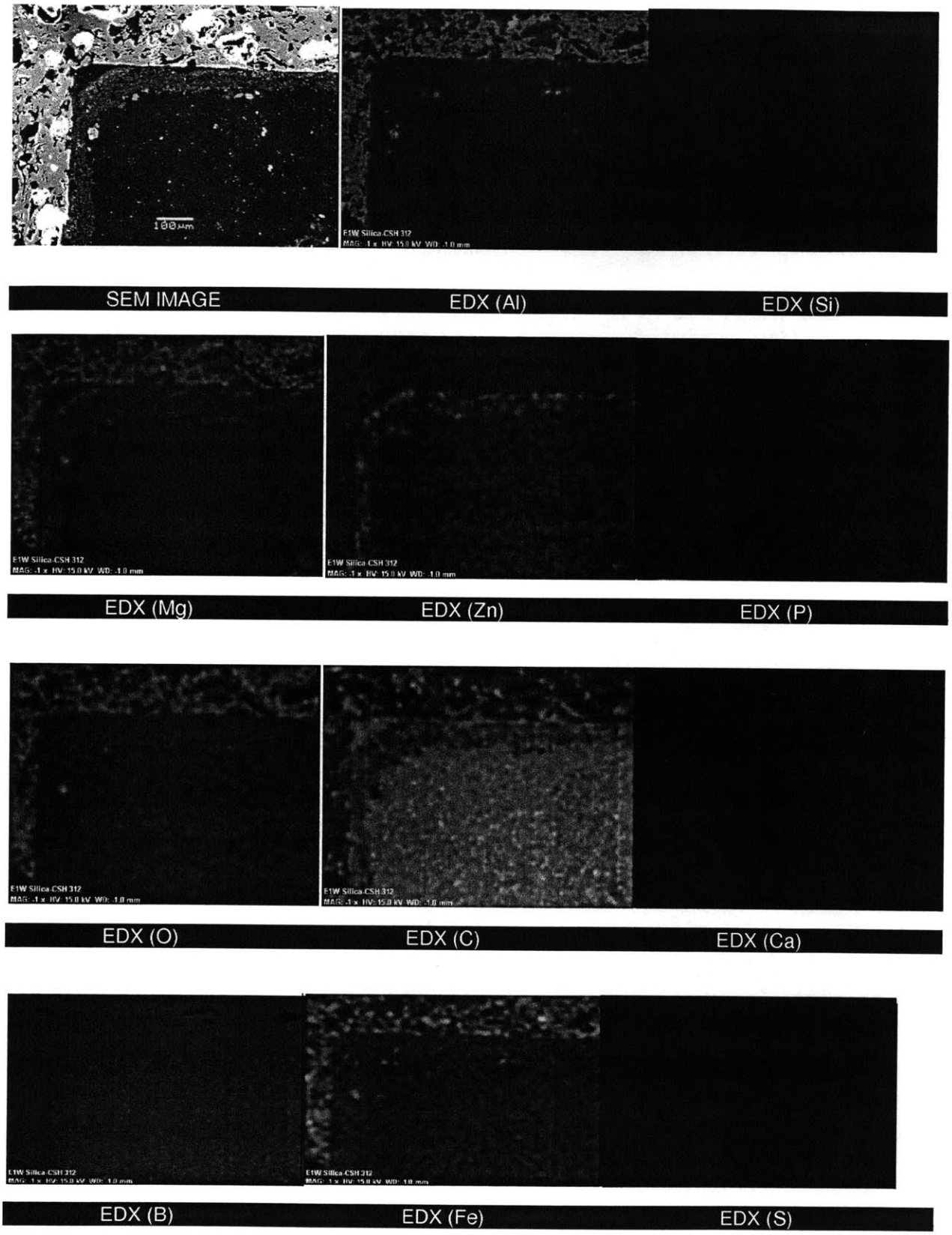

Figure A- 10. EDX Images for Mg + ZDDP Test Case

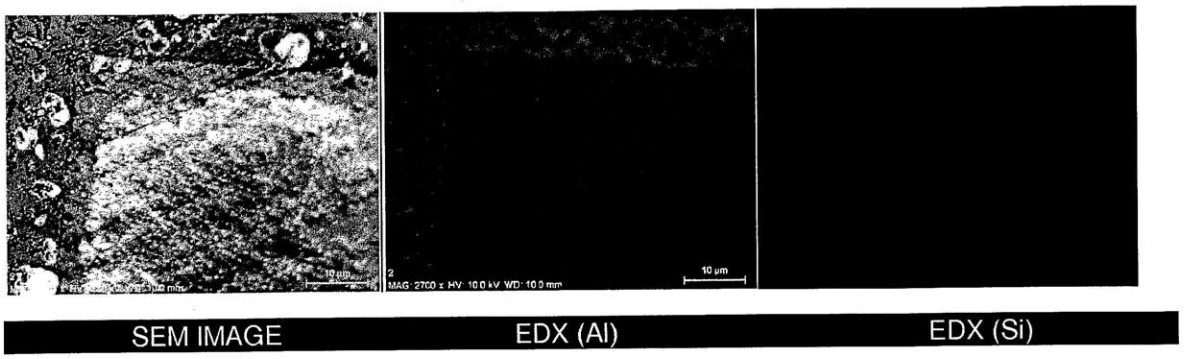

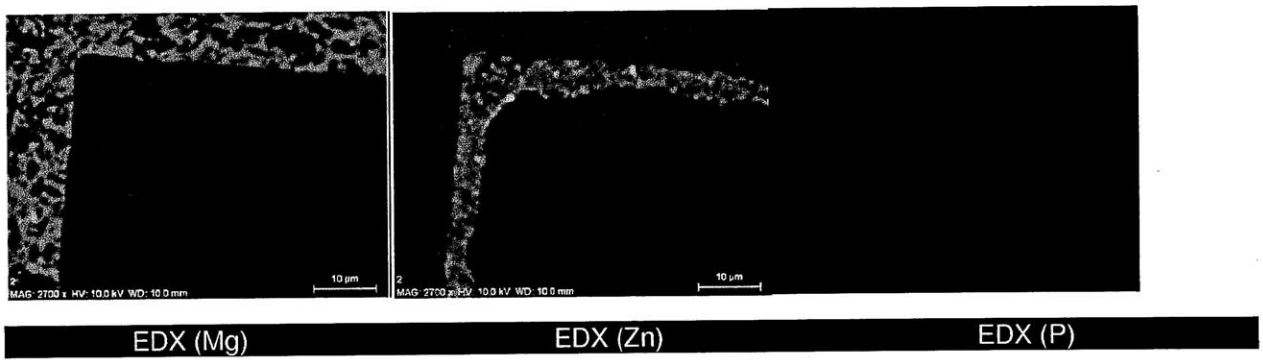

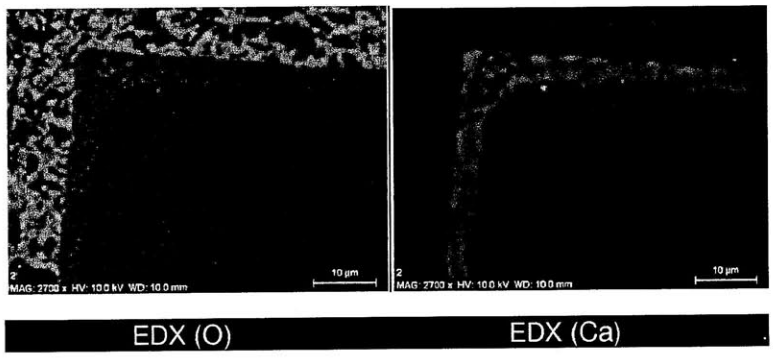

Figure A- 11. EDX Images for Ca + ZDDP Test Case

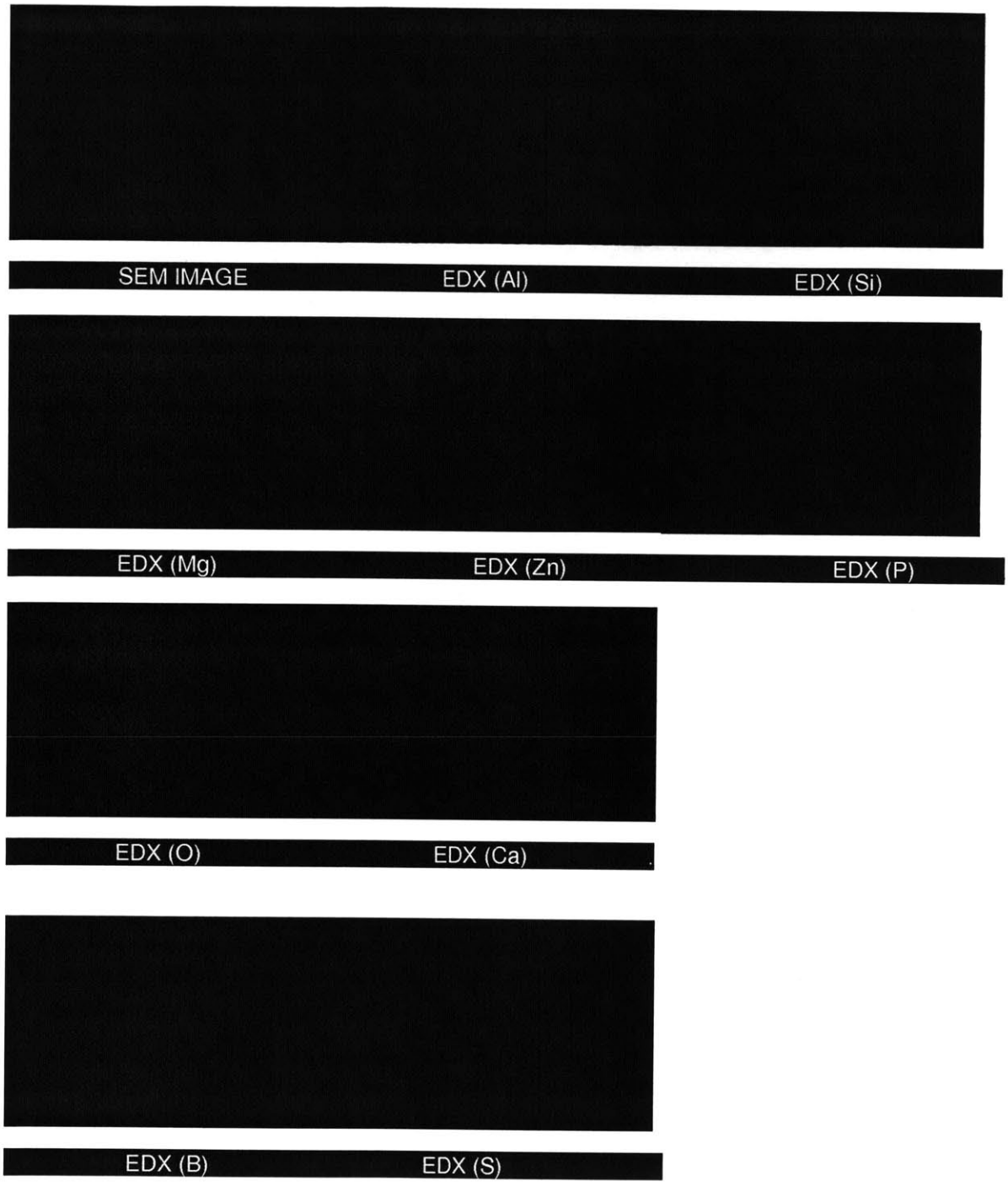

Figure A- 12. EDX Images for base + Mg Test Case